BIOELECTROCHEMICAL SYSTEMS AS TOOLS TO STUDY SUBSURFACE BIOGEOCHEMICAL PROCESSES

A Dissertation Presented

to the Faculty of the Graduate School

of Cornell University

In Partial Fulfillment of the Requirements for the Degree of

Doctor of Philosophy

by

Elliot Sam Friedman

January 2014

© 2014 Elliot Sam Friedman

BIOELECTROCHEMICAL SYSTEMS AS TOOLS TO STUDY SUBSURFACE BIOGEOCHEMICAL PROCESSES

Elliot Sam Friedman

Cornell University 2014

Microbes capable of extracellular electron transfer have been identified, characterized, and isolated from a wide variety of environments, including many soils and sediments. These uniquely-adapted microbes have been extensively studied in bioelectrochemical systems, such as microbial fuel cells, microbial electrolysis cells, and microbial three-electrode systems. These bioengineered systems capitalize on their ability to respire with insoluble electron acceptors, including solid-state electrodes. However, the role that these microbes play within the microbial community and biogeochemistry of the soils and sediments in which they are naturally found is less clear. Subsurface microbial communities perform many functions, including: degrading organic matter, controlling carbon and nutrient availability for primary producers, producing greenhouse gases, and mitigating anthropogenic pollutants. Therefore, it is critical to understand the complex community dynamics that govern soil microbiome structure in subsurface environments, and to link microbial processes with landscape level ecosystem function. To this end, I developed a cost-effective and field-ready potentiostat, capable of long-term operation in remote areas with poised subsurface electrodes and measuring respiration of iron- and humic acid-reducing microbes. I integrated these systems with measurements of greenhouse gas emission from soils and characterization of microbiome structure to link the microbial and landscape scales. I applied these techniques to two environments: (1) Arctic peat soils outside Barrow, Alaska to study the impacts of dissimilatory metal-reduction and microbial community structure on greenhouse gas emissions; and (2) sediments in a riparian zone near Ithaca, New

York to study differences in biogeochemistry across hydrologic and spatial gradients. In the Arctic, potentiostatic monitoring of bacterial respiration revealed a correlation with soil temperature and the activation of microbes at deeper depths as the thaw progressed. Furthermore, bioelectrochemical manipulation altered microbial community structure, enriching for proteobacteria, bacteroidetes, and verrucomicrobia phyla, and these changes impacted landscape-scale processes by increasing methane emissions 15-43%. This work demonstrates a new technique for linking the microbial and landscape scales, the fragility of carbon-rich high latitude soils, and the potential for increased methane emissions in response to small shifts in biogeochemistry. In riparian zones, which are often critical to the mitigation of anthropogenic nitrogen and phosphorus pollution in aquatic ecosystems, I found that microbial processes are highly variably across relatively small spatial gradients (~50 m). One location had lower methane emissions which did not change as a result of bioelectrochemical manipulation; however, at another site which had higher control methane emissions (factor of 2), bioelectrochemical manipulation severely (50%) inhibited methane emissions. Despite these differences in landscape scale response, microbial community structure at both sites was altered by manipulation. The work from both locations (Arctic and New York State) demonstrates the complexity of subsurface microbial community dynamics, their ability to be influenced by small changes in conditions, and the tangible impact that these processes have on landscape-scale processes. Understanding the links between the microbial and landscape scales will be essential to predicting response to external stimuli, such as anthropogenic pollution and climate change.

BIOGRAPHICAL SKETCH

Elliot Friedman earned a B.S. in Environmental Engineering from Lehigh University in 2009. During his undergraduate education, he spent a summer working with Dr. Stephen C. Dexter on marine biocorrosion at the College of Earth, Ocean, and Environment at the University of Delaware. After completing his undergraduate degree he began work towards his M.S./Ph.D. at Cornell University in the Department of Biological & Environmental Engineering. Working with Dr. Largus T. Angenent, he became interested in the role of dissimilatory metal-reducing bacteria within soil biogeochemical cycles. Elliot spent four summers in Barrow, Alaska investigating iron- and humic acid-reduction and the implications for the carbon balance in high-latitude peat soils. During this time he collaborated heavily with Drs. David A. Lipson (Department of Biology, San Diego State University) and Ted K. Raab (Carnegie Institution for Science). While at Cornell University, Elliot also worked on bioengineered systems, including microbial fuel cells and microbial electrolysis cells for recovering value from waste streams, and collaborated with Dr. M. Todd Walter (Department of Biological & Environmental Engineering, Cornell University) to study microbial activity in the sediments of riparian zones. He was also the president of the Cornell University Chapter of the Alpha Epsilon Honor Society for Agricultural, Biological, and Food Engineering, the treasurer for the Department of Biological and Environmental Engineering Graduate Student Association, and active member of the Biogeochemistry, Environmental Sciences and Sustainability (BESS) Graduate Student Association.

This dissertation is dedicated to my soon-to-be wife, Victoria Drobit-Blair; my parents, Russell & Irene Friedman; and my sister, Jeannie Friedman; all of whom have given me unconditional love and support.

ACKNOWLEDGEMENTS

First, I would like to acknowledge the continuing support of my special committee: Dr. Daniel Aneshansley, Dr. James Gossett, and Dr. Bruce Land. I would also like to acknowledge the support of my colleagues in the Angenent Lab, especially: Michaela TerAvest, Dr. Miriam Rosenbaum, Devin Doud, Dr. Matthew Agler, Dr. Jeff Werner, Joseph Usack, Catherine Spirito, and Juan Guzman, who all provided intellectual and social support. I have been lucky enough to work with many collaborators during my time at Cornell University, many of whom I worked with in the field either in Alaska or New York. I would like to thank Dr. David Lipson, Dr. Ted Raab, Kim Miller, Marguerite Mauritz, Jim Miller, and Cristina Solis for their help in Alaska, and Lauren McPhillips and Dr. M. Todd Walter for their help in New York. Finally, I would like to extend my heartiest thanks to Dr. Largus Angenent for advising and teaching me, working with me, and allowing me the opportunity to grow both scientifically and personally.

The work in Chapters 3 and 4 was supported by the National Science Foundation (grant number: 0808604). For the work in Chapter 5, we were supported by the Atkinson Center for a Sustainable Future at Cornell University, as well as the Cornell University Program in Cross-Scale Biogeochemistry and Climate, which is supported by NSF-IGERT and the Atkinson Center for a Sustainable Future.

TABLE OF CONTENTS

LIST OF FIGURES

Note: AX denotes appendix X, and figures in appendices are placed in the table to follow the chapter they support.

LIST OF TABLES

CHAPTER 1.

INTRODUCTION : CENTRAL HYPOTHESIS AND SUMMARY OF THE EXPERIMENTS

Central Hypothesis

Dissimilatory metal reducing bacteria (DMRB), which are capable of respiring with extracellular electron acceptors *via* a variety of mechanisms, have been found across both terrestrial and aquatic ecosystems. Scientists and engineers have utilized these unique microbes in bioengineered systems called bioelectrochemical systems, which capitalize on the ability of DMRB to transfer electrons outside of their cell membranes and respire with electrically poised, solid-state electrodes. Over the past twenty years, interest in these systems has grown tremendously, with researchers investigating the conversion of organic waste streams to electrical power in microbial fuel cells, the production of valuable chemical products (i.e., H_2, CH_4, H_2O_2) in microbial electrolysis cells, biocomputing platforms using these bacteria, and biosensing of chemical compounds. Consequently, we know a great deal about how DMRB function in pure- and mixed-culture bioengineered systems; the state of these systems and outlook for application is discussed in a literature review (Chapter 2).

However, the role of these uniquely adapted microbes in natural systems is less clear. Thermodynamically, dissimilatory metal reduction lies in the middle of the anaerobic hierarchy; it is less favorable than denitrification, but more favorable than sulfate reduction or methanogenesis. Despite this, little is known about the role that DMRB play in the biogeochemical cycles of soils and sediments. As microbes play a critical role in carbon and

nutrient cycling, understanding the drivers of interspecies competition is essential for improving climate models, driving best management practices, and informing policy decisions. In the environment, it is unlikely that microbiome structure is driven by thermodynamics alone; it is more likely to be influenced by a complex mixture of spatial and temporal gradients (e.g.., environmental factors, substrate availability). Due to their unique adaptation allowing them to respire with extracellular electron acceptors, and their position in the anaerobic thermodynamic hierarchy, DMRB could play a critical role in regulating the biogeochemical cycles of soils and sediments.

First, we hypothesized that bioelectrochemical systems could be used to measure respiration of DMRB in the environment. We investigated this hypothesis with the following experiments:

1) **Developing a field potentiostat capable of operating continuously in remote environments and acting as a sensor for microbial respiration.**

- We designed a low-power, microcontroller-based potentiostat that we manufactured for a fraction of the price of commercially available units, and tested its accuracy against a commercially available potentiostat. CHAPTER 3.
- We deployed eight microcontroller-based potentiostats (24 channels total) across ecosystem gradients in peat soils outside Barrow, Alaska, quantified microbially-produced electrical current, and analyzed changes in microbial respiration over time. CHAPTER 3.

Second, we hypothesized that microbial communities influence ecosystem-scale processes, and that enriching for DMRB would alter community composition and inhibit less thermodynamically favorable metabolic processes (i.e., methanogenesis). We investigated this hypothesis with the following experiments:

2) **Linking subsurface microbial communities to ecosystem-scale processes by integrating potentiostatic-manipulation of redox environments with measures of greenhouse gas emissions.**

- We used microcontroller-based potentiostats to enrich for iron(III)- and humic-acid-reducing microbial communities and measured the impact on greenhouse gas fluxes from the associated soils. CHAPTER 4.
- We performed a 16S rRNA gene characterization of soils and biofilms grown on poised and unpoised electrodes to link changes in microbial communities to differences in ecosystem-level function (greenhouse gas emissions). CHAPTER 4.

Thirdly, we hypothesized that DMRB is an important process in riparian zone sediments, and that bioelectrochemical manipulation designed to enrich for DMRB would impact other anaerobic processes, including denitrification and methanogenesis. We investigated this hypothesis with the following experiments:

3) **Studying the role of dissimilatory metal reduction in riparian-zone sediments through potentiostatic-manipulation, and linking subsurface microbiomes to biogeochemical cycles.**

- We enriched for iron(III)- and humic-acid-reducing microbes in a stream riparian area and measured the effect on other forms of anaerobic respiration. CHAPTER 5.
- We performed a 16S rRNA gene survey of biofilms from poised and unpoised electrodes to determine the impact of potentiostatic-manipulation on soil microbiomes across spatial and temporal gradients. CHAPTER 5.

Finally, results from these experiments are summarized and recommendations are made for future work to improve our understanding of the role that DMRB play in important biogeochemical cycles (Chapter 6).

CHAPTER 2.

LITERATURE REVIEW: ENGINEERING IMPROVEMENTS TO INCREASE THE PRACTICAL FEASIBILITY OF BIOELECTROCHEMICAL SYSTEMS

2.1 Introduction

Although the ability of certain microbes to generate electrical current has been known since the first half of the 20th century, the majority of research towards utilizing this process for various applications has occurred in the past fifteen to twenty years [1-3]. Bioelectrochemical systems (BESs) utilize these unique microbes for energy production (microbial fuel cell), product generation (microbial electrolysis cell), or microbial research and biosensing (three-electrode systems). BESs are a unique combination of science and engineering; as a result there are various biological (e.g., metabolism, biofilm structure), chemical (e.g., ionic strength, pH, dissolved oxygen), and physical factors (e.g., reactor design, materials) that influence system performance. Understanding the effects of these factors on system performance is crucial in the effort towards practical implementation of BESs. There has been extensive work towards understanding metabolic pathways and microbial physiology in BESs [4-9]; alternatively, design improvements in BESs have led to increased performance, although many of these systems are laboratory scale and the effects of scale-up are difficult to predict [10-14]. For the purposes of this review, however, only the engineering aspects of BESs will be discussed. This will include reactor design, materials, operating conditions, and the implications for pilot and full-scale systems. Ultimately, the engineering and microbial design considerations must be merged to maximize performance if practical implementation of BESs is to become feasible.

2.2 Microbial Fuel Cells

Overview. In nature, certain bacteria found in sediments are capable of extracellular electron transfer, where they use solid iron, manganese, or other mineral species as terminal electron acceptors during anaerobic respiration [15-19]. BESs rely on the ability of these unique metal-reducing bacteria to respire with solid electron acceptors (electrodes). Microbial fuel cells (MFCs) are designed to physically separate the microbial oxidation of substrate (at the anode) from the corresponding reduction of the terminal electron acceptor (at the cathode). The chambers are separated by an ion exchange membrane (which allows ion exchange to maintain electroneutrality), while metabolically generated electrons travel through an external circuit to generate electrical power (**Fig. 2.1**) [20].

At the anode, there are at least four means by which bacteria transfer electrons to electrodes: (1) redox mediators (or shuttles) [6, 21]; (2) direct contact via outer membrane cytochromes [8]; (3) conductive nanowires [7, 22]; and (4) conductive biofilms [23-25] (**Fig. 2.1**). Recently, two additional mechanisms have been reported: (5) electrokinesis, a cell behavioral response to the presence of an electrode or redox active mineral that is manifested via increased swimming speeds and lengthened motion paths [26]; and (6) a hybrid mechanism involving the transfer of electrons from outer-membrane-bound c-type cytochromes to self-secreted flavins [27, 28]. A variety of substrates have been used as electron donors, including municipal, food, and animal wastewater [29]; molasses wastewater [30]; industrial wastewater [31], landfill leachate [32], industrial dyes [33], and laboratory substrates (e.g., glucose, sucrose, acetate). The strength and characteristics of the substrate can influence MFC performance through substrate availability, conductivity, and toxicity.

The cathode chamber of an MFC involves biotic or abiotic reduction reactions using the electrons from the anode (**Fig 2.1**). In most MFCs, this is the abiotic reduction of oxygen to hydroxide [34]; this reaction is ideal because it generates the largest cell potential (**Fig. 2.2**), although reaction potentials in MFC cathodes are below the standard potential due to the well known difficulties of the oxygen reduction reaction [35-38]. These difficulties, known as overpotentials, are defined as the difference between the theoretically determined reaction potentials (determined from Gibbs free energies) and the experimentally observed potentials [39]. These overpotentials result in energy loss in BESs, and are a major obstacle in the development of applicable BES technology. In laboratories, the abiotic reduction of ferricyanide is often used, however, this is impractical for scaleup or long-term use because it is unsustainable and expensive [40].

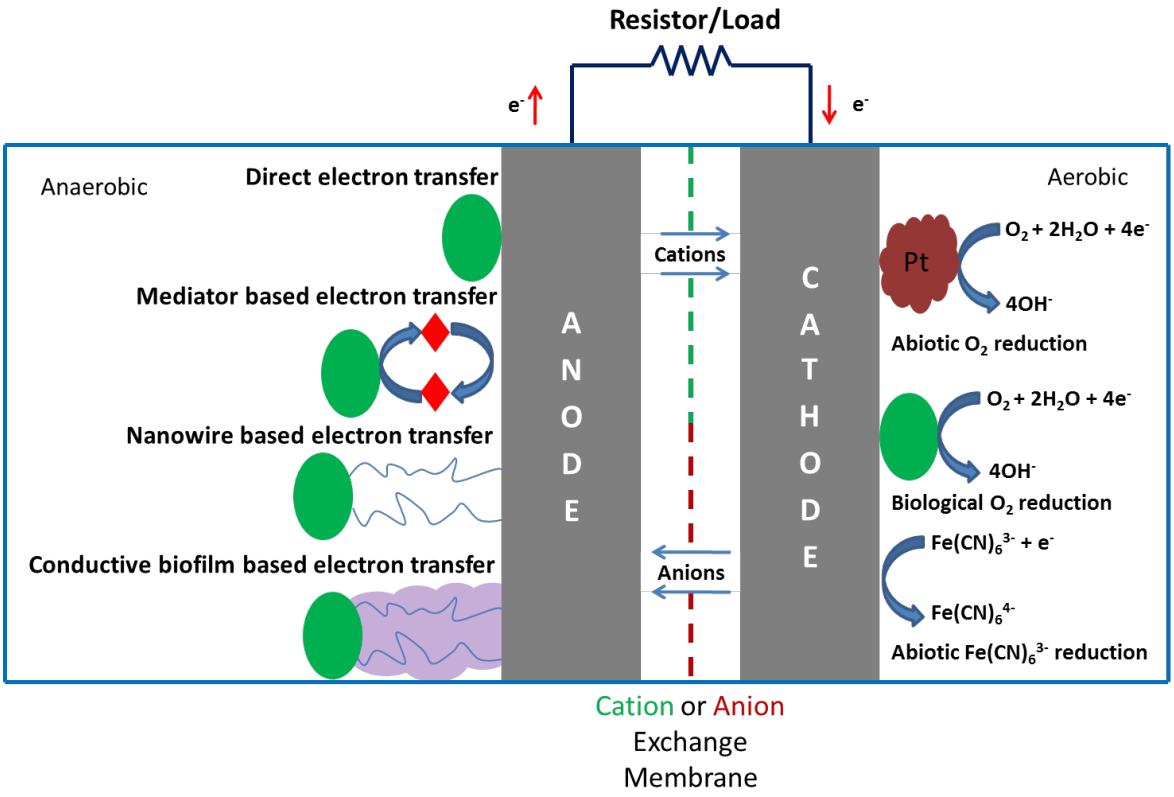

Figure 2.1: A schematic of an MFC, showing four of the possible extracellular electron transfer mechanisms used by anodic microbes; recently, additional mechanisms have been proposed, including electrokinesis and hybrid mediators [26, 27]. The abiotic and biotic reduction of oxygen to hydroxide is shown on the cathode, as well as the reduction of ferricyanide, which is an unsustainable catholyte used for laboratory studies. The anode and cathode chambers are separated by either a cation or anion exchange membrane, which allows for the flow of ions to maintain electroneutrality. Electrons generated at the anode travel through the external circuit to generate electrical power, which can be used to drive a load (practical application) or dissipated through a resistor (laboratory studies).

Power generated in MFCs is dictated by the cell potential, which is a direct result of reaction potentials, and is governed by fundamental electrochemical concepts. Theoretical cell voltage in MFCs can be derived from standard reduction potentials (**Fig. 2.2**) using Equation 1.

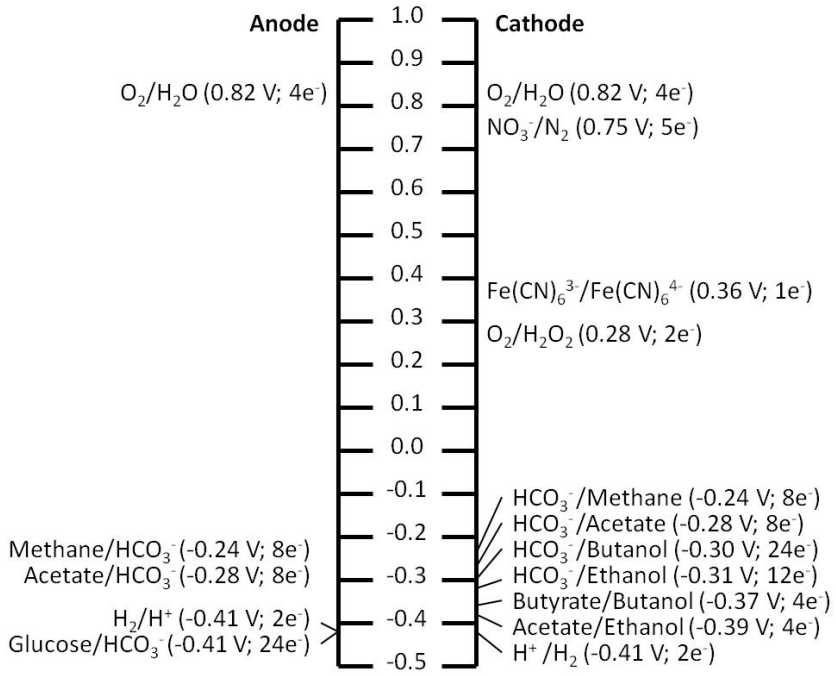

Figure 2.2: Standard reaction potentials ($E^{'}_{o}$) and number of electrons transferred for typical anodic and cathodic reactions in bioelectrochemical systems (BESs). A positive cell voltage (cathode potential minus anode potential) results in power generation (MFC). For product synthesis at the cathode (MEC), power must be added to overcome a negative cell voltage. All potentials are *vs.* standard hydrogen electrode (SHE) at pH 7. Adapted from [39, 41, 42].

$$E_{cell} = E_{cathode} - E_{anode} \qquad \text{Eqn. 1}$$

For example, the theoretical potential of an MFC with an acetate oxidizing anode and an oxygen reducing cathode can be calculated using Eqn. 1 and values from **Figure 2.2** (Eqn. 2).

$$E_{cell} = E_{O_2} - E_{acetate} = 0.82 - (-0.28) = 1.0\,V \qquad \text{Eqn. 2}$$

In practice, the half-reaction potentials in reactor conditions differ from standard values (mainly in regards to pH), and can be calculated using the Nernst equation (Eqn. 4). This equation can also be used to predict the whole cell potential; consider a whole cell reaction of the following form, where A_r is the anode reactant, A_p is the anode product, C_r is the cathode reactant, C_p is the cathode product, and α, β, γ, δ are their respective stoichiometric coefficients (Eqn. 3).

$$\alpha A_r + \beta C_r \rightarrow \gamma A_p + \delta C_p \qquad \text{Eqn. 3}$$

The theoretical cell potential can then be calculated using the Nernst equation (Eqn. 4):

$$E_{rxn} = E^0 + \frac{RT}{nF}\log\left(\frac{A_p^{\gamma} C_p^{\delta}}{A_r^{\alpha} C_r^{\beta}}\right) \qquad \text{Eqn. 4}$$

Where E^0 is the standard reaction potential (i.e., not already corrected to pH 7), R is the gas constant, T is absolute temperature in Kelvins, n is the moles of electrons transferred per mole reaction, and F is Faraday's constant. For most MFCs in which protons or hydroxyl ions are involved in the anode or cathode reaction, the Nernst equation predicts that an increase of one pH unit results in a 0.059 V decrease in cell potential [43].

This potential loss due to pH imbalance is one type of potential loss in BES; the others are ohmic losses, activation losses, and concentration losses. Potential losses prevent theoretically calculated potentials from being achieved in practice. As mentioned, the first type of losses are pH losses, which result in a decrease in cell potential of 0.059 V/pH unit.

These pH losses can occur as a result of membrane processes, which will be discussed in detail in section 2.3. Another source of pH losses is the increase in proton concentration at the surface of biofilm colonized electrode due to slow transfer of protons out of the biofilm into the bulk solution [44]. This can be especially inhibiting in high current systems, where the rate of organic substrate oxidation, and thus proton production is increased [45, 46]. To date, most MFCs exhibit pH imbalances where the catholyte pH increases and the anolyte pH decreases, and cell potential decreases [43]. Recently it has been suggested that a catholyte pH below the anolyte pH could increase MFC performance by reducing the overpotential of oxygen reduction [43, 47, 48], however, more work needs to be done to understand the underlying mechanisms.

The second type of losses are ohmic losses, which occur as a result of solution conductivity and resistance of system components (**Fig. 2.3**) [43]. Solution conductivity can be particularly inhibiting in BESs treating real wastewater, which have very low conductivities [20]. Activation losses, the third type of potential losses, are any losses associated with electrode electron transfer reactions, and include bacterial metabolism, anode overpotentials, and cathodic activation energy losses (overpotential) (**Fig. 2.3**) [49].

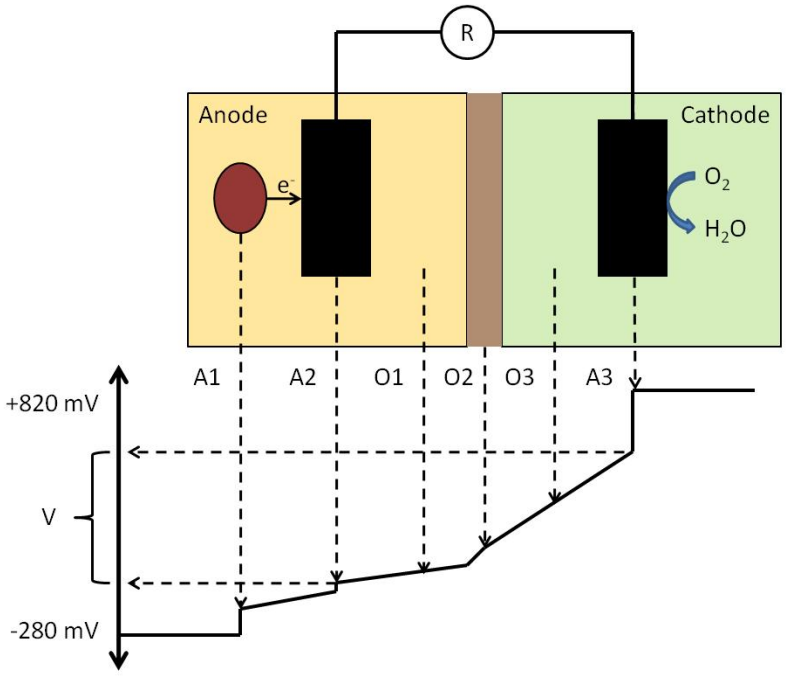

Figure 2.3: Ohmic (O#) and activation (A#) potential losses in an air cathode MFC, occurring as a result of: bacterial metabolism (A1), anodic overpotentials (A2), anolyte resistance (O1), membrane resistance (O2), catholyte resistance (O3), and cathodic overpotentials (A3). The measured cell potential (V) is shown in relation to the standard potentials of the anodic and cathodic reactions. Usable voltage is below the measured voltage due to ohmic losses (O#). Adapted from [20, 50].

The fourth type of losses is due to concentration losses, which occur as a result of inhibited mass transport of reactants and/or products. Insufficient substrate transport can limit bacterial metabolic rates, and thus the current produced. Certain products of bacterial metabolism, if they are allowed to accumulate to high concentrations, can be toxic to the bacteria themselves. These losses can be decreased with increased advection, however, excessive advection can damage bacterial biofilms, which are essential to MFC operation [45]. In addition, the low solubility of O_2 can make efficient mass transfer to the cathode difficult and increase concentration losses in oxygen reduction cathodes [49]. When measuring the cell potential using a multimeter, the

measured voltage is above the usable potential; the cause of this is termed internal resistance, which is defined at the resistance resulting from both electrolytes and the membrane [20].

During operation, different potential losses can dominate based on the operating conditions (**Fig. 2.4**). This can be seen in a polarization test, which is used to measure the performance of an MFC. During a polarization test, the external resistance is varied from open to short circuit, and the cell potential is recorded (**Fig. 2.4**).

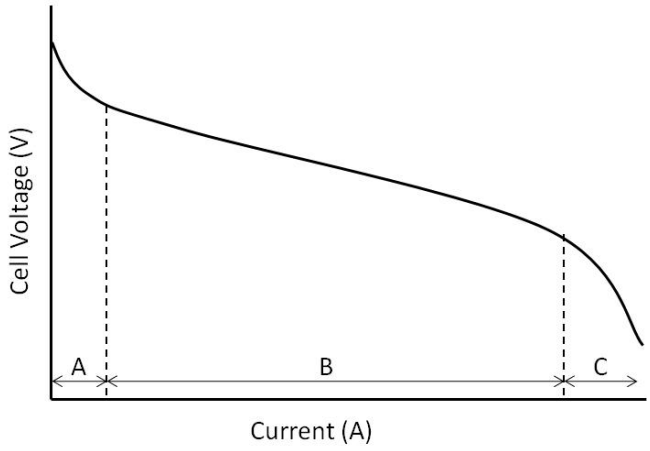

Figure 2.4: Typical polarization curve of an MFC, showing the three regions of polarization: the low current region (A), the medium polarization region (B), and the maximum polarization region (C). Different potential losses are dominant in different regions: in the low current region (A), activation losses dominate; in the medium polarization region (B), ohmic losses dominate; and in the maximum polarization region (B), concentration losses dominate [51].

Based on the measured cell potential and chosen external resistance, the current and power can be calculated using Ohm's Law and Joule's First Law, respectively.

$$\text{Ohm's Law: } I = \frac{E}{R} \qquad \text{Eqn. 5}$$

$$\text{Joule's First Law: } P = IE = I^2R \qquad \text{Eqn. 6}$$

Current density and power density can be calculated based on electrode surface area, and the maximum power point (MPP) can be determined. MFC power output is maximized when the external resistance (or load) is equal to the internal resistance [52]; it has been shown that up to 50% of the electrical power can be lost if the resistances are not matched [53]. Manual optimization of the external resistance is difficult, as the internal resistance is complex and can fluctuate based on a variety of factors, including pH, ionic strength, and mass transport. As such, the development of real-time automated system for load optimization will be crucial to full-scale MFC applications. This can be achieved using maximum power point tracking (MPPT), the same method used to optimize output from photovoltaic cells [52, 53]. Two types of MPPT algorithms (multiunit optimization [MU] and perturbation and observation [P/O]) have been tested for use in MFCs. MU, which is the more complex algorithm, has proven to be faster than P/O and more effective when handling high-frequency perturbation. However, MU is more complex and difficult to employ. In addition, Woodward et al. showed that the MU method will be most applicable to stacks of very similar MFCs, and small differences in individual cells could prevent effective optimization [53, 54]. Alternatively, P/O is relatively simple, effective, and robust; P/O works by changing the external resistance (R_{ext}) at a predefined increment ΔR until power is optimized (Eqn. 7).

$$R_{ext_{k+2}} = R_{ext_{k+1}} + \Delta R sign\left(\frac{P_{MFC_{k+1}} - P_{MFC_k}}{R_{ext_{k+1}} + R_{ext_k}}\right) \quad \text{Eqn. 7}$$

Where P_{MFC} is the power and *k* is the iteration number. Given Eqn. 7, it is evident that a smaller ΔR will result in smaller oscillations at the optimal R_{ext}; however, it will take longer to converge to the optimal value. Initial testing has shown that application of MPPT, especially the P/O

algorithm, leads to increased power production in MFCs [52], and further work to optimize external circuitry promises to yield improved performance.

Electrochemical Techniques. Electrochemical techniques, including cyclic voltammetry (CV), chronoamperometry (CA), and impedance spectroscopy (IS), can be used to identify electrode-respiring bacteria, quantify the redox properties of a system, and examine the resistances in BESs. Central to these techniques is the use of a potentiostat, which is a device that allows the user to control the potential of a working electrode of a three-electrode cell [55]. In such systems, the electrode of interest is deemed the working electrode (WE). The potential of the WE is controlled against a reference electrode (RE), while the third electrode (the counter electrode [CE]) serves as a current drain for the cell.

CV is the cyclic scanning of the WE potential through a range of values at a user-defined scan rate (mV/s), while the current is recorded. This technique is used to understand the fundamental chemical and biological processes in a system and to identify the potential at which chemical and/or biological components (mediators, bacteria, etc.) are electrochemically active [56, 57]. In addition, CV can be used to determine the reversibility of redox processes; this can be used to quantify the efficiency of mediator cycling in a system. The user-defined scan rate is crucial in these tests, as slower scan rates will allow the system to further approach equilibrium conditions as each potential step. In CA, the potential of the working electrode is held constant and the current is recorded with respect to time. This can be used to mimic anode or cathode processes, and is especially helpful in screening potential organisms. IS, which quantifies the impedance, Z_i, of an electrical circuit to current flow, can be used in MFCs to determine the contribution of different system components to internal resistance (R_i) [58-62]. As internal resistance is directly linked to potential losses and power production, IS is a powerful technique in determining areas

of BESs that require the most improvement. However, IS may lose power if the MFC factors are too complex due to biofilms, polysaccharides on electrode, etc.

Design & Engineering. Engineering aspects of MFCs, including reactor design, electrode material, and membrane selection, have profound influence on the chemical and biological components, and influence overall performance (power production) and efficiency. These design aspects can influence factors, such as cell resistance, pH, microbial yield, coulombic efficiency, and power generation.

Reactor Design. Although there have been many variations, the majority of MFC configurations fit into one of four categories: H-type, plate, upflow, and benthic (**Fig. 2.5**).

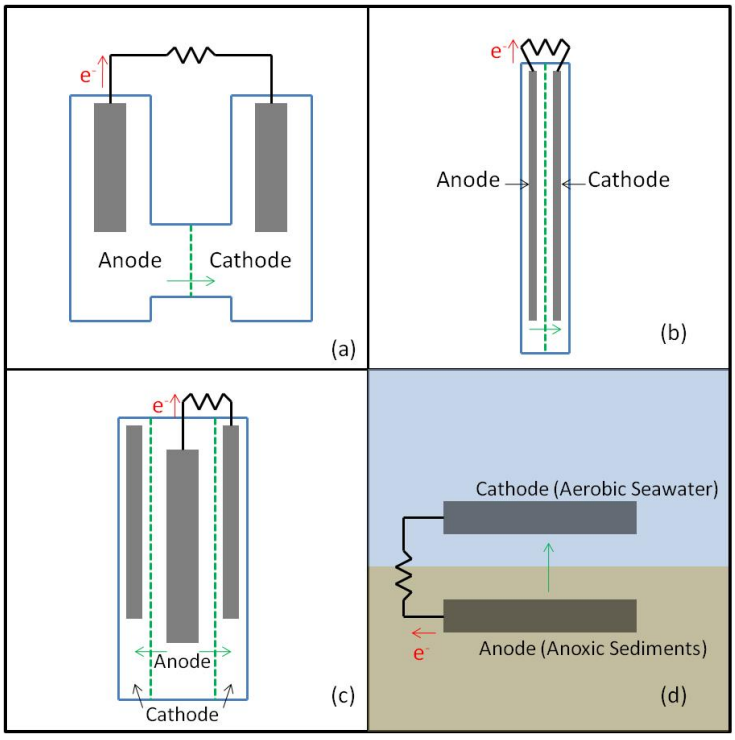

Figure 2.5: Schematics of H-type (a), flat-plate (b), upflow (c), and benthic (d) MFC configurations, showing the anode and cathode as well as the direction of electron and cation movement.

The H-type MFC was the first configuration to be used, which consisted of two vessels connected by salt bridge, and which allowed for ion transport from anode to cathode [63]. The use of a salt bridge, while effective, contributes to high internal resistance and subsequently low power outputs, and was quickly replaced by ion exchange membranes [41]. The H-type configuration is severely limited by the small surface area of the membrane relative to the anode volume, leading to poor ion transport [64]. Additionally, these types of MFCs typically have high internal resistances due to poor reactor design, large distance between electrodes, and inefficient ion transport [12, 41]. A low surface area to volume ratio further decreases efficiency, as power and current are often reported per unit volume [41]. As a result, H-type MFCs are mainly run as batch systems in laboratories to study MFC parameters, including materials, substrates, or microbial communities, and are considered impractical for scale-up. Since they are run in batch mode, H-type MFCs are usually inaccurate for testing parameters relating to continuous operation (e.g., organic loading rate, flow rate, flow patterns, etc.).

Plate MFCs consist of two thin chambers separated by a membrane. This design is similar to hydrogen fuel cells, where use of thin chambers serves to maximize the electrode surface area to substrate volume ratio while minimizing the distance between the electrodes [34]. In these systems, the flow of substrate across the electrode surface can be strictly controlled by cutting channels in the electrode or reactor, which serves to maximize substrate contact with the electrode and decrease dead zones and eddies. In addition, flat-plate designs have an increased membrane surface area for improved ion transport, but may allow for oxygen (cathode to anode) or substrate crossover through the membrane.

A third type of MFC is the upflow (or tubular) MFC (UMFC), which integrates the principles of an upflow anaerobic sludge blanket (UASB) reactor with MFCs. UASB's were developed in the

1970s to eliminate the need for mechanical mixing in anaerobic digesters [65]. These reactors allow for high-rate treatment of waste by producing microbial aggregates, which select for a highly efficient and resilient microbe population. UMFCs were designed in an effort to decrease internal resistance by reducing the distance between the electrodes, and can be used with traditional graphite anode materials (cloth, rods, etc.) or employ granular graphite materials [66, 67]. Although the anode in UMFCs is always designed as a tubular upflow system, different cathode configurations have been used. First, the cathode can be located above the anode, which is separated by a membrane, although this system employed an unsustainable chemical cathode (potassium hexacyanoferrate) and had a similar distance between electrodes as a H-type MFC [67]. Second, an interior U-shaped cathode was shown to produce a high power density per electrode surface area [59]. Third, a configuration using the cation exchange membrane as the physical boundary of the upflow anode, with a chemical or air cathode facing outwards, was operated [66]. Various configurations of UMFCs have been shown to produce high power densities during continuous operation [66, 67]. One study used a UMFC with an internally facing cathode with carbon dioxide addition to prevent a pH imbalance [43]. Additionally, some UMFCs designs have eliminated the ion exchange membrane, allowing for a decreased distance between electrodes [68]. This can be employed when a gaseous cathode is used, and a cloth material is used to separate the anode and cathode; this is advantageous because membranes contribute to internal resistance and are cost-prohibitive in larger MFCs, but can contribute to additional difficulties during scale-up. While UMFCs have provided valuable insights to the biological, chemical, and engineering aspects of MFCs, there are inherent problems that make industrial operation of UMFCs unlikely. IS analysis has shown that electrolyte resistance in UMFCs is inhibiting due to low ionic strengths and the large distance between electrodes [59].

Most systems have been operated with synthetic wastewater; in reality, electricity production from real wastewater will be lower due to high ionic resistances [67]. Traditional UASB reactors, with which UMFCs were designed to compete, generate 49 times more electricity than UMFCs [67]. Finally, material and operational costs are too high to compete with other forms of renewable energy [66].

Finally, benthic microbial fuel cells (BMFCs) have been designed for use in marine environments. Here, the anode is placed in anoxic sediment rich in organic material, and the cathode is placed in oxygenated seawater above the anode [69, 70]. Later designs included a semi-enclosed anode, which served to enhance mass transport of substrate by means of mechanical mixing or natural advection [71, 72]. Additionally, power production can be increased by intermittent mechanical pumping of the BMFC chamber to increase the mass transfer of anodic substrate while removing reaction products [73]. The use of a rotating cathode in a BMFC has been shown to increase mass transport of oxygen to the cathode, leading to currents 70% greater than BMFCs with fixed cathodes [74]. However, in the employment of techniques; such as mechanical pumping and rotation of the cathode, the energy costs of mechanical components must be weighed against increased performance. BMFCs have sustained high power densities for long times (over 1 year), although they can fail from perturbation or biofouling [71, 73, 75]. Pilot scale studies have shown the capability of powering oceanographic sensing equipment, and the development of power management equipment is underway [75, 76].

Electrodes. In addition to reactor configuration, the type, size, and properties of both electrodes have a large impact on overall performance of MFCs. The anode requires a material that is highly conductive, corrosion resistant, stable, and conducive to biofilm formation. The presence of a biological component eliminates certain metals (e.g., silver, copper) used in

electrochemical fuel cells, as they can be toxic to the microbial population. Typically, graphite is used in the form of plates, rods, granules, cloths, or fibers. In some cases stainless steel has been used as an anode [77] although careful analysis of the anolyte and selection of an appropriate steel grade must be taken to prevent corrosion. Stainless steel and gold have also been used as current collectors in conjunction with graphite electrodes [78-80]. When selecting the type of graphite material, a delicate balance between surface area, pore size, and cost must be reached. Materials with high surface areas, including fibers, felts, and foams, have performed better than those with lower surface areas, such as rods, plates, and blocks. However, these higher surface area materials are typically more difficult to manufacture, and thus more expensive, which can become cost-prohibitive in larger systems. A new material used in the aerospace industry, reticulated vitreous carbon (RVC), has also worked well in MFCs due to its high surface area [67]. However there are concerns about clogging the anode chamber when using a material with a small pore size, such as RVC, in a long term reactor with a dense biofilm. Some groups have attempted to enhance performance by modifying the electrode surface to improve electron transfer from microbes. The pretreatment of carbon cloth with ammonia, which increased surface charge and improved electron transport to the electrode, lead to a power increase of 20% over an untreated anode [81]. In addition, the use of platinum and polyanilins as electrocatalysts on graphite anodes to lower overpotentials increased current generation at the anode by electrochemically oxidizing microbial fermentation products while remaining stable in microbially aggressive environments normally hostile towards traditional catalysts [82]. By improving anode efficiency through the selection of an ideal material and properly engineering the anode chamber around the selected material, additional improvements in efficiency can be made.

The selection of an effective cathode material is based on the desired reaction. As previously mentioned, many MFC laboratory experiments are conducted using ferricyanide as electron acceptor. In this case, the electrode material is usually a graphite material, although the type of graphite is trivial due to the low reduction overpotential of ferricyanide. In more practical systems, oxygen is used as the final electron acceptor. In this case, the cathode material has a large effect on system performance, because the reduction of oxygen at carbon electrodes has slow kinetics and high overpotentials. Typically, platinum catalysts are used to enhance rates of oxygen reduction in laboratory MFCs [69, 83], but the feasibility of their use for long-term or scaled-up MFCs is doubted due to high costs and susceptibility to poisoning over time. Other materials have been identified as possible catalysts for oxygen reduction at MFC cathodes, including pyrolyzed iron(II) and Co tetramethoxyphenyl porphyrin (CoTMPP) [84], although the synthesis of these materials is difficult and studies are needed to determine their long-term stability. In the past few years, there has been increased interest in biological cathodes (biocathodes), where microbes use the electrode as an electron donor. A main advantage of this configuration is the elimination of the expensive chemical catalyst, as microbes serve to mediate the transfer of electrons from the electrode to a final electron acceptor [85]. An additional benefit could be the use of biocathodes for the denitrification of wastewater [42]. The feasibility of biocathodes for large-scale reactors is undetermined, although they show promise for increasing the practicality of MFCs for large-scale, long-term applications.

Membranes. The membrane in an MFC is responsible for allowing ions generated at one electrode to pass into the other chamber to maintain electroneutrality. In addition, the membrane serves as a physical means of separating the two chambers, preventing reactant or product crossover. An effective membrane allows for maximum transport of ions while preventing

diffusive transport of other species (e.g., oxygen, fuel, etc.). Ideally, only protons [H^+] or hydroxyl ions [OH^-] should move between the anode and cathode chambers of an MFC; the movement of other ions leads to inhibited proton or hydroxyl ion transport and results in a pH gradient [51].

Initially, Nafion®, which is a perfluorosulfonic acid membrane manufactured by DuPont, was used in MFCs due to its proven use as a proton exchange membrane (PEM) in polymer electrolyte membrane fuel cells (PEMFCs) [86, 87]. However, unlike MFCs, PEMFCs operate at very low pH, allowing for exclusive proton transport through the PEM. The complexity of anodic substrates and the neutral pH found in MFCs results in the presence of additional cation species, decreasing the effectiveness of Nafion® and other PEMs in MFCs [88]. Specifically, increased concentrations of additional cations, such as Na^+, K^+, Ca^{2+}, and Mg^{2+}, at orders of magnitude greater than that of protons (~10^{-2} to 10^{-3} M for other cations *vs*. ~10^{-7} M for protons), results in insufficient conditions for selective proton transport [51]. These additional cations dominate ionic transport, leading to an accumulation of protons (pH decrease) at the anode and of hydroxyl ions (pH increase) at the cathode; this pH imbalance results in potential loss as explained by the Nernst equation (Eqn. 4, Section 2.1). In addition, Nafion® is prohibitively expensive; as such, other, less expensive membranes have been used in MFCs.

Anion exchange membranes (AEMs) and cation exchange membranes (CEMs) are charge selective monopolar membranes and are similar in that aspect to PEMs [89]; in fact a PEM is a specific type of CEM. Ideally, the use of these in MFCs would select for the transport of either protons, from anode to cathode (CEM), or hydroxyl ions, from cathode to anode (AEM). However these membranes are subject to the same limitations as PEMs, in that transport is dominated by ions other than [H^+] or [OH^-], and, as in PEMs, pH gradients develop. In

laboratory systems, the addition of expensive pH buffers can mitigate these effects, but for scale-up and long-term operation membrane problems will need to be addressed [11].

Bipolar membranes (BPMs), which consist of an AEM and CEM mounted together, have also been tested in MFCs [90]. In these cases, water-splitting occurs in a transition zone between the AEM and CEM, and resulting [H^+] and [OH^-] move through the CEM and AEM to the cathode and anode, respectively [89, 91]. This water splitting requires 22 Wh, which corresponds to a membrane polarization of ~820 mV [51, 89]. However, the non-ideality of the AEM and CEM results in the presence of electrolyte salts in the transition zone; this causes a leakage current, which, in BES, is relatively large compared to the total ion flux. Under these conditions, protons and hydroxyl ions are transported to the anode and cathode, respectively (opposite of desired transfer), resulting in the same pH seen in monopolar membranes [89].

Each membrane has advantages and disadvantages; from the perspective of power production AEMs and CEMs work best, however, they are not as effective in overall proton and/or hydroxyl ion transport as BPMs [90]. Further complicating the situation, diffusion layers can develop on all types of membranes as a result of flow patterns in either chamber; this layer can affect the transport resistance of ions [92]. By directing the flow away from the membrane and increasing circulation speeds, the diffusion layer thickness is decreased and current density increases [92].

Due to the complexity of membrane processes, there is much interest in alternative methods of separating anode and cathode chambers. MFCs have been designed to operate without membranes by using either air cathodes [93] and/or cloth separators [94]. Ion transport is only one impact that membranes have one MFC performance; the physical presence of the membrane contributes to the ohmic (internal) resistance of the cell. Membrane properties including

thickness, porosity, charge, and charge density, in addition to the physical configuration of the membrane in the cell, can contribute to ohmic resistance. To minimize resistance, electrodes should be placed as close to each other (and thus to the membrane) as possible, although substantial oxygen diffusion through the membrane into the anode chamber may decrease efficiency by providing a competing electron acceptor. However, some recent work has shown that small amounts of oxygen increased current densities over anaerobic anodes by increasing active biomass levels and allowing for more efficient utilization of substrate [9, 95].

Outlook & Potential for Application. MFCs are a promising technology addressing a global need and significant advances have been made in a relatively short time period, but there is still much work to be done before MFCs can be operated on a large scale. Recent demonstrations of BMFCs capable of powering oceanographic sensing equipment are promising [75, 76], however, for recovery of energy from wastewater, significant advances in understanding bacterial biochemical pathways involved in extracellular electron transport and the engineering of efficient systems must be made. The use of MFCs as a significant source of energy may still be impractical due the dilute nature of wastewater feeds and comparatively low fossil fuel costs. In the best-case scenario, MFCs would be one of many players in the renewable energy arena contributing to the reduction or elimination of fossil fuel use. Primarily, the benefits of MFC technology lie in the sustainable treatment of wastewater, and, as such, would be optimized for maximum current production; under these conditions power production is typically low. Additionally, when considering practical implementation of MFCs technology, extensive studies to determine the viability of wastewater streams on an individual basis will be crucial to ensuring positive investment returns.

The low cost of fossil fuel energy, dilute nature of MFC substrates, and high operating costs present significant barriers towards implementation of MFCs for wide-scale power generation. Even with significant performance improvements, life cycle assessment (LCA) of MFC technology has suggested that it may not be more valuable than traditional anaerobic treatment methods [96]. Additionally, costs of materials used in laboratory and some pilot-scale MFCs, specifically membranes and platinum catalysts, is expected to become cost-prohibitive in full-scale systems [97]. Therefore, for practical implementation to become feasible, increased performance must be congruent with lower construction and operating costs. To this end, a greater understanding of extracellular electron transfer mechanisms, microbe-material interactions, and the effects of design and operating parameters on MFC performance must be achieved.

2.3 Microbial Electrolysis Cells

Overview. With significant barriers towards practical power generation with MFCs, alternative uses for BES technology are being sought. By replacing the load or resistor in the external circuit with a power supply, which applies a small voltage to poise the cathode at potentials high enough to overcome overpotentials for desired reactions, a chemical can be produced at the cathode of an MEC. In MECs, anodic processes remain similar to those in an MFC, while the cathodic reactions change. Therefore, the electrons flowing in the MEC circuit are still derived from microbial substrate oxidation at the anode. Cathodic reactions can be aerobic or anaerobic, and can occur on bare electrodes, chemically catalyzed electrodes, or biocathodes. This flexibility opens the door to a wide variety of potential products and uses, including the production of valuable chemicals and the remediation of pollutants (Table 1). Processes where

chemicals are produced by using the cathode as an electron donor for bacteria has been termed microbial electrosynthesis [98].

Cathode Reaction	Cathode type	$\Delta G^{o'}$ (kJ/mol)	Interest	Reference(s)
$\mathbf{8H^+} + 8e^- \rightarrow \mathbf{4H_2}$	Abiotic	-39.8	Product generation	[99, 100]
$\mathbf{CO_2} + 8H^+ + 8e^- \rightarrow \mathbf{CH_4} + 2H_2O$	Biocathode (UMC†)	-131.0	Product generation	[101-103]
$8H^+ + \mathbf{4O_2} + 8e^- \rightarrow \mathbf{4H_2O_2}$	Abiotic	-134.3	Product generation	[104]
$8H^+ + \mathbf{2CO_2} + 8e^- \rightarrow 2H_2O + \mathbf{CH_3COOH}$	Biocathode (*S. ovata*)	-94.9	Product generation	[98]
$\mathbf{C_6H_5ClO} \rightarrow \mathbf{C_6H_6O}$*	Biocathode (*A. dehalogenans*)	-156.9	Pollutant remediation	[105]
$\mathbf{C_2Cl_4} \rightarrow \mathbf{C_2H_2Cl_2}$*	Biocathode (*G. lovleyi*, UMC†)	-100.5	Pollutant remediation	[106, 107]
$\mathbf{NO_3^-} + 2e^- + 2H^+ \rightarrow \mathbf{NO_2^-} + H_2O$	Biocathode (UMC†)	-163.2	Pollutant remediation	[108, 109]
$\mathbf{U^{6+}} + 2e^- \rightarrow \mathbf{U^{4+}}$	Biocathode (*G. sulfurreducens*)	-21.0	Pollutant remediation	[110]

*exact reaction undetermined; †UMC=undefined mixed culture; $\Delta G^{o'}$ values from [111-115]

Table 1.1: Abiotic and biotic (biocathodes) cathodic MEC reactions for product generation and pollutant remediation, showing the main reactants and products in bold. Additional reactions are possible with the use of external mediators [116].

Powering MECs. To drive cathodic reactions in MECs, an exogenous potential is applied using either a potentiostat or power supply, each of which has advantages and disadvantages. An advantage to the use of a potentiostat is the ability of most commercial potentiostats to automatically adjust parameters (such as applied potential) for maximum performance based on real-time operational data. Commercial potentiostats can be quite elaborate, allowing the user to perform a wide variety of techniques (voltammetry, cyclic voltammetry, chronoamperometry,

chronocoulometry, impedance spectroscopy, etc.) and include computer interfaces. Unfortunately, many commercial potentiostats are prohibitively expensive ($5000+); this could ultimately inhibit the economic feasibility of some BESs systems. In addition, although they can be used to operate lab-scale MECs, commercial potentiostats are not designed to operate at larger currents that will be required for full-scale industrial MECs. Due to these factors, some researchers have designed and fabricated more cost-effective potentiostats, using microcontrollers and operational amplifiers (op-amps) (**Fig. 2.6**) [55].

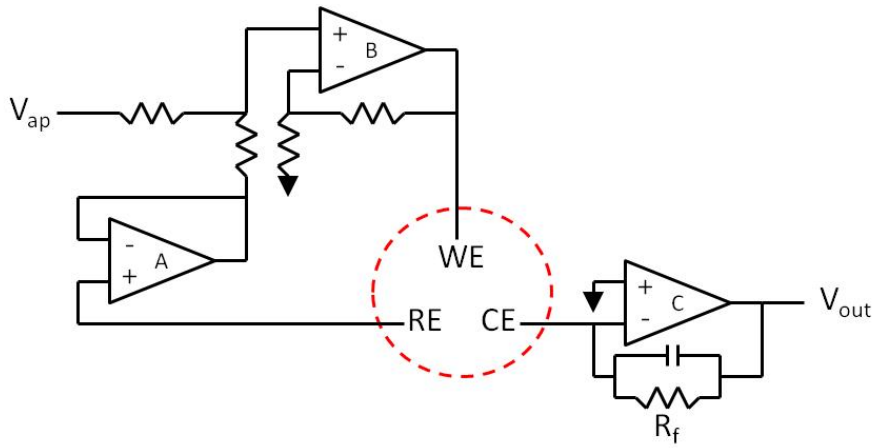

Figure 2.6: Schematic of basic potentiostat circuitry connected to a three-electrode cell. The applied potential (V_{ap}) is applied to the working electrode (WE) *vs.* the reference electrode (RE) *via* a voltage following (A) and summing (B) op-amps. The current at the counter electrode (CE), which is equal and opposite that at the working electrode, is converted to a voltage (V_{out}) via a third op-amp (C). Current is calculated using Ohm's Law (V=IR), where R is the feedback resistor (R_f) of the current-to-voltage converting op-amp (C).

An alternative option to the use of a potentiostat for MEC operation is to use a power supply to apply the required voltage while recording operational parameters (current, cell potentials) using a multimeter. Power supplies, which are capable of handling the large currents that will be experienced in full-scale MECs, and are more economical (~$250) than potentiostats, have been used in pilot-scale MECs [117]. However, commercially available power supplies do not offer

the same level of control over a system as potentiostats; any changes to a power supply-controlled system must be made manually. The design of a novel system, integrating automated control (similar to MPPT in MFCs) with low costs and the ability to handle large currents, holds promise to increase performance and economic feasibility of MECs.

Products.

Hydrogen. Based on a growing interest in sustainable hydrogen production [118], the production of hydrogen in BESs was identified as a higher-value product than electric current [99, 100]. Advantages of hydrogen production in MECs over other methods include increased efficiency and lower voltage requirements. Compared to MFCs, the anaerobic cathode in a hydrogen-producing MEC, which significantly lowers oxygen penetration to the anode chamber, increases overall productivity [100, 119]. However, the collection of a gaseous product from the cathode chamber presents new challenges unforeseen in MFCs. There are also safety concerns when generating, collecting, and storing a highly combustible gas. Due to its high diffusivity, loss of hydrogen can occur by diffusion through the membrane to the anode chamber or into the atmosphere through any tubings or fittings in the system. Additionally, in systems using undefined mixed culture anodes, consumption of hydrogen by bacteria in the anodic chamber could increase the diffusion of hydrogen to the anode. Nafion® is frequently used as a membrane in hydrogen producing MECs [100, 119], making these systems susceptible to the same pH problems experienced in many MFCs (Section 2.2).

Methane. Methane is a combustible gas that has been produced in anaerobic bioprocesses for many years. Using combined heat and power (CHP) systems, methane is burned to offset energy and heating costs at farms, breweries, and wastewater treatment plants. Cathodic methane production in MECs can be achieved using abiotic cathodes with metal catalysts, but high

overpotentials make biocathodes more favorable [120]. In this case, the cathode serves as an electron donor for mixed microbial communities capable of the direct production of methane or the production of H2 and subsequent conversion to methane by hydrogenotrophic methanogens [102, 103]. This process has increased the efficiency of methane recovery by 65% over abiotic cathodes [103, 121]. However, the reduction of carbon dioxide to methane by microbes is highly pH dependent, which, as previously discussed, can change drastically during long term operation of BESs due to membrane processes. Methane production by MECs is a promising area, and improvements can be made in catalysts for abiotic cathodes as well as microbe isolation and enrichment for bio-cathodes. However, the low value of methane as an energy source in the United States must accounted for when considering the potential for large scale application of MECs [122]. One interesting application of methane-producing MECs is the conversion of CO_2 in anaerobic digester biogas to pipeline grade gas (>95% CH_4), which will increase efficiencies, value, and usability of biogas; this technology requires investigation to determine feasibility.

Liquid Biofuels. Liquid biofuels, such as ethanol, are another potential product of MECs; interest in these products has grown due to large fluctuations in the liquid petroleum market from increased demands and uncertain politics [123]. Ethanol can be produced by mixed culture biocathodes, however, the addition of a redox mediator is required [120]. Currently, efficiencies in this system are low due to high overpotentials, low cathodic recovery of ethanol (49%), and competition with other cathodic products (e.g., methane, hydrogen, and n-butyrate) [116]. Efficiency is further decreased due to the loss of the expensive mediators during long term operation and diffusion of ethanol through the membrane to the anode chamber. The diffusion of ethanol is particularly inhibiting, since in addition to decreasing recovery levels, the presence of ethanol at high enough concentrations at the anode can be toxic to bacteria.

Production of other liquid fuels with longer carbon chains is of particular interest based on higher energy content and the ability to integrate such fuels (e.g., butanol) into existing petroleum-based infrastructure [98]. Another advantage is that these fuels can be produced from carbon dioxide, meaning this process could be coupled to a CO_2 generating process to decrease CO_2 releases to the atmosphere. However, work in this area is relatively new and only small amounts of products have been generated [98], although there is potential for increasing yields through genetic manipulation and engineering [4].

Like anodes of MFCs (**Fig. 2.1**), there are different mechanisms by which electrons are transferred from the cathode to microbes. First, direct electron uptake via *c*-type cytochromes is known to occur from solid electron donors, and is likely a mechanism of electron transfer to bacteria in biocathodes [85]. A second mechanism is mediated electron transfer to a periplasmic hydrogenase, and a third, hybrid mechanism, has been proposed involving cytochrome-hydrogenase partnerships. In addition, artificial mediators can be used to transfer electrons from the cathode to microbes; however, these are often impractical for any type of application and are best used to study underlying mechanisms of extracellular electron transfer [85]. A final mechanism is the use of microbially produced mediators, such as phenazines from *Pseudomonas* spp. [6, 9] and flavins from *S.oneidensis* [124, 125]. This mechanism is especially promising since these mediators can be used by other microbes than the producer and react at different cellular locations [85]. Further work on the mechanisms of cathodic electron transfer to microbes should increase functionality of biocathodes, since the energy gain of bacterium involved in biocathodes is directly influenced by the mechanism of electron transfer.

Hydrogen Peroxide & Caustic Soda. Hydrogen peroxide (H_2O_2) is a valuable oxidant used in industries such as paper bleaching, chemical synthesis, and textile bleaching [126]. Recent work

has demonstrated the potential use of H_2O_2 in anaerobic wastewater treatment processes to increase methane yield and lower biosolids production [127]. Production of H_2O_2 using MECs is promising, since in MFCs the open circuit potentials for bare carbon materials are closer to the theoretical potential of oxygen reduction to hydrogen peroxide than they are to water [120]. This two-electron reduction, which is undesirable in MFCs and is circumvented by the application of catalysts to the cathode, could prove to produce a value-added product in MECs. Recently it was shown that small amounts of H_2O_2 (0.13 wt %) can be efficiently generated in MECs on bare carbon cathodes [104]. While promising, there are still significant improvements to be made for this process to become useful.

Peroxide production (Eqn. 8) competes with oxygen reduction to water (Eqn. 9), and dominance is determined by system conditions (pH, temperature, supporting electrolyte) and electrode materials.

$$O_2 + 2H^+ + 2e^- \rightarrow H_2O_2 \qquad E^o = 0.695 \text{ V} \qquad \text{Eqn. 8}$$

$$O_2 + 2H_2O + 4e^- \rightarrow 4OH^- \quad E^o = 1.229 \text{ V} \qquad \text{Eqn. 9}$$

Electrochemical H_2O_2 production occurs in both alkaline (pH 13) and acidic (pH 2) solutions without the presence of mediators [128-133]. The fact that hydrogen peroxide can be degraded by reduction to water (Eqn. 10), as well as homogeneous chemical decomposition, further complicates the operation of H_2O_2 producing MECs.

$$H_2O_2 + 2e^- + 2H^+ \rightarrow 2H_2O \qquad \text{Eqn. 10}$$

At high pH (>13) and/or high temperatures (>50^{o}C), the homogenous decomposition becomes prevalent; at pH 13 and 50^{o}C, 100% of H_2O_2 decomposed within 96 h [132, 133]. Certain

properties of H_2O_2 present challenges to its production in MECs: H_2O_2 can be toxic to microbes, and diffusion to the anode through the membrane can cause the entire MEC to fail. In addition, for many uses of H_2O_2, the product must be more concentrated (at least 3 wt %) than those seen in MECs thus far.

An alternative to H_2O_2 production is the production of a caustic solution [134]. This mixture of mainly sodium and/or potassium hydroxides capitalizes on the pH gradient caused by many cation exchange membranes to generate a mixture used in industries, including paper manufacturers, breweries, and diary plants. Like many MECs, this is a relatively new area and further work needs to be done to increase microbial efficiency and overall process design.

Design Considerations. Many of the design parameters for MFCs also apply to MECs; the electrodes should be as close together as possible to reduce ohmic losses, the reactor should be designed to minimize electrical resistance, and the membrane should be optimized for ion transport to prevent pH gradients. However, it has recently been suggested that hydrogen-producing MECs could benefit from a high anolyte pH and low catholyte pH, which results in a decrease of the overpotential for hydrogen evolution at the cathode [135]. This presents a potential solution to the significant losses associated with pH imbalance in MECs, but further work is needed to understand the underlying mechanisms. The anode chambers of MFCs and MECs are nearly identical in most cases, and a suitable electrode material should be selected with low resistance, high surface area, and proper pore space to prevent clogging. The main differences in MEC design come in the cathode chamber and overall reactor design.

In MECs, the cathode material is chosen based on the desired product. In the case of hydrogen, expensive catalysts, such as platinum, can be used with carbon electrodes to reduce the

overpotential and increase productivity [136]. However, these catalysts have the same limitations as in MFCs;, therefore alternative cathode materials have been investigated for hydrogen production. Hydrogen production occurs on bare carbon electrodes, and it has been shown that a one thousand fold increase in surface area led to a six thousand fold increase in current [38, 137]. Thus, high surface area materials including activated carbon and reticulated vitreous carbon foam could be used to increase productivity, and the identification and application of additional high surface area materials is promising for improved results. Stainless steel can be used for hydrogen evolution and it has been shown that the grade of steel used can have significant impacts on hydrogen evolution rates. Specifically, steel grades with higher nickel contents showed increased hydrogen production rates [138]. Stainless steel brushes have been used in MECs for hydrogen evolution, although the corrosion resistance and long term performance of stainless steel materials needs to be further investigated for practical applications [139]. The use of more complex, rigorously manufactured electrode materials can contribute to higher system costs. Even though increases in efficiency are necessary for practical use of BESs, it is crucial to consider the impact of cost when conducting research.

For methane and ethanol production using biocathodes, the electrode must be an effective material for biofilm growth. Porous, high surface area graphite materials are promising since the rate of direct electron transfer to bacteria is directly proportional to surface area. For long-term operation of biocathodes, susceptibility to biofouling must be investigated to ensure continued operation. In mediated biocathodes (such as ethanol), cathode material is less important, although these mediated systems are not practical for scale-up.

In the case of hydrogen peroxide or caustic soda generation, bare carbon electrodes can be effective cathodes (Section 4.1), however there has been little work on different types of carbon

or alternative cathode materials to increase productivity. Certain carbon materials have been shown to be naturally selective towards peroxide production as opposed to the four electron reduction to water [120]. In addition, titanium electrodes have shown promise in purely electrochemical systems, but have yet to be tested in MECs [140]. The long term stability of this process must be further examined, since at high concentrations hydrogen peroxide has the potential to damage the cathode as well as other parts of the reactor [104].

Reactor configuration can also have large effects on overall performance of MECs. Electrode spacing has been identified as a major contributor to ohmic losses, and reduction of spacing has led to improved product production [141]. In addition, the elimination of a membrane is possible with a gaseous cathode, although this has led to high diffusion of hydrogen into the anode in pilot-scale studies [117]. In this case, a cloth material is often used to allow close electrode spacing (0.3 mm) while still preventing the crossover of reactants between chambers; this has led to improvements in overall performance [142]. Another promising concept is the use of a bipolar plate configuration in MECs (**Fig. 2.7**).

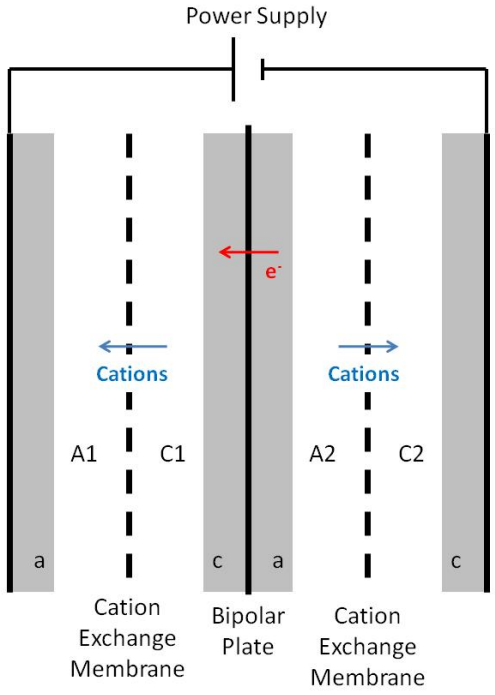

Figure 2.7: Schematic of a bipolar plate stack, showing the anode chambers (A1, A2), anodes (a), cathode chambers (C1, C2), and cathodes (c). In this configuration, both electrodes are in electrically connected to the bipolar plate, and the electrons from an anode travel to a different cathode than the cations. These systems can be expanded to include additional cells.

Although this configuration has been used in MFCs, it has led to cell reversal at high power densities and may be more feasible in MECs, where current is more important than power [10, 143, 144]. This configuration is advantageous because it decreases ohmic losses by allowing the electrons to flow a more direct path from the anode to the cathode. In MECs, the applied voltage necessary for product generation can be applied across the entire stack, eliminating external circuitry and further lowering overall system resistance. This configuration holds promising potential to increase MEC performance, although it requires much investigation.

Outlook & Potential Applications. MECs hold promise as a method to recover value from a wide variety of wastewaters including municipal, agricultural, and industrial streams. While a wide variety of products have been generated, the processes need to be both better understood and

more effectively engineered to garner feasible systems for real-world application. When considering pollutant removal technologies, high efficiencies must not only be achieved, but sustained reliably over long periods of times since failure in these cases means that a potentially harmful pollutant goes untreated. For practical applications, long term feasibility studies are needed to determine reliability and establish confidence in the technology.

To date, only one pilot-scale test of an MEC has been published, where winery waste was used to produce hydrogen in a 1,000 L MEC without a membrane. In this study, Cusick et al. [117] showed that there are still significant improvements to be made before wide scale application is feasible, and that many issues with lab-scale MECs were exacerbated by scaleup. First, the capture of a reactive and highly diffusive product proved difficult without a membrane, as a majority of H_2 produced was converted to methane before recovery. Second, the use of stainless steel cathode supported high currents, but the long term corrosion resistance needs to be investigated. Third, the distance between the electrodes was too large. Finally, it was shown that specific care needs to be taken in selecting and enriching an inoculum to avoid long startup time; this is especially crucial for large reactors [117]. Despite these obstacles, the ability to produce value-added products including hydrogen, methane, ethanol, and hydrogen peroxide from readily available substrates is a promising technology that deserves continued investigation.

2.4 Three Electrode Systems

The third and final type of BES to be discussed in this review is the three electrode system (M3C). This configuration, which is based on the electrochemical half cell, is used when either microbial oxidation or reduction with an electrode is of sole interest. Controlled by a potentiostat, an M3C contains a working electrode (WE), counter electrode (CE), and reference electrode (RE) (**Fig. 2.8**).

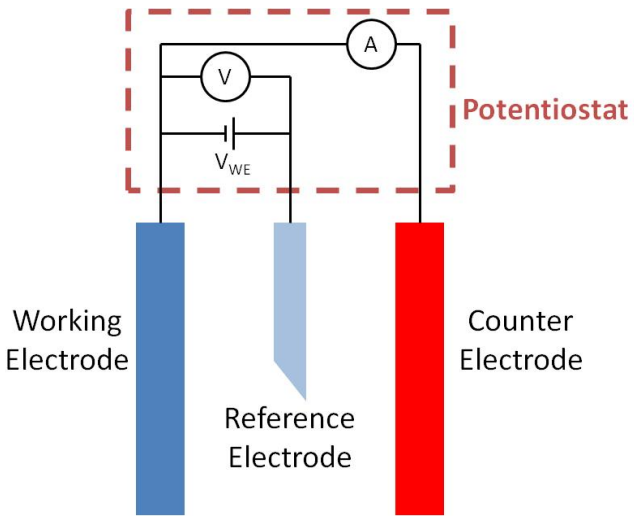

Figure 2.8: Schematic of a three electrode system (M3C). Here the process of interest, either microbial oxidation or reduction, occurs on the working electrode. The potential of the working electrode is controlled against the reference electrode, and the current either into (oxidation) or out of (reduction) the working electrode is recorded. The counter electrode serves as a current drain for the system so that no current passes through the reference electrode.

M3Cs can be a powerful tool for studying microbial processes and interactions in pure and defined mixed cultures [9, 145]. Specifically, M3Cs provide a valuable tool for the identification of the most efficient microbes for oxidation and reduction at electrodes, and can be used to identify organisms capable of power production in MFCs. In addition, these organisms have been studied in M3Cs to determine the effects of electrode potential on overall productivity [146]. Using M3Cs to study the mechanisms of extracellular electron transfer and underlying microbial processes can provide invaluable information necessary in making BESs practical for real-world applications. M3Cs can also be used as biosensors to monitor environmental variables, including microbial respiration and the presence of chemicals, although these techniques still need to be developed. Another application is biocomputing, where biological systems transduce certain inputs to produce digital outputs, thus forming Boolean logic gates [147]. This has potential applications in smart medical devices capable of making decisions

based on *in-situ* real time biosensing of the system. Additionally, M3Cs could be used for the monitoring and control of various biological processes such as activated sludge treatment, fermentation, and pollutant remediation. This area is relatively new, and further work promises to result in additional applications.

2.5 Dissimilatory Metal-Reduction in the Environment

All of the aforementioned BESs are based on the ability of DMRB to respire with electron acceptors located outside of the cell membrane. DMRB is a form of anaerobic respiration; naturally, these bacteria respire with metal oxides through different forms of extracellular electron transfer, including direct electron transfer (DET) and mediated electron transfer (MET) utilizing electron shuttles [5, 148, 149]. In the environment, dissimilatory-metal reduction is one of a host of potential processes (**Table 2.2**) that can occur in soils and sediments.

Process	Reaction	ΔG_r^0 [kJ/($^1/_6$ mol glucose)
Aerobic Respiration	$C_6H_{12}O_6 \longrightarrow 6CO_2 + 6H_2O$	-487.046
Denitrification	$5C_6H_{12}O_6 + 24NO_3^- \longrightarrow 6H^+ + 12N_2 + 30HCO_3^- + 12H_2O$	-433.16
Iron oxide reduction	$C_6H_{12}O_6 + 24(Fe(OH)_3) + 42H^+ \longrightarrow 24\ Fe^{2+} + 6HCO_3^- + 36H_2O$	-263.606
Sulfate Reduction	$C_6H_{12}O_6 + 3\ SO_4^{2-} \longrightarrow 3H_2S + 6HCO_3^-$	-76.017
Methanogenesis	$C_6H_{12}O_6 \longrightarrow 3CO_2 + 3CH_4$	-57.559

Table 2.2. Hierarchy of select microbial respiratory processes, including reactions and standard state Gibbs energies (organic matter represented as glucose, $C_6H_{12}O_6$) . Adapted from Regnier, et al [150].

Specifically among anaerobic processes, iron oxide reduction yields a higher amount of energy for microbes than sulfate reduction and methanogenesis, but less than denitrification [150, 151]. However, in the environment, competition between these processes is subject to a wide array of temporal and spatial gradients, and the dominant process may not be easily defined by thermodynamics alone [152, 153].

Anaerobic microbial processes, including dissimilatory metal-reduction, are of special concern in saturated soils and sediments, such as those found in wetlands worldwide. Microbes play an essential role in biogeochemical cycles, decomposing organic material and making carbon and nutrients available for plant growth [154-157]. Furthermore, different forms of respiration result in different products; for example, denitrification results in the formation of dinitrogen gas, while iron oxide reduction results in carbon dioxide (or bicarbonate, depending on pH) and methanogenesis produces methane. Dinitrogen gas is an inert gas that is the main component in our atmosphere, while carbon dioxide and methane are both greenhouse gases that contribute to global climate change. Methane is a potent greenhouse gas, with a global warming potential 24 times that of carbon dioxide. Currently, wetlands account for the single largest source of methane emissions to the atmosphere; however, there is a large amount of uncertainty associated with the range of emissions predicted in models [158, 159]. Accurate modeling of anaerobic microbial processes is one of the main barriers to improving predictions of wetland methane emissions [158].

High-latitude wetlands are of particular interest, as these soils contain massive carbon stocks (~1672 Pg) [160] and are predicted to contribute up to 30% of global CH_4 emissions from wetlands [158]. Changes in climate could: (1) release dormant carbon stocks through permafrost thaw; (2) alter soil biogeochemistry; (3) influence hydrology of wetlands normally underlain with permafrost; and (4) impact plant communities, net primary productivity, and the amount of carbon fixed by plants through photosynthesis [154, 158, 161, 162]. Due to their remoteness and difficulty of accessibility, high-latitude peat soils are considered vastly understudied compared to other wetlands, and information on microbial processes in these soils is especially lacking [163-166].

Anaerobic microbial processes are essential players in the biogeochemical cycles of saturated soils and sediments such as wetlands. Competition between different forms of anaerobic respiration is complex, and likely driven by a variety of factors, including temporal and spatial gradients. Many wetland environments contain substantial carbon stocks, and predicting how these environments will respond to climate change is important for setting regulatory policies, informing best management practices, and elucidating future concerns. However, models of wetland processes are limited by our knowledge of competing microbial processes in soils and sediments; elucidating the underlying mechanisms driving microbial competition is essential for improving ecosystem- and global-level models.

2.6 Conclusion

MESs are emerging technologies working to address global needs by capitalizing on the ability of microbes to use a solid-state electrode as either an electron acceptor (anode) or donor (cathode). In the case of MFCs and MECs, the recovery of value from an ever-increasing amount of organic waste will prove essential to the continued social, political, and economic success of the civilization. M3Cs have promising applications in the areas of environmental sensing, process control, and smart medical devices. However, in most cases, BESs require significant advances in efficiency and overall production to warrant large scale use. In MFCs and MECs, the knowledge of microbial processes must be merged with practical engineered systems to increase efficiency. Selection of the best electrode materials, as well as reactor configuration, must be optimized for the given system as this can play a major role in system performance. Electrode spacing has a drastic effect on overall efficiency, and should be optimized in conjunction with other parameters. In addition, the factors decreasing performance in BESs, mainly membranes and internal resistance, must be examined so that they can be properly

addressed. Finally, economic analysis and life cycle assessments of these systems must be performed to find the most useful applications of BESs.

CHAPTER 3.

A COST-EFFECTIVE AND FIELD-READY POTENTIOSTAT THAT POISES SUBSURFACE ELECTRODES TO MONITOR BACTERIAL RESPIRATION

Adapted from: Friedman, Rosenbaum, Lee, Lipson, Land, & Angenent. Biosensors & Bioelectronics. February 2012. 32(1): 309-313.

Note: Supplementary information can be found in Appendix 1, and is denoted in the text as A1.SX, where X is the appendix section.

Abstract

Here, we present the proof-of-concept for a subsurface bioelectrochemical system (BES)-based biosensor capable of monitoring microbial respiration that occurs through extracellular electron transfer. This system includes our open-source design of a three-channel microcontroller-unit (MCU)-based potentiostat that is capable of chronoamperometry, which laboratory tests showed to be accurate within 0.95 ± 0.58% (95% Confidence Limit) of a commercial potentiostat. The potentiostat design is freely available online: http://angenent.bee.cornell.edu/potentiostat.html. This robust and field-ready potentiostat, which can withstand temperatures of -30°C, can be manufactured at relatively low cost ($600), thus, allowing for *en-masse* deployment at field sites. The MCU-based potentiostat was integrated with electrodes and a solar panel-based power system, and deployed as a biosensor to monitor microbial respiration in drained thaw lake basins outside Barrow, AK. At three different depths, the working electrode of a microbial three-electrode system (M3C) was maintained at potentials corresponding to the microbial reduction of iron(III) compounds and humic acids. Thereby, the working electrode mimics these compounds

and is used by certain microbes as an electron acceptor. The sensors revealed daily cycles in microbial respiration. In the medium- and deep-depth electrodes the onset of these cycles followed a considerable increase in overall activity that corresponded to those soils reaching temperatures conducive to microbial activity as the summer thaw progressed. The BES biosensor is a valuable tool for studying microbial activity *in situ* in remote environments, and the cost-efficient design of the potentiostat allows for wide-scale use in remote areas.

3.1 Introduction

Bioelectrochemical systems (BESs), including microbial fuel cells and microbial electrolysis cells, have been designed to utilize the ability of dissimilatory metal-reducing bacteria to respire with a solid-state electrode [13, 29, 67, 83, 101, 117, 120]. In addition to waste treatment and energy or product recovery, BESs can be used as biosensors. Often for biosensor function, the working electrode (WE) is poised at a specific potential to mimic an electron acceptor (e.g., iron[III], humic acids) or an electron donor (e.g., iron[II]). This is accomplished with a microbial three-electrode system (M3C) for which the potential of a WE is controlled with respect to a reference electrode (RE). The current flowing into or out of the working electrode is measured via an equal and opposite current produced at the counter electrode (CE). A potentiostat is used to control the potential at the WE and to record the current. The resulting current produced by electrode-respiring bacteria can be directly linked to other parameters, including metabolic activity [167], biological oxygen demand [168, 169], or biodegradable organic matter [170].

Currently, biosensing applications of BESs are limited by the price of potentiostats, which can cost up to $6000 per channel and are often unsuitable for long-term field use. Here, we present the design of an accurate, cost-effective, open-source, and field-ready potentiostat and

demonstrate its use as a biosensor to study bacterial respiration in Arctic peat soils. Although other microcontroller-unit (MCU)-based potentiostats have been described in the literature for cyclic voltammetry [55], to the authors' knowledge, this is the first open-source design of an inexpensive potentiostat that is field ready for long-term chronoamperometry. We demonstrated the use of this MCU-based potentiostat as part of a fully-functional and stand-alone BES biosensor capable of operation in harsh environments (down to -30°C) without electrical grid capabilities. The low cost of our open-source MCU-based potentiostat allows many to be employed across an ecosystem or as a sensor network; indeed, 24 potentiostatically-controlled BESs were deployed at different depths across four drained thaw lake basins around Barrow, AK. For at least five weeks, the WEs were poised at +0.1 V_{SHE} to mimic iron(III) compounds and humic acids; the resulting currents showed high variability across both drained thaw lake basin age and electrode depth. The most interesting results were the distinct increases in microbial respiration at deeper electrodes as the thaw progressed, indicating that elevated temperatures are stimulating microbial activity deeper into soils.

3.2 Experimental

3.2.1 Potentiostat Design

Logical Structure. The MCU-based potentiostat consists of four distinct parts: i. the MCU (ATmega 644, Atmel, San Jose, CA), which serves as a central processing unit, distributing power and running all the other functions (additional information in **A1.S1**, supplementary information); ii. the secure digital (SD) card, which stores the gathered data; iii. the user interface, which consists of an liquid crystal display (LCD) and push buttons; and iv. the operational amplifier (op amp) circuitry, which provides the core of the potentiostat and interfaces between the MCU and the electrodes.

Hardware Design. The electronic signal between the MCU and electrodes is processed by a series of op amps (**Fig. 3.1**), which is based on a previous MCU-based potentiostat by Gopinath and Russell [55] and other basic potentiostat sources (complete parts list available in **A1.S4**, supplementary information). The potential of the working electrode is applied in hardware from MCU output pins through a voltage divider and a 10 kΩ potentiometer. To apply the potential to the WE, the voltage of the RE is passed through a voltage follower (OA-1, LT1097; **Fig. 3.1**), and then summed with the potential from the potentiometer so that the applied potential on the WE is with respect to the RE. To apply a negative potential, the potentiometer voltage is inverted with another op amp (OA-3, LT1097; **Fig. 3.1**) before being applied to the WE. The voltage polarity can be switched by bypassing this op amp via a jumper located on the circuit board. The current entering the WE is measured through a corresponding current at the counter electrode, where it is converted to voltage through a current-to-voltage converting op amp (OA-4, LT1007; **Fig. 3.1**). The feedback resistor (R) on the current-to-voltage converter sets the range of readable current (four choices: 200 μA; 400 μA; 1 mA; and 2 mA). The range is manually adjusted *via* a series of jumpers located on the circuit board. Since the internal ADC reads voltages between 0 and 1.1V, the incoming voltage is shifted by half (550mV) on the auxiliary board so that the range is centered around the origin (i.e., -500μA to 500μA in the 1mA range) (OA-6, LT1097; **Fig. 3.1**). This signal is read by the ADC input pins on the MCU and converted to a digital signal. The user is able to set the time and WE potentials *via* the user interface, which consists of a LCD (MTC-C162DPRN-2N, Truly Semiconductors Ltd., Hong Kong) and four push buttons. In addition, the LCD allows the user to obtain real-time data for easy monitoring at the field site during operating periods. The LCD screen was designed on its own circuit board to allow it to be

disconnected and stored between uses, since it cannot be left in extreme temperatures for extended operating periods.

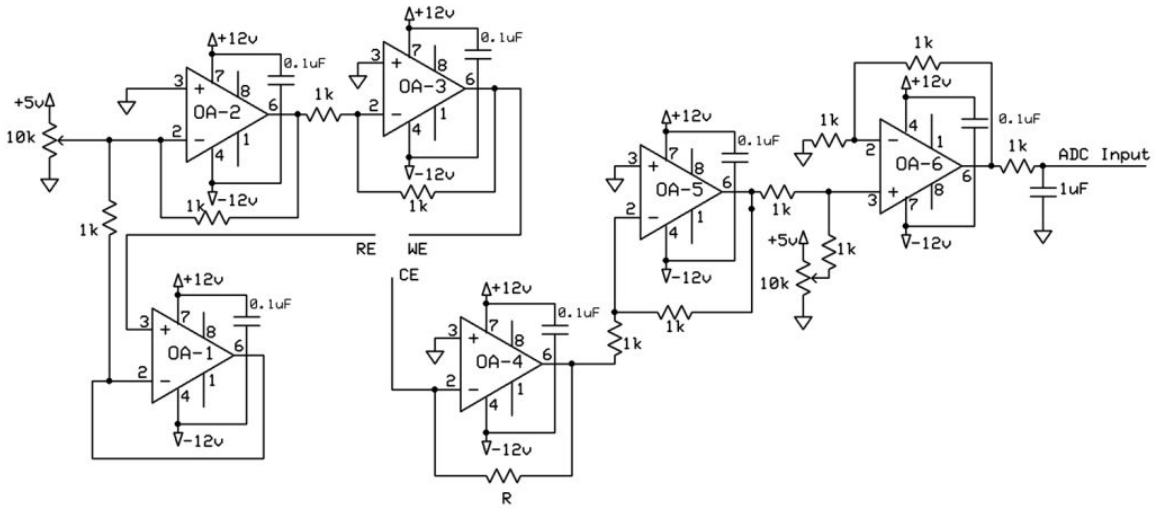

Fig. 3.1: Op amps (OA) that provide the core potentiostat circuitry. The working-electrode (WE) potential is poised with respect to the reference electrode (RE). The current necessary to maintain this potential is measured at the counter electrode (CE), and processed through a series of op amps before being read *via* analog-to-digital conversion. OA-3 inverts the applied potential to allow the application of a negative potential, and can be bypassed when a positive potential is required. A current-to-voltage conversion is performed at OA-4 through a precision resistor that sets the measurement range of the channel. The feedback resistor (R) for current-to-voltage conversion can be changed through a series of jumpers.

Software Design. Software was written in C using AVR Studio v.4 (Atmel, San Jose, CA) – this is included in the open source potentiostat design (additional information in **A1.S1.2**, supplementary information). To minimize the impact of electronic noise from the MCU and the surrounding environment, recorded data points were averaged over fifty individual measurements taken within five milliseconds. The internal ADC converts the analog values to digital values, and the raw ADC input is converted the appropriate current or applied potential. These values, along with the time of the measurement and operating parameters, are recorded to the SD card (WPSDC256M-EAISI, Pretec, Taiwan).

3.2.2 Field Location and Experimental Setup

Units were deployed at four different aged drained thaw lake basins – young (0-50 years), medium (50-300 years), old (300-2000 years), and ancient (3000-5000 years) – outside of Barrow, Alaska (**Fig. 3.2a**) [171]. The medium-aged basin is located at the Biocomplexity Experiment in the Barrow Environmental Observatory and has AC power lines. However, the other sites do not have power lines. At each site we installed two potentiostats (eight total) with each potentiostat controlling three-electrode systems at each of three depths (7, 10, and 14 cm). Thus, we operated a total of 24 electrode systems. The three depths correspond to the aerobic, micro-aerobic, and anaerobic soil zones [172]. Potentials of +0.1 V_{SHE} were applied to the WE starting in late June (2011) to stimulate microbial respiration during an operating period of five to seven weeks. The soil temperature (5-10 cm below surface) was recorded every 30 min using a data logger (CR3000, Campbell Scientific, Logan, Utah) with a temperature probe (Model 107, Campbell Scientific) at the medium-aged drained thaw lake basin (AC power available).

3.2.3 Electrode Construction

For the WE and CE, 8 cm x 2.7 cm x 0.6 cm blocks were machined from medium-extruded graphite plates (GT001135, Graphite Store, Buffalo Grove, IL), and 1.6129-mm holes were drilled in the top of the blocks. The exposed end of a 2.4-m length of 1.628-mm copper wire (ID Booth, Ithaca, NY) was tightly inserted into the hole and sealed using urethane adhesive (4024, Ellsworth Adhesives, Germantown, WI) ($R \leq 0.5\ \Omega$ per connection). Electrodes were housed vertically in 5.1-cm polyvinyl chloride (PVC) piping with lengths of 7, 10, and 14 cm for shallow, medium, and deep electrodes, respectively (**Fig. 3.2b**).

Holes (2.7 cm x 0.6 cm) were drilled in 5.1-cm PVC knockout caps and the electrodes were affixed so that 6 cm of the electrode lengths were outside the piping, giving the electrodes a functional surface area of 41.2 cm^2. In the center of the 5.1-cm PVC piping, 1.3-cm PVC piping was inserted to allow the placement of a reference electrode (Ag/AgCl saturated KCl). The space between the 1.3-cm and 5.1-cm PVC tube was filled with a silica gel desiccant (Bulk Silica Gel, Veritemp, Encino, CA), and the ends were sealed using urethane adhesive. Groups of three electrodes (shallow, medium, and deep) were held together using a hose clamp (**Fig. 3.2b**). Ag/AgCl saturated KCl reference electrodes were connected to 2.4-m lengths of copper wire similar to the other electrodes (additional information in **Fig. A1.S2**, supplementary information).

3.2.4 Field Deployment

The potentiostats were housed in secure waterproof cases (SE-120, Seahorse Cases, La Mesa, CA). A hole was drilled in the case for power, reference electrode, and electrode wires. The cases included desiccant packets (5 g Silica Gel Tyvek Desiccants, VeriTemp, Encino, CA) to prevent any moisture from damaging the electronics, and were locked to prevent tampering in the field. All external electrical connections were made using Buccaneer IP68 waterproof circular connectors (Bulgin, Essex, England).

AC power was used at the medium-aged site; 12-V power adapters (RS-15-12, TRC Electronics, Lodi, NJ) were added to the MCU-based potentiostats that were operated at this site. At the young-, old-, and ancient-aged sites, systems were powered using a combined solar panel-car battery system. A twenty-watt solar panel (BP Solar, Warrenville, IL) charged a 50-Ah deep cycle gel battery (Optima Batteries, Milwaukee, WI) (**Fig. 3.2c**). A solar controller (SunSaver

MPPT, Morningstar Corporation, Newton, PA) regulated the current to the battery from the solar panel to prevent overcharging, and also controlled the power supply to the potentiostats. Each solar panel-battery system directly powered two potentiostats (i.e., six electrode systems).

Fig. 3.2: Biosensing application in arctic peat soils: (a) Map of the area surrounding Barrow, AK where the subsurface biosensor was employed. The area of interested is denoted by a red box on a map of the entire state of Alaska (inset), and general area of research sites are denoted with a red star; (b) Set of electrodes before being buried in the soil. There is a working and counter electrode at each of three depths (7cm – top, 10 cm – bottom right, 14 cm – bottom left). The reference electrodes are inserted from the surface through a tube between the counter and working electrodes; and (c) MCU-based potentiostats with electrodes and solar panel-powered system deployed at a drained thaw lake basin.

3.3 Results & Discussion

3.3.1 Lab Tests of our MCU-Based Potentiostat

To ensure precision and accuracy, performance of the MCU-based potentiostat was compared against a commercial potentiostat (VSP, Biologic, Claix, France) using a resistor-capacitor (RC) circuit (Test Box #4, Biologic, Claix, France) (additional information in **A1.S2**, supplementary information). This showed that our MCU-based potentiostat was accurate within 0.95±0.58% (95% Confidence Limit) on the microamp scale throughout the 1 V operation range (V_{WE} = -0.5 to 0.5 V_{REF}) (**Fig. A1.S1**).

3.3.2 A Biosensor to Study Biogeochemical Processes

Our BES biosensor is a valuable tool for environmental sensing, and can be used to aid the understanding of biogeochemical processes. The biosensor can be used in many different environments. We tested our system with peat soils in the arctic (**Fig. 3.2a and 3.2c**). These soils are a major carbon reservoir (containing up to 1.7 X 10^{18} g [160]); however, little is known about the underlying biogeochemistry and the effects that continued climate change will have on carbon stored in these dense and organic-rich soils [160, 162, 164, 173-175]. Microbial processes are at the heart of the carbon cycle in peat soils, and small changes in environmental factors (e.g., temperature, pH, dissolved oxygen) can alter the dominance of microbial processes responsible for either CH_4 or CO_2 production [176-178]. The reduction of iron(III) and humic acids *via* dissimilatory metal-reducing-like bacteria is a microbial process that competes with methanogenesis in the environment [5, 149, 179-182]. The production of CH_4 with methanogens rather than CO_2 with dissimilatory metal-reducing-like bacteria has considerable impact on climate change because of the 21 times higher climate-forcing potential of CH_4 *vs*. CO_2. Iron(III) and humic acids are present in high concentrations in drained thaw lake basins that dominate Alaska's North Slope [172]. Therefore, a mechanistic understanding of the underlying biogeochemistry of these peat soils is crucial when predicting the long-term effects of climate change.

3.3.3 Field Operation Reveals Weather-influenced Subsurface Microbial Activity

We operated eight MCU-based potentiostats (24 channels) as *in-situ* biosensors in the field at four different sites for a period of five-seven weeks. At three sites, we operated them off-grid with solar panel–battery powered systems. Our 20-W photovoltaic systems at each site provided adequate power for the entire operating period (midnight-sun conditions), including at the ancient-aged drained thaw lake basin site for which we show data here (**Fig. 3.3**).

At the ancient-aged site, the electric current from our subsurface electrodes during the first 2-3 weeks of the operating period was higher for the shallow-depth electrode compared to the medium- and deep-depth electrodes (~100 μA compared to ~80 μA and ~70 μA, respectively) (**Fig. 3.3a**). Our system does not distinguish between electric current from abiotic and biotic reactions at the set potential; however, we anticipate that abiotic reactions are catalyzed without a lag period and then exist at a relatively constant rate controlled by the diffusion of oxidized redox species to the WE. On the other hand, for biotic reactions we observe lag periods to grow cells and a considerable sensitivity to temperature changes. For example, we have observed diurnal changes in electric current from pure cultures of *Geobacter sulfurreducens* in a microfluidic system that was not temperature controlled and that closely followed the daily temperature changes of our laboratory (data not shown). Here, we observe daily cycles of electric current, which were evident within a week at the shallow depth with daily maximums occurring between 15:00 and 18:00 and daily minimums occurring between 6:00 and 9:00. These cycles correlated closely to daily changes in soil temperature (a microbial growth parameter), which indicates that the electric current associated with these cycles is biotic (additional information in **Al.S3**, supplementary information). However, further experiments are necessary to ascertain the ratios of abiotic and biotic current responses. The diurnal electric current cycles became more distinct as the summer progressed.

Currents in the medium- and deep-depth electrodes, which were initially lower compared to the shallow-depth electrode, experienced an increase in average current during the third week of operation (July 13th to 20th) to ~120 μA and ~90 μA, respectively (**Fig. 3.3a**). In addition, the daily cycles that were initially present only at the shallow-depth electrode became evident at the medium- and deep-depth electrodes following the July 13th-20th increase in electric current. This

increase in current corresponded to an increase in medium-depth soil temperature of ~2°C (**Fig. 3.3b**); prior to July 13th the average temperature was 3.66 ± 0.81°C, while after July 20th the average temperature was 5.44 ± 0.71°C. This correlation with our system indicates that microbial activity is limited by growth conditions and not by the availability of terminal electron acceptors (i.e., the electrode). This finding supports the theory that climate-driven increases in temperature could stimulate further increases in subsurface microbial activity, but only if enough natural electron acceptors are present in the soil.

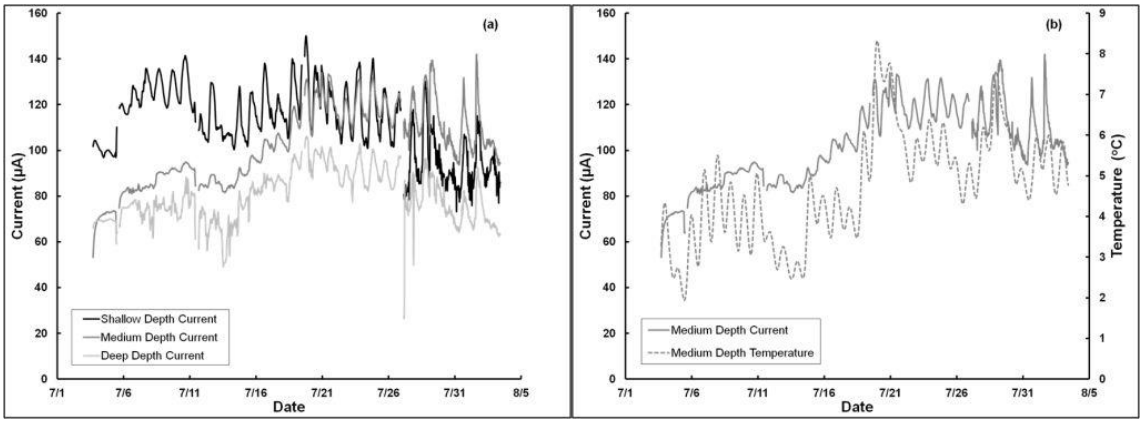

Fig. 3.3: Chronoamperometric data from potentiostatically-controlled system operated at an ancient-aged drained thaw lake basin: (a) The MCU-based potentiostat applied a potential of +0.1 V_{NHE} to working electrodes (WEs) at shallow (7 cm), medium (10 cm), and deep (14 cm) depths; and (b) The electric current at the medium-depth WE overlaid with soil temperature (5-10 cm probe depth located at the medium-aged site, which was one mile from the ancient-aged site). The increase in current production and onset of daily cycles corresponds to the increase in soil temperature between July 13th and July 20th.

By the end of the operating period, the average current with the medium-depth electrodes had surpassed the shallow-depth current. In addition, the current for the deep-depth electrode system was comparable to the shallow-depth electrode system (**Fig. 3.3a**). This indicates that the deeper and denser soils, which are richer in organic substrates, have the potential for higher microbial activity if they experience increased thaws.

This is another indication that continued climate change could unlock previously dormant carbon from tundra soils, although further investigation is necessary to fully comprehend these processes. We are planning to continue our monitoring in future years to reveal the effects of climate change on these microbial communities. It is important to understand, however, that our biosensor systems are just one tool for research and that the electrochemical results must be correlated to many other environmental measurements and information from molecular biology tools to eventually predict the true impact of climate change on these fragile Arctic ecosystems.

3.3.4 Other Possible Biosensor Applications for our MCU-based Potentiostat

As increased monitoring of the environment is necessary to fully comprehend the effects of climate change; this potentiostatically-controlled BES provides a tool to monitor microbial activity *in situ* and in real-time. Furthermore, it is a stand-alone, weatherproof system, allowing it to be deployed in remote areas with no existing infrastructure (i.e., electrical power, buildings). The design of the low-cost MCU-based potentiostat was essential to this application because it enabled biosensors to be deployed in large numbers (24 BESs) across a highly varied ecosystem. The MCU-based potentiostat has the potential for other applications, including *in-situ* pollutant remediation and industrial process control.

The development of these biosensing systems are advantageous because they allow for real-time and *in situ* monitoring, and could alleviate the need for time-intensive and laborious analysis methods. Furthermore, the design presented here could be easily augmented with additional features to improve usability with minimal additional hardware components; this could include wireless monitoring and control or the performance of additional electrochemical techniques (i.e., linear sweep voltammetry, cyclic voltammetry).

3.4 Conclusions

Here, we describe the design and operation of an accurate, field-ready, cost-effective, and MCU-based potentiostat and demonstrate its use as part of a novel subsurface BES-based biosensor. The field-ready MCU-based potentiostat is accurate within 0.95±0.58% (95% Confidence Limit) of commercial potentiostats and can be manufactured for a fraction of the cost, enabling many systems to be utilized across a large area as *in-situ* biosensors. The potentiostatically-controlled BES presented functions as a standalone system, allowing for deployment in remote areas. The application of this system as a novel subsurface biosensor was demonstrated through its use in monitoring microbial respiration in Arctic peat soils. Daily cycles in microbial activity were evident, and results indicate that microbes in deeper soil layers became increasingly active as the soil temperature increased throughout the summer.

3.5 Acknowledgements

The authors would like to acknowledge Dr. Ted K. Raab and Eric Slessarev (Stanford University), Kim Miller (San Diego State University), and Jim Miller (Cleveland Heights High School) for assistance in conducting field work. This work was funded by the U.S. NSF Grant #0808604.

CHAPTER 4.

POTENTIOSTATICALLY POISED ELECTRODES MIMIC IRON OXIDE AND INTERACT WITH SOIL MICROBIAL COMMUNITIES TO ALTER THE BIOGEOCHEMISTRY OF ARCTIC PEAT SOILS

Adapted from Friedman, Miller, Lipson, & Angenent. Accepted to Minerals.

Note: Supplementary information can be found in Appendix 2, and is denoted in the text as A2.SX, where X is the appendix section.

Abstract

Dissimilatory metal-reducing bacteria are ubiquitous in soils worldwide, possess the ability to transfer electrons outside of their cell membranes, and are capable of respiring with various metal oxides. Reduction of iron oxides is one of the more energetically favorable forms of anaerobic respiration, with a higher energy yield than both sulfate reduction and methanogenesis. As such, this process has significant implications for soil carbon balances, especially in the saturated, carbon-rich soils of the northern latitudes. However, the dynamics of these microbial processes within the context of the greater soil microbiome remain largely unstudied. Previously, we have demonstrated the capability of potentiostatically poised electrodes to mimic the redox potential of iron(III)- and humic acid-compounds and obtain a measure of metal-reducing respiration. Here, we extend this work by utilizing poised electrodes to provide an inexaustable electron acceptor for iron- and humic acid-reducing microbes, and by measuring the effects on both microbial community structure and greenhouse gas emissions. The application of both nonpoised and poised graphite electrodes in peat soils stimulated methane emissions by 15%–

43% compared to soils without electrodes. Poised electrodes resulted in higher (13%–24%) methane emissions than the nonpoised electrodes. The stimulation of methane emissions for both nonpoised and poised electrodes correlated with the enrichment of proteobacteria, verrucomicrobia, and bacteroidetes. Here, we demonstrate a tool for precisely manipulating localized redox conditions *in situ* (via poised electrodes) and for connecting microbial community dynamics with larger ecosystem processes. This work provides a foundation for further studies examining the role of dissimilatory metal-reducing bacteria in global biogeochemical cycles.

4.1 Introduction

High-latitude soils contain vast reservoirs of carbon (nearly twice the amount in the atmosphere) and currently act as a net carbon sink [160, 183, 184]. However, it is unclear how Arctic warming, which is projected to be greater than average global warming [185], will alter the balance between carbon uptake via photosynthesis and release through microbial decomposition [154, 161, 166]. Globally, wetlands are the single largest natural methane source, and those located in high-latitude regions account for 10%–30% of wetland methane emissions [158, 159]. Global methane models are highly subject to assumptions and small changes in parameters, including those related to redox inhibition, can change predicted outputs by as much as a factor of two [159]. The subsurface microbiota that decomposes organic matter play a crucial role in carbon cycling in wetland soils and sediments, however, the dynamics of competing microbial populations are poorly understood [163, 164, 166]. Competing forms of microbial respiration have different nutrient requirements, growth rates, and metabolic products, which can have implications for other ecosystems members (e.g., plants, invertebrates). To better

model greenhouse gas emissions and carbon dynamics at the landscape and global scales, we need to further our understanding of the underlying microbial biogeochemistry [186].

Over the past 25 years, it has become apparent that bacteria capable of reducing insoluble compounds (*i.e.*, metal oxides and humic substances) are ubiquitous in soils and sediments [70, 149, 187, 188]. These bacteria achieve extracellular electron transfer through a variety of different mechanisms and can be utilized to produce power in microbial fuel cells [29, 41, 67], produce chemicals in microbial electrolysis cells [85, 102, 117], and remediate organic contaminants in the subsurface [105, 106, 189, 190]. While humans have successfully exploited the ability of microbes to perform extracellular electron transfer in bioengineered systems, the role that extracellular electron transfer plays in natural environments, such as soils, is less clear [191]. The impact that extracellular electron transfer processes have on carbon cycling in anoxic soil is of particular interest because dissimilatory metal-reducing bacteria (DMRB) may compete with other forms of anaerobic respiration for carbon sources and nutrients. Extracellular electron processes dominate microbial processes in peatland ecosystems ranging from mid- (46 °N) to high- (71 °N) latitudes [192-194]. For example, recent work has shown that the reduction of ferric iron and humic substances is a major respiratory process in Arctic peat soils, accounting for between 40%–63% of total ecosystem respiration [193, 194], with similar results found in an ombrotrophic (*i.e.*, a hydrologically isolated environment receiving all water and nutrients from precipitation) bog in Michigan, USA [192]. However, it is relatively uncertain how competition between different microbial respiratory pathways affects larger-scale ecosystem processes (e.g., carbon release).

Previously, we have demonstrated the ability of subsurface bioelectrochemical systems (BESs) to interact with DMRB *in situ* [195]. In these soil-based BESs, an inexhaustible electron

acceptor (poised graphite electrode mimicking the redox potential of iron(III)- and humic acid-compounds) is provided for iron- and humic acid-reducing microbes. Here, these BESs were installed as a tool to manipulate localized redox conditions (via poised electrodes) of tundra peat soils and examine changes in both microbial community structure and ecosystem function (e.g., greenhouse gas emissions). We hypothesized that the addition of an inexhaustible source of electron acceptor for DMRB would outcompete microbial processes with a lower thermodynamic yield (*i.e.*, methanogenesis). Soil chambers were installed in three replicate ice-wedge polygons within a medium-aged drained-thaw lake basin outside Barrow, Alaska. Some soil chambers contained no electrodes, while others contained nonpoised or poised electrodes at either shallow (6 cm) or deep depths (14 cm) below the soil surface. For the poised electrodes, we potentiostatically controlled (0.1 V_{SHE}) the working electrode (WE) of these three-electrode BESs within soils chambers for a period of five weeks. This potential is used in laboratory BESs to grow DMRB at electrodes, and was chosen to promote favorable conditions for DMRB in the subsurface. We measured methane and carbon dioxide emissions from all soil chambers three times per week, and also measured environmental parameters (*i.e.*, soil temperature, pH, dissolved oxygen, soil conductivity, oxidation-reduction potential). At the end of the experiment, biofilms from nonpoised and poised electrodes, as well as control soils, were collected for soil microbiome characterization.

4.2 Results and Discussion

4.2.1. Electrodes Stimulate Methane Emissions Compared to Soils without Electrodes

For electrodes located at both shallow (6 cm) and deep (14 cm) depths, the chambers with graphite electrodes (nonpoised and poised) had higher methane emissions than control chambers (**Fig. 4.1a**); there were no significant differences in CO_2 emissions ($p > 0.48$; **Fig. 4.1b**).

Nonpoised electrodes at shallow and deep depths increased methane emissions by 15% (p = 0.13) and 22% (p = 0.03), respectively. The poised electrodes stimulated methane emissions by 43% at the shallow depth and 38% at the deep depth compared to the control chambers (p < 0.0001 for both depths) (**Fig. 4.1a**).

To account for temporal variations in methane emissions due to, for example, changing weather conditions during the course of the experiment, we compared methane emissions from different chambers by calculating the daily methane emission ratio for chambers with one electrode (either nonpoised and poised) *vs.* control chambers with only soil. These ratios confirmed that nonpoised electrodes at shallow depths did not significantly alter methane emissions (**Fig. 4.2a**). Conversely, poised electrodes at both depths and nonpoised electrodes at deep depths did significantly increase methane emissions (p < 0.001, **Fig. 4.2b**).

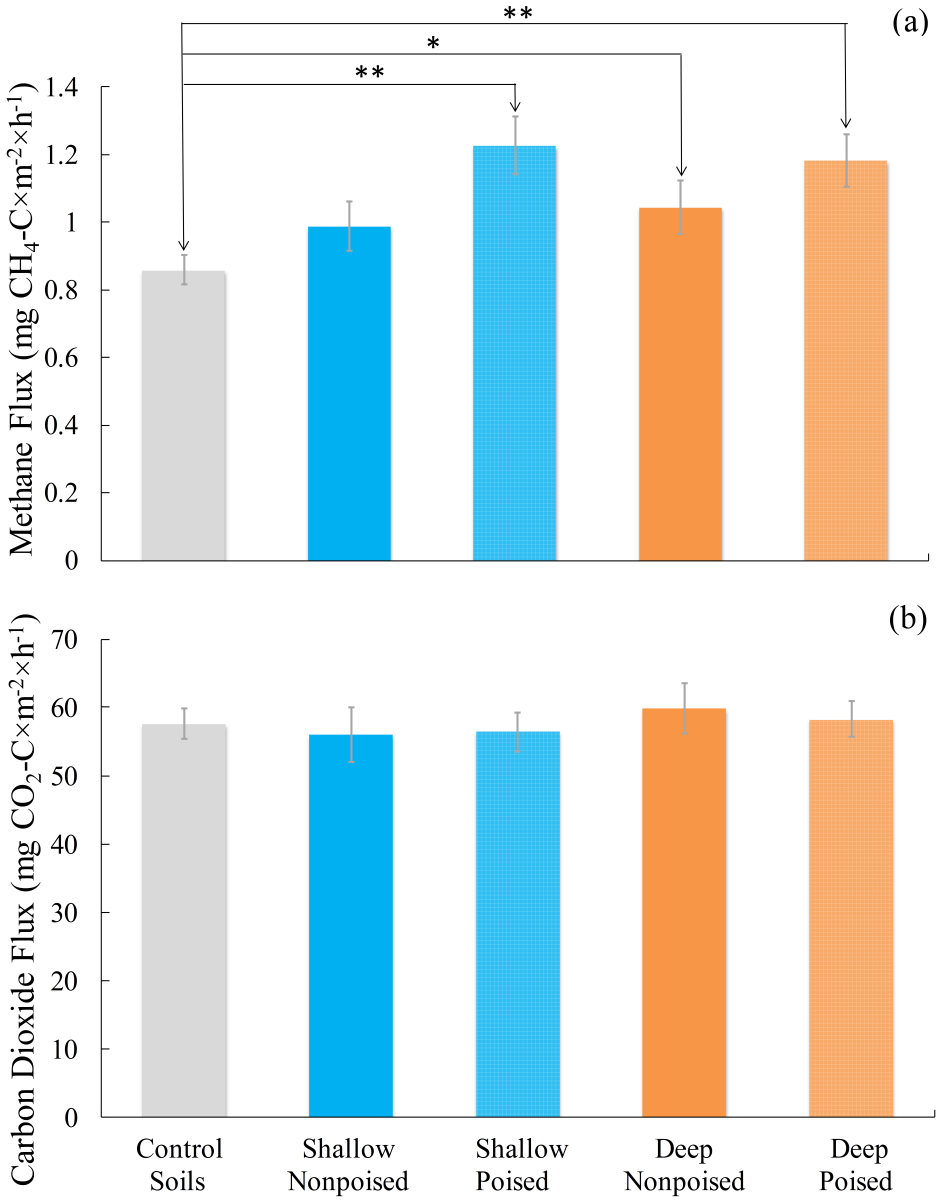

Figure 4.1. Average (**a**) methane and (**b**) carbon dioxide fluxes from the five different soil chamber types over a five-week experimental period. Chambers with nonpoised electrodes had higher methane fluxes (**a**) than the control chambers, but the largest differences from the control were in the chambers with poised electrodes. There were no significant differences in carbon dioxide emissions between different chamber types (**b**). Error bars indicate standard error and statistically significant differences at the $p = 0.05$ (*) and $p = 0.0001$ (**) are noted. We used two-sample *t*-test.

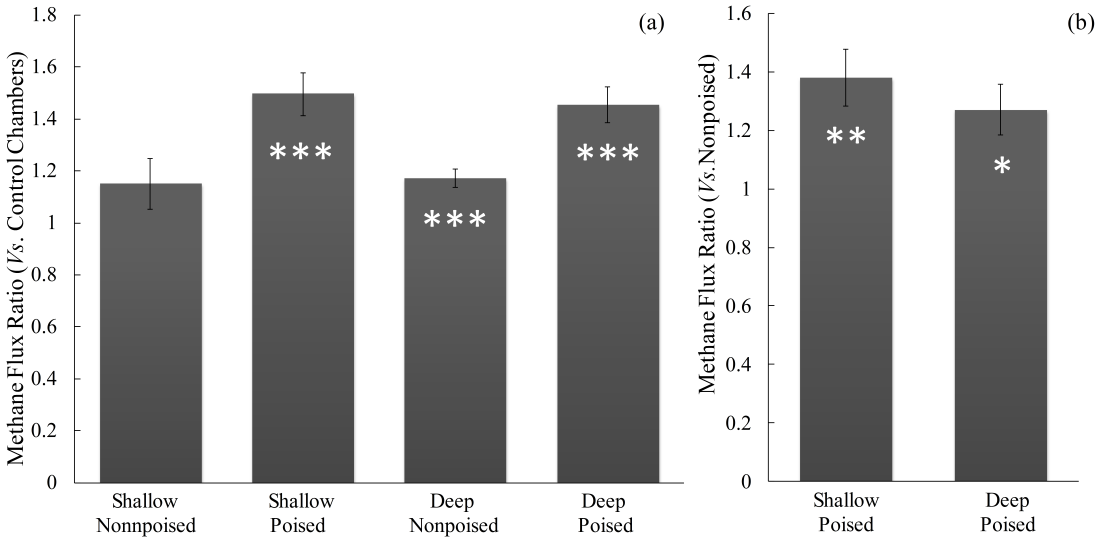

Figure 4.2. Average (**a**) methane flux ratios for the chambers with electrodes *vs.* the control chambers and (**b**) for the chambers with poised electrodes *vs.* those with nonpoised electrodes. Ratios were calculated on each measurement day to account for temporal variations in methane flux based on temperature, precipitation, and other variables. The values shown in the graphs represent the average methane flux ratio over the course of the experiment, and error bars indicate standard error. Significant differences at $p = 0.05$ (*), $p = 0.01$ (**), and $p = 0.001$ (***) using Bonferroni correction are noted.

4.2.2 Electrodes Stimulate a Change in Microbiome

At the end of the five-week experiment, biofilms were harvested from both nonpoised and poised working electrodes and soils in the control chamber to determine the effects of bioelectrochemical manipulation on microbial community structure. We analyzed the microbiomes of 24 samples and with a total sequence count used in our analysis of 4,620,649, the average assigned sequences per sample was 140,166. We achieved an average operational taxonomic units (OTU) assignment of 72.6%. Characterization of 16S rRNA gene sequences revealed significant changes in community structure when electrodes were deployed; the most noticeable differences occurred at the shallow depth. At this depth, the largest differences occurred in the phyla of proteobacteria, acidobacteria, verrucomicrobia, and bacteroidetes (**Fig. 4.3**). In all three types of samples (*i.e.*, soil, nonpoised electrode, and poised electrodes), these

four phyla accounted for 80%–85% of the total microbial populations. The phylum proteobacteria, which includes many DMRB [196-198], accounted for 30.5% of the microbial community in control soils, but comprised 41.6% and 48.7% of the community in biofilms harvested from nonpoised and poised electrodes, respectively. In addition, bacteroidetes, which are carbohydrate-consuming anaerobic bacteria and are commonly found in soils and sediments, were also more prevalent in nonpoised (23.5%) and poised (20%) electrode communities than soil communities (13.3%). Meanwhile, percentages of acidobacteria and verrumicrobia decreased in electrode samples (**Fig. 4.3**). Acidobacteria, which are oligotrophs that prefer low pH environments, had a higher relative abundance in control soils (23.5%) than nonpoised (12.2%) and poised (11%) electrode communities; this result suggests an increase in carbon and/or nutrient availability with electrode deployment, as acidobacteria have been shown to be outcompeted by other microbes when conditions shift from nutrient-poor to nutrient-rich [199]. Verrucomicrobia populations were also lower in poised (5%) and nonpoised (4.4%) samples than control soils (13.3%). Verrucomicrobia is a diverse group of microbes which include species with many possible homologies to proteobacteria [200], and which include species that are capable of methane oxidation [201, 202]. The latter poses the possibility that increased methane fluxes from chambers could be due to a decrease in methane utilization, rather than or in addition to stimulating methane production. However, this would need to be verified experimentally, while a mechanism for this is elusive.

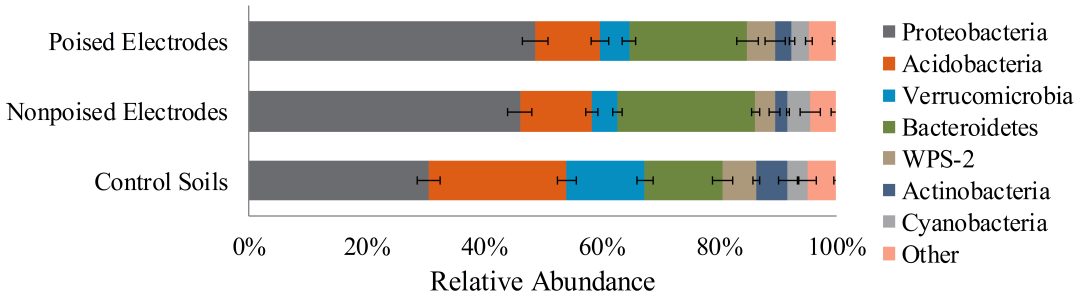

Figure 4.3. Relative abundance of the seven most prevalent bacterial phyla from shallow soil and biofilm samples at the end of a five-week experimental period. Proteobacteria, acidobacteria, verrucomicrobia, and bacteroidetes accounted for >80% of the microbial communities in all three sample types. Error bars indicate standard error, calculated from taxonomic composition of all samples from a given type (*i.e.*, soils, nonpoised electrodes, poised electrodes).

Beta diversity, which is the differentiation in community structure between individual samples, was calculated using both unweighted and weighted UniFrac distances [203]. Principal coordinates analysis of the UniFrac distances (**Fig. 4.4**) showed that the weighted method explained more (62%, **Fig. 4.4b**) of the variation in community structures than the unweighted method (26%, **Fig. 4.4a**) in the first two principal coordinates. This makes sense because the weighted method includes the relative abundance of OTUs within samples, while the unweighted method does not (it only differentiates based on OTU variation), and we already found abundance differences (**Fig. 4.3**). In both unweighted and weighted methods, microbial communities from control soil samples were more similar to each other than those from electrode biofilm samples. We did not observe an obvious grouping of electrode communities based on the depth of application, whether the electrode was nonpoised or poised, or based on the specific polygon that the sample was from. This beta diversity analysis mirrors our results from alpha diversity analysis in which electrodes *vs*. soils showed a diversion in community composition, while the composition was more similar between nonpoised and poised electrodes (**Fig. 4.3**).

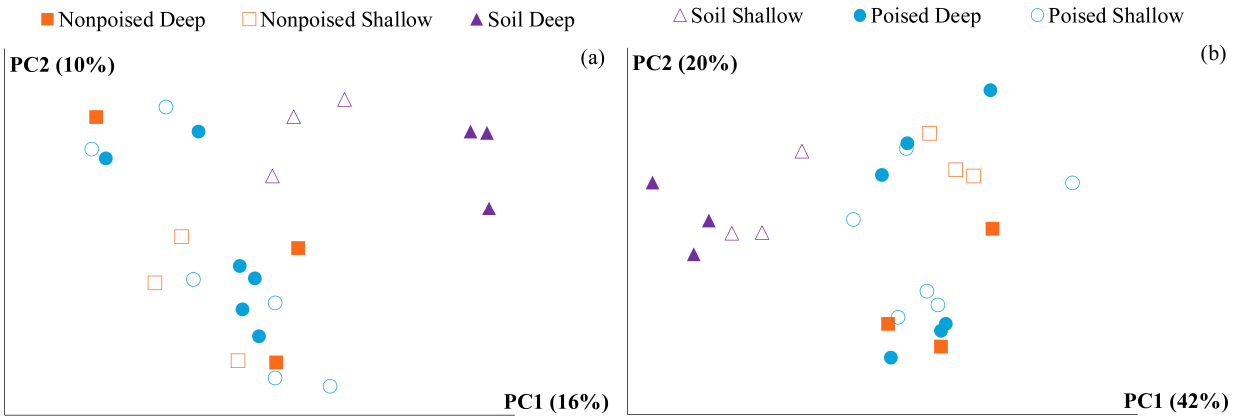

Figure 4.4. Beta diversity analysis of microbial communities showed using both unweighted (**a**) and weighted (**b**) UniFrac principal coordinates. Both unweighted and weighted analysis reveals clustering of soil samples at deep (filled triangles) and shallow (open triangles) depths, however difference in communities from nonpoised (squares) and poised (circles) electrodes are less distinct. Weighted UniFrac, which takes the sequence abundance into account, explains more of the variation in the first two principal coordinates (62% of variation explained) than the unweighted UniFrac analysis (26% of variation explained).

To determine which OTUs were predictive of sample type (*i.e.*, control soil, nonpoised electrode, or poised electrode), we applied a machine learning method using the pamR package for R [204]. This approach developed an algorithm to predict the sample type of an unknown sample based on microbiome structure by identifying specific OTUs that are predictive (*i.e.*, the OTUs that have characteristic changes between sample types). This algorithm utilized 30 phyla to predict sample type; of the eight most highly predictive phyla, only two (proteobacteria and bacteroidetes) had positive machine learning scores for the electrodes (*i.e.*, high abundance of these phyla indicated the sample was from an electrode community) (**Fig. 4.5a**). Using three sample types yielded a high error rate of 0.312 (*i.e.*, the algorithm would incorrectly predict the sample type of an unknown sample 31.2% of the time). However, when nonpoised and poised electrodes were grouped together and analyzed against soil communities, the machine learning approach was able to predict sample history (*i.e.*, soil *vs*. electrode) with a low error rate (0.081) (**Fig. 4.5b**). In this case, there were 43 predictive phyla utilized in the algorithm; of the 16 most

predictive of these phyla, only four (proteobacteria, bacteroidetes, firmicutes, and fibrobacteres) had positive machine learning scores for electrode samples (*i.e.*, a higher abundance of these communities in a sample was indicative of an electrode sample). The remaining 12 phyla had negative machine learning scores for electrode samples. These results suggest that inserting an electrode into the soil: (i) changes the community structure in a nonrandom fashion (predictive); and (ii) decreases overall microbiome diversity, increasing the abundance of a few prominent phyla at the expense of less prominent community members.

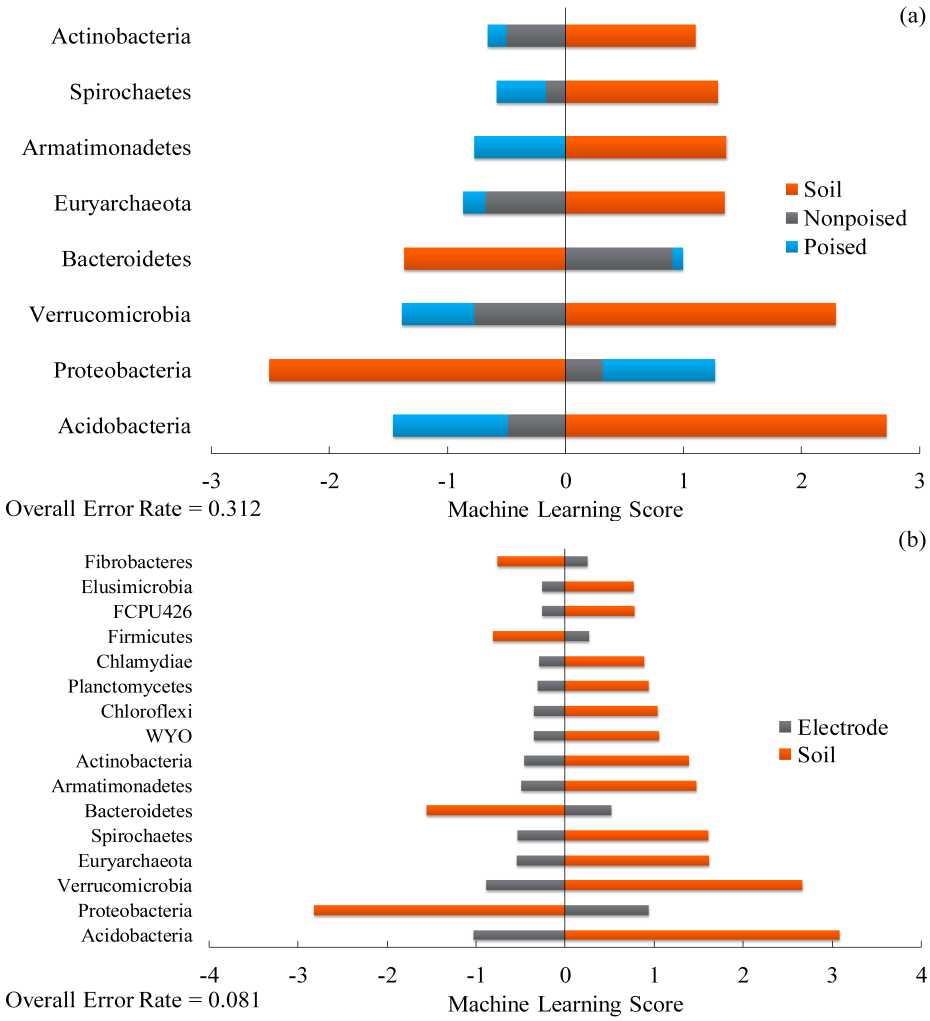

Figure 4.5. Machine learning analysis of soil and biofilm communities from shallow samples reveals the major difference is between communities with an electrode and those without one. When communities are grouped into soil, nonpoised electrodes, and poised electrodes (**a**), of the 30 phyla used to create the algorithm, there are eight phyla that are highly predictive of sample type, however the error rate is high (0.312) and trends (positive or negative scores) are always the same between nonpoised and poised electrodes. Grouping all electrode samples (both nonpoised and poised) together (**b**) results in a better ability to predict sample history (error rate = 0.081). In addition, there are 43 phyla used to predict sample history and, of the 16 most predictive phyla, higher abundance of 12 phyla predict the sample to be from a soil sample.

Alpha diversity, beta diversity, and machine learning analysis of microbial communities all revealed distinct shifts in microbiome structure when an electrode was added to soil, regardless of whether the electrode was nonpoised or poised. One possible explanation for this shift is that

the large conductive graphite electrode allows for electron transport over longer distances (*i.e.*, beyond the microbial scale) (especially if the nonpoised electrode spans oxygen gradients in which case the graphite acts as a bioelectrochemical snorkel [205]). Another possible explanation for this shift is that the graphite electrode provides a surface for biofilm growth, which could enrich for biofilm-producing microbes and alter nutrient and substrate dynamics. This alteration in nutrient and substrate dynamics could make certain microbes better suited for growth, and promote their abundance over other less well-suited community members. A nonconductive material could be used to tease apart the mechanisms of community change on the nonpoised electrodes (*i.e.*, biofilm attachment effects *vs.* conductivity of the electrode).

4.2.3. Changes in Methane Emissions Correspond to Changes in Microbial Communities

Chambers with either nonpoised or poised electrodes exhibited stimulation in methane emissions and a shift in microbial community structure compared with control chambers. Although the soils in chambers containing nonpoised and poised electrodes were disturbed when electrodes were installed and the soils in the control chambers were not, it is unlikely that this had a significant effect on microbial community structure or greenhouse gas emissions since the chambers and electrodes were installed a week prior to the beginning of measurements, which allowed ample time for the saturated soils to recover from any perturbation [206]. While a hypothesis based on a thermodynamic analysis of microbial respiratory processes would have forecasted a decrease in methane emissions with our BES tool that provided an enlarged chance for iron(III)- and humic acid-reduction, we observed the opposite here (an increase in methane emission). In another study where we placed these electrodes in anaerobic sediments of riparian zones (*i.e.*, an area of land adjacent to a river or stream) in the Northeast of the U.S., the hypothesis based on thermodynamics did hold and we observed a lower methane emission rate

[207]. The deviation from the hypothesis here may be specifically related to the peat soils in which we placed our electrodes.

The Arctic climate is known to inhibit decomposition of plant matter [208], which suggests the existence of a buildup of nondegraded organic material (*i.e.*, lignocellulose) in these ecosystems. Since the decomposition of plant matter is achieved via a complex mixed microbial community [209], a bottleneck at the top of this microbial food web would result in retarded downstream processes (e.g., fermentation, iron reduction, and methanogenesis). If either nonpoised or poised electrodes stimulated the breakdown of nondegraded organic material through syntrophic product removal (*i.e.*, increasing the consumption of inhibitory products), the bottleneck at the top of the microbial food web would have widened, resulting in a larger carbon flux through the ecosystem. In other words, the placement of electrodes may have stimulated the breakdown of complex organic matter into acetate, CO_2, and hydrogen (H_2) to fuel both iron reduction and methanogenesis. This possibility is supported by the marked increase (50%–76%) in bacteroidetes abundance in samples from electrodes (**Fig. 4.3**), because bacteroidetes are known for their ability to degrade complex organic matter [210]. This theory would provide an explanation for the increases in methane emissions that we observed in chambers with either nonpoised or poised electrodes.

4.2.4. Poised Electrodes Further Stimulate Methane Emissions with Minimal Changes in Microbiome Structure

Applying a potential to electrodes further stimulated overall methane emissions (mg CH_4-C × m^{-2} × h^{-1}) beyond those observed in chambers with nonpoised electrodes (**Fig. 4.1.a**), although the difference between overall average emissions from chambers with nonpoised and poised

electrodes was not significantly different at the shallow (24% increase in emissions, $p = 0.07$) or deeper depths (13% increase in emissions, $p = 0.26$) (**Fig. 4.1a**). To again account for temporal variations in methane emissions, we calculated daily methane emission ratios of chambers with poised electrodes *vs.* nonpoised electrodes. These ratios indicated that poised electrodes did stimulate methane emissions at both depths compared to nonpoised electrodes ($p < 0.01$, **Fig. 4.2b**), and suggests that poising electrodes further stimulated the breakdown of nondegraded organic material. Differences between electrodes located at shallow and deep depths are most likely due to a variety of factors, including: a higher mean soil temperature at shallow depths (5.8 °C *vs.* 7.0 °C for shallow and deep depths, respectively [$p < 0.0001$]); differences between carbon stocks, hydrology, redox conditions, and nutrient availability between depths [211]; and the potential for gases produced at deeper soil depths to be consumed by methane oxidizers or trapped in the subsurface due to diffusion limitations [212].

Alpha diversity of microbial community structure (**Fig. 4.3**) and principal coordinates analysis of UniFrac distances (beta diversity, **Fig. 4.4**) did not reveal any differences between microbial communities located at nonpoised and nonpoised electrodes. Another way of visualizing differences between communities is to look at the UniFrac distance between different samples (where a UniFrac distance of 0 indicates identical communities and a distance of 1 indicates completely distinct communities) (**Fig. 4.6**). In this case, we looked at two scenarios using both unweighted and weighted UniFrac distances: (1) the average distances between samples of different types (*i.e.*, control soils, nonpoised electrodes, poised electrodes) (**Fig. 4.6a,c**); and (2) the average distances between samples from poised electrodes within the same polygon and across replicate polygons (**Fig. 4.6b,d**). Samples from control soils were more similar than samples from nonpoised and poised electrodes (**Fig. 4.6a,c**) using both the unweighted UniFrac distances

(ANOVA $p = 0.06$) and weighted UniFrac distances (ANOVA $p = 0.003$), which suggests that the electrodes changed microbial communities but not in a uniform way across different samples. This was confirmed by looking at the average UniFrac distances between poised electrode samples within and across replicate polygons (**Fig. 4.6b,d**). The average UniFrac distance between samples across replicate polygons was greater than the distance between samples within polygons for both the unweighted UniFrac distances ($p = 0.004$) and weighted UniFrac distances ($p = 0.07$), indicating that the response of microbiomes to bioelectrochemical manipulation was similar within a given polygon but different across polygons. Despite their proximity to one another, the replicate polygons did have slight differences in environmental conditions, suggesting that communities will respond differently to bioelectrochemical manipulation depending on specific environmental factors (e.g., temperature, pH) (**Fig. 4.7**).

Despite minimal changes in microbial community structure, poising electrodes increased methane emissions. It is possible that while there were minimal changes in microbial community structure, poising an electrode resulted in changes in the metabolic processes of certain microbes, eventually leading to stimulation in methane emissions. This would require proteomic and transcriptomic investigation to determine the specific metabolic functions of microbes. Regardless, it is clear that applying a potential to electrodes in Arctic soils stimulates methane emissions, however the mechanisms are unclear and were not elucidated by analysis of microbiome structure.

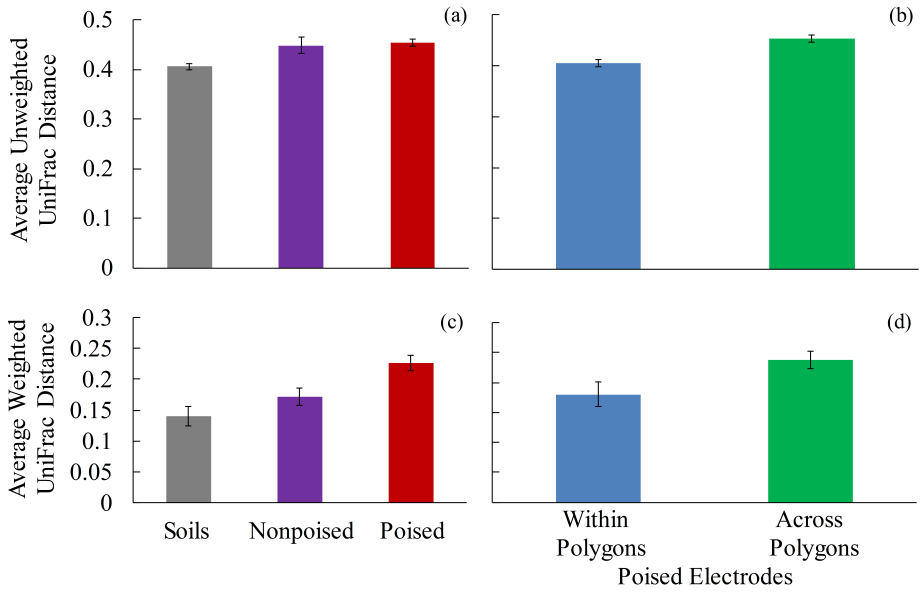

Figure 4.6. Average unweighted (**a**,**b**) and weighted (**c**,**d**) UniFrac distances between samples of different types. Microbial communities in soil samples from different polygons were more similar than communities from nonpoised and poised electrodes using both unweighted (one-way ANOVA, $p = 0.06$) and weighted UniFrac (one-way ANOVA, $p = 0.008$) distances (**a,c**). Additionally, microbial communities from poised electrodes within the same polygon were more similar than communities from poised electrodes in the other polygons using both unweighted (two-sample *t*-test, $p = 0.004$) and weighted (two-sample *t*-test, $p = 0.07$) UniFrac distances (**b**,**d**).

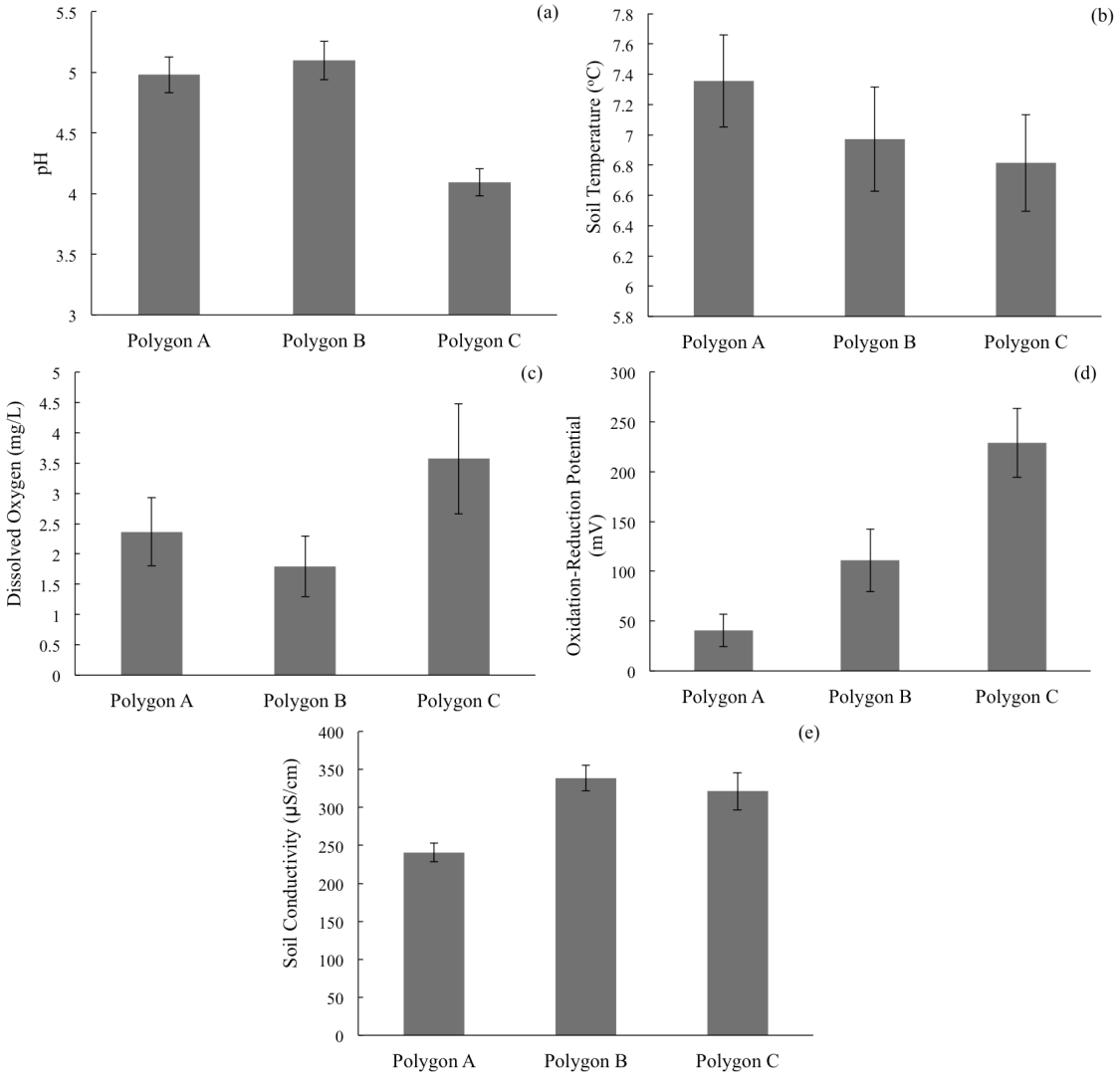

Figure 4.7. Environmental data from the three polygons studied during this experiment: (**a**) pH; (**b**) soil temperature; (**c**) dissolved oxygen; (**d**) oxidation-reduction potential; and (**e**) soil conductivity. Data was collected from both 7 and 10 cm depths over the five-week long experiment. Despite the close proximity (all within a ~10 m radius), there were differences in pH (**a**), dissolved oxygen (**c**), oxidation-reduction potential (**d**), and soil conductivity (**e**) across polygons. Polygon C had a lower pH and higher dissolved oxygen than polygons A and B, while polygon A had a lower soil conductivity than polygons A and C. Oxidation-reduction potential showed the largest difference across polygons; polygon A had the lowest (most reducing) potential while polygon C had the highest (most oxidizing) potential.

4.3 Experimental Section

Field Location and Experimental Setup. Field experiments were located in the Biocomplexity Experiment site, which is a medium-aged (50–300 years old) drained-thaw lake basin located within the Barrow Environmental Observatory in Barrow, AK [171, 213, 214]. Nine soil chambers were deployed in the depressed center of each of three adjacent ice-wedge polygons (total of 27 soil chambers), which are saturated for most or all of the summer [194]. Within each polygon, we installed three control chambers (with only soil and no electrode), two chambers with nonpoised electrodes (one chamber with an electrode at 6 cm and one chamber with an electrode at 14 cm below soil surface), and four chambers with poised electrodes (two chambers with an electrode at 6 cm and two chambers with an electrode at 14 cm below soil surface). Both soil chambers and electrodes were inserted after first making small incisions with a serrated knife to minimize disruption to the soil. In the control chambers, an electrode incision was not made, because a void without subsequently placing in an electrode could have provided an artificial avenue for prolonged oxygen diffusion into anaerobic soils.

Bioelectrochemical Systems. For the working and counter electrodes, 8 cm × 2.5 cm × 0.6 cm blocks were machined from medium-extruded graphite plates (GT01135, Graphite Store, Buffalo Grove, IL). Holes (1.5875 mm) were drilled in the top of the blocks and the exposed end of a 3 m length of 18-gauge stranded copper wire was inserted into the hole. The electrical connection was reinforced with a conductive carbon adhesive (#12664, Electron Microscopy Sciences, Hatfield, PA, USA), and the connection was sealed using a urethane adhesive (#4024, Hardman, Sound Bend, IN, USA). The working electrode was poised at 0.1 V_{SHE} using a microcontroller-

based potentiostat [195] and an Ag/AgCl reference electrode (RE), and electrical current was recorded (**Fig. A2.S1**).

Soil Chamber Construction. Soil chambers were constructed from 20 cm lengths of 10.15 cm diameter polyvinyl-chloride (PVC) pipe. When buried in the soil, 14 cm of each chamber was below the soil surface, with 6 cm above the surface. An 8 cm × 8 cm portion was removed from the subsurface section of the soil chamber, and replaced with an anion exchange membrane (AMI-7001S, Membranes International, Glen Rock, NJ, USA). The WE and RE were placed inside the soil chamber, while the counter electrode was placed outside the chamber to ensure that cathodic activity did not influence gas flux measurements. A 10.15 cm PVC slip cap was used as the top of the soil chamber. To ensure an airtight seal, a rubber gasket was placed around the outside of the soil chamber and the cap was then placed on the chamber over the gasket. Two 0.635 cm barbed brass pipe fittings were attached to the top of the cap and sealed with urethane adhesive, and 45 m of 0.318 cm tubing (#57328, U.S. Plastics, Lima, OH, USA) was attached to each fitting. One tube was connected to the input of a gas analyzer (Fast Greenhouse Gas Analyzer, Los Gatos Research, Mountain View, CA, USA) while the other tube was connected to the output. Connections to the gas analyzer were made using Swagelok tube fittings (SS-405-2 & SS-400-6, Swagelok Western New York, West Henrietta, NY, USA). A 0.635 cm cylindrical septum (AT6526, Grace Davison Discovery Science, Deerfield, IL, USA) was affixed to the PVC cap with urethane adhesive, and during measurements the chamber was vented with a 21G needle (#305129, VWR, USA) to prevent pressure differentials within the soil chamber.

Measurements. Carbon dioxide and methane concentrations were measured every Monday, Wednesday, and Friday using the gas analyzer. To do this, the PVC cap was placed on the soil chamber and measurement of CH_4 and CO_2 concentrations (ppm) began. There was a delay of

approximately 45 s between the time that the PVC cap was placed on the chamber and the time that CH_4 and CO_2 concentrations began to increase. Data was recorded every s for 5 min from the point when CH_4 and CO_2 concentrations began to increase. After analysis was complete, the PVC cap was removed from the chamber, placed on its side, and ambient air was pumped through the tubing and gas analyzer for 3 min before beginning the next measurement. CH_4 and CO_2 flux rates were calculated as the slope of the linear regression line over the 5 min measurement period (300 data points). R^2 values for all 405 measurements were greater than 0.7, and were greater than 0.9 for 399 of the 405 measurements.

Soil temperature (°C), pH, redox potential (mV), dissolved oxygen (mg/L), and soil conductivity (µS/cm) were measured with a portable multiparameter meter and probes (Orion* 5-Star Meter, pH/ATC Triode 9107WMMD, DO probe 083010MD, Conductivity cell 013010MD, Thermo Scientific, Pittsburgh, PA, USA). Measurements were taken at 7 cm and 10 cm below the soil surface from two locations in each polygon. Soil water was collected weekly from within each soil chamber for analysis of Fe^{2+} and Fe^{3+} using porous soil moisture samplers (#220300, Rhizosphere, Wageningen, The Netherlands) and vacutainers (VT6430, BD, Franklin Lakes, NJ, USA).

Microbial Community Analysis. Soil samples were collected from each of the three polygons for sequencing on 8, 15, 28, July and 11, August 2012. Background samples were collected from both the depressed, saturated centers of the polygons and the elevated, dry rims. Soils were sampled using a sterile serrated knife from two depths (0–7 cm and 7–14 cm below the surface) and stored in Bitran bags (#19-240-150, Fischer Scientific, Waltham, MA, USA). Upon the completion of the experiment, biofilm samples were collected from all working- and counter-electrodes by scraping the biofilms into a 15 mL centrifuge tube (#93000-026, VWR, Radnor,

PA, USA) with a sterile razor blade. Both soil and biofilm samples (~0.25–3g) were placed on wet ice in the field and stored at −20 °C within 2 h of collection. Genomic DNA was extracted using a PowerSoil® DNA Isolation Kit (MoBio, Carlsbad, CA, USA), and samples were PCR amplified and sequenced according to the protocols from the Earth Microbiome Project [215]. In short, triplicate 25 µL PCR reactions were conducted using: 13 µL grade water, 10 µL mastermix (5 Prime Hot MasterMix, Catalog # 2200110, 5 Prime, Fischer Scientific, USA), 0.5 µL 515f forward primer [216], 0.5 µL 806r barcoded reverse primer [216], and 1 µL template DNA. Reactions were run under the following conditions: 94 °C for 3 min; then 94 °C for 45 s, 50 °C for 60 s, and 72 °C for 90 s (repeated 25 times); 72 °C for 10 min, and then hold at 4 °C. Triplicate PCR products were pooled, confirmed with gel electrophoresis, cleaned using the MoBio UltraClear PCR Clean-Up Kit (#12500, MoBio, Carlsbad, CA, USA) according to the manufacturer's instructions, pooled at equimolar ratios, and sequenced using an Illumina HiSeq (Illumina, San Diego, CA, USA) (Online sequence data access: http://www.microbio.me/emp/; study id: 1692; study name: Friedman_arctic_peat_soil). The resulting sequences were assigned to barcodes, grouped into OTUs, and analyzed using the Quantitative Insights Into Microbial Ecology (QIIME v1.6) platform [217]. Machine learning analysis was performed using the pamR package in R [204, 218].

4.4 Conclusions

This work demonstrates a research tool combining electrochemical, ecological, and microbial techniques to study complex subsurface ecosystems. Both nonpoised and poised electrodes stimulated methane emissions (15%–43%) from Arctic peat soils and altered microbial community structure. Analysis of alpha and beta diversity of soil communities and the application of machine learning techniques demonstrated that there was a large difference in

microbial communities between samples (enrichment for already dominant proteobacteria and bacteroidetes phyla) from soils and those from either nonpoised or poised electrodes, although there were minimal differences in microbiome structure between samples from nonpoised and poised electrodes. Despite this, poising the electrode did stimulate methane emissions beyond those from nonpoised electrodes. We suspect that the stimulation of methane emissions is due to a bottleneck in the microbial food web at the initial breakdown of nondegraded organic material that is stimulated by both nonpoised and poised electrodes, which in turn stimulates downstream microbial processes (including methanogenesis). The mechanism of this stimulation is unknown, but could be due to physical effects from the electrode, electron transport across the electrode surface, or the stimulation of syntrophic product removal. Regardless, these results suggest that there is a potential for increased carbon release from Arctic soils under changing conditions, and we must understand the biogeochemical relationships that govern microbial processes to be able to predict the responses of these systems to changing conditions.

4.5 Acknowledgements

The authors would like to acknowledge the Earth Microbiome Project (EMP) and Rob Knight (University of Colorado at Boulder) for 16S rRNA gene amplification and sequencing, Cristina Solis (LA Academy) for assistance in conducting field work, and Jeffrey Werner (SUNY Cortland) and James Gossett (Cornell University) for helpful discussions. This work was funded by the U.S. NSF Grant #0808604.

CHAPTER 5.

CHANGES IN MICROBIAL COMMUNITY STRUCTURE AND METHANE EMISSIONS FROM RIPARIAN ZONE SEDIMENTS IN RESPONSE TO BIOELECTROCHEMICAL MANIPULATION

In preparation for *JGR-Biogeosciences*.

Note: Supplementary information can be found in Appendix 3, and is denoted in the text as A3.SX, where X is the appendix section.

Abstract

Dissimilatory metal-reducing bacteria (DMRB) are widespread in terrestrial ecosystems, especially anaerobic soils and sediments. Energetically, dissimilatory metal-reduction is more favorable than methanogenesis and sulfate reduction, but less favorable than denitrification and aerobic respiration; as such, this process can be prominent in anaerobic sediments. Subsurface microbial processes impact: (1) carbon and nutrient cycling; (2) plant productivity; (3) pollutant remediation; and (4) greenhouse gas emissions from soils. It is therefore critical to understand the complex relationships that govern microbial competition and coexistence in anaerobic soils and sediments. Here, we attempt to elucidate these relationships by deploying potentiostatically-poised graphite electrodes mimicking ferrous iron, which DMRB can use to respire, in the sediment of a stream riparian area adjacent to an agricultural field. At two sites within the riparian zone, we measured nitrous oxide (N_2O) and methane (CH_4) fluxes from soil chambers containing the poised and unpoised electrodes over the course of six weeks, and harvested biofilms from the electrodes on a weekly basis to quantify changes in microbial communities

over time and treatment. At one site, which was further upstream, had less vegetation cover, and had higher soil temperatures than the downstream site, the poised electrodes inhibited methane emissions by nearly 50%. Methane emissions were not significantly impacted at the second (downstream) site, which was ~50 m away. Meanwhile, nitrous oxide fluxes were generally low at both sites and were not impacted by poised electrodes. There was an increase in the relative abundance of proteobacteria populations and a decrease in bacteroidetes populations over time on poised electrodes that corresponded with lower methane fluxes from the upstream site.

5.1 Introduction

Riparian zones, which are the areas of land adjacent to streams, are often hotspots for biogeochemical transformations [219]. These ecosystems provide valuable services by acting as buffers and preventing nutrients and pollutants from entering aquatic environments. Within riparian zones, subsurface microbial communities play a major factor in biogeochemical cycling – impacting carbon and nitrogen availability, and by extension, plant productivity [220, 221]. Extensive work has examined denitrification processes in riparian zones, as these areas typically provide the last opportunity to mitigate excess nitrate in groundwater before it reaches the stream. Studies have found that the main regulators of denitrification (e.g., nitrate, anaerobic conditions, availability of other electron acceptors and carbon sources) are spatially and temporally heterogeneous, which makes modeling these landscape-level processes particularly difficult [219, 222-224]. Therefore, it is essential to have a full understanding of the underlying biogeochemistry to inform landscape level models, determine best management practices, and guide regulatory policies.

Bioelectrochemical systems (BESs) are bioengineered systems that capitalize on the ability of dissimilatory metal-reducing bacteria to respire with solid-state electrodes *via* extracellular

electron transfer [24, 41, 97, 120]. BESs have been used to: produce power in microbial fuel cells [29, 43, 67, 225]; produce chemical products in microbial electrolysis cells [85, 102, 104, 117, 141]; remediate pollutants [105, 110, 226]; sense environmental and chemical parameters [170, 227], and; produce logic gates in biocomputing devices [147, 228]. In the environment, potentiostatically-poised electrodes (i.e., electrodes held at a constant electrical potential using an electrical device called a potentiostat), can mimic iron(III)- and humic acid-compounds and act as the terminal electron acceptor for dissimilatory metal-reducing bacteria [195, 229-231]. In this application BESs can be a powerful tool for precise manipulation of environmental conditions for *in-situ* experimentation.

Dissimilatory metal reduction has been shown to dominate a wide variety of anaerobic soils and sediments from the tropics to poles [155, 192-194, 232]. Thermodynamically, iron- and manganese-reduction yield less energy than denitrification but more than sulfate reduction and methanogenesis [150, 151]. However, these calculations occur under ideal conditions and do not take into account the ecological and physiological factors encountered *in-situ*. For example, recent work in Arctic peat soils has shown that bioelectrochemical manipulation designed to enrich for dissimilatory metal reduction actually increased methane emissions from soils. In this case, there was likely a bottleneck in the degradation of plant organic matter, which was widened by bioelectrochemical manipulation and stimulated the production of fermentation-like products [229].

Modeling efforts are generally concerned with landscape-level function, such as pollutant removal or greenhouse gas emissions, but these parameters can vary by several orders of magnitude within an ecosystem and it can be difficult to accurately distill these processes into a function of easily obtained environmental parameters [164, 233, 234]. Therefore, it is critical to

elucidate the links between microbiome structure and ecosystem processes [235, 236]; here, we combined *in-situ* bioelectrochemical manipulation with quantitative measurements of community structure (16S rRNA gene sequences), environmental parameters (i.e., soil temperature, pH), and greater ecosystem function (CH_4 and N_2O fluxes) to strengthen our understanding of this essential link.

At two distinct sites within the riparian zone of Fall Creek in Freeville, NY, we measured CH_4 and N_2O emissions from soil chambers contained both unpoised (control) and potentiostatically-poised (mimicking iron(III) compounds) electrodes for a period of six weeks. We also gathered environmental data over the course of the experiment, including: soil temperature, pH, dissolved oxygen concentration, conductivity, iron concentrations and speciation, and anion concentrations. Once per week, bacterial biofilms were harvested from both poised and unpoised electrodes for 16S rRNA gene sequencing to determine the microbial community structure. It will be crucial to understand the complex links between microbial-, landscape-, and global-scales to predict the effects of climate change, mitigate anthropogenic pollutants, and guide best management practices. Here, we demonstrate the capability of small alterations to redox conditions to impact carbon release to the atmosphere, and provide a foundation for future examinations of biogeochemical cycling using *in-situ* bioelectrochemical manipulations.

5.2 Materials & Methods

Field Location and Experimental Setup. This experiment was conducted within Fall Creek, a 3rd order steam in Central New York that passes through the Homer C. Thompson Vegetable Research Farm, a Cornell University facility in Freeville, NY (42^{o}31'N, 76^{o}20'W) [237]. Six soil chambers were installed at each of two sites, which are separated by ~50 m. At each site, three of

the chambers contained unpoised graphite electrodes (control), while the other three contained potentiostatically-poised graphite electrodes (experimental). Both soil chambers and electrodes were installed by making small incisions with a serrated knife, and then inserting the chambers/electrodes into the soil. The experiment ran from April 25th through June 6th, 2013.

Soil Chamber Construction. Soil chambers were constructed from one-gallon plastic buckets (#2860, U.S. Plastic Corp., Lima, OH). To create the base of the chamber, the bottom 2-cm of the bucket was removed leaving a 17-cm-long cylinder; when placed in the soil, 11-cm of the soil chamber was below the surface and 6-cm extended above the soil surface. From each chamber, a 8.5-cm x 4.5-cm section of the subsurface area was removed and replaced with an anion exchange membrane (AMI-7001S, Membranes International, Glen Rock, NJ). To create a cap for the soil chamber, the top 4-cm were removed from another one gallon plastic bucket. The bottom edge of the plastic bucket was reinforced with foam insulation tape and duct tape to ensure an airtight seal between the soil chamber and the chamber cap. Two 0.635-cm cylindrical septa (AT6526, Fisher Scientific, USA) were affixed to the top of the chamber cap and sealed with urethane adhesive. During measurements, the chamber was vented with a 21G needle (#305129, VWR, USA) through one of the septa to prevent induced pressure differentials in the soil chamber [238]. Gas samples were taken through the other septum.

Bioelectrochemical Systems. The working and counter electrodes were machined from medium-extruded graphite plates (GT001135, Graphite Store, Buffalo Grove, IL). The counter electrodes (CE) consisted of a 6-cm x 6-cm block of 0.635-cm thick block (surface area = 87.24 cm^2), while each working electrode (WE) consisted of six 6-cm x 6-cm x 0.635-cm blocks connected in parallel (total surface area = 523.44 cm^2). Having multiple electrodes in parallel for the WEs allowed for the harvesting of biofilms during different stages of the experiment. The WE and RE

were placed inside the chamber, while the CE was placed outside the chamber on the opposite side of the membrane to maintain an electrical connection while preventing cathodic hydrogen or methane production inside the soil chamber. Electrodes were connected to microcontroller-based potentiostats [195] by inserting the exposed end of a 3-m length of 18-gauge stranded copper wire into a 1.5875-mm hole drilled in the top of each graphite block. A conductive carbon adhesive (#12664, Electron Microscopy Sciences, Hatfield, PA) was used to ensure a good electrical connection (resistance < 0.5 Ω), and the junction was sealed with a urethane adhesive (#4024, Hardman, South Bend, IN). The working electrodes in experimental chambers were poised at 0.1 V_{SHE} using a microcontroller-based potentiostat [195] and an Ag/AgCl reference electrode (RE) made in house; electrodes in the control chambers were not poised.

Measurements. Measurements were taken every Monday and Thursday over the course of the six-week experiment. Denitrification was measured using the acetylene inhibition method, where acetylene is added to the soil to inhibit reduction of N_2O to N_2, allowing measurement of N_2O fluxes to quantify denitrifiction [239-241]. We prepared and used beeswax-coated calcium carbide tablets, which react with water to form acetylene gas, as described by Thompson [240]. Six beeswax-coated calcium carbide tablets were inserted between into each soil collar 45 min prior to gas sampling at a depth of 7-15 cm. We measured acetylene concentrations in the gas samples to ensure that ample acetylene (>1% v/v) was being produced to inhibit N_2O reduction [240]. Nitrous oxide and methane fluxes were measured from the chambers by placing the cap on the chamber and collecting 12 mL of the headspace gas at four time points (0, 10, 20, 30 min). Gas chromatography analysis of N_2O, CH_4, and C_2H_2 was performed on an Agilent 6890N gas chromatograph equipped with a HP 7694 Headspace Autosampler (Hewlett-Packard Company, Palo Alto, CA). N_2O separation was performed using a Supel-Q™ PLOT capillary column (30m

x 0.32mm; Supelco Inc., Bellafonte, PA) with ultra-pure helium carrier gas (2.6 mL min^{-1}) and 95:5 Ar:CH_4 make-up gas (8.2 mL min^{-1}) and a μECD (electron capture detector) set to 250°C. CH_4 and C_2H_2 separation was performed using a Carboxen 1006 PLOT capillary column (30m x 0.32mm; Supelco, Inc.) and an FID (flame ionization detector) set to 200°C with H_2 gas (30 mL min^{-1}), air (400 mL min^{-1}), and N_2 makeup gas (25 mL min^{-1}) . The oven temperature was initially set to -22°C for 4.7 min, then increased to 30°C for 0.85 min and finally increased to 80°C for 2.5 min to allow for elution of all three gases of interest. Calibration curves were made using serial dilutions of 1ppm N_2O, 20 ppm CH_4, 2.5% C_2H_2 (Airgas Inc.). Fluxes were calculated as the slopes of the linear regression curves for each measurement period.

Soil temperature, pH, dissolved oxygen, and conductivity were measured at 7-cm depth directly adjacent to each soil chamber using a portable multiparameter meter (Orion Star A329, Thermo Scientific, Pittsburgh PA) and probes (ROSS Ultra Triode pH/ATC electrode, DuraProbe conductivity probe, Orion RDO probe, Thermo Scientific, Pittsburgh, PA). Soil water was collected from within each soil chamber using porous soil moisture samplers (#220300, Rhizosphere, Wageningen, The Netherlands), vacutainers (VT6430, BD, Franklin Lakes, NJ), and 21G needles (#305129, VWR, USA). These samples were analyzed for nitrate, nitrite, chloride, and sulfate using a Dionex ICS-2000 Ion Chromatograph with IonPac AS-18 analytical column and 25-μL sample loop. Immediately following the collection of soil water 0.5 mL of each sample was transferred to another vacutainer containing 0.5 mL of 0.5 N HCl; these samples were analyzed for Fe^{2+} and total Fe using the ferrozine assay [242].

Microbial Community Analysis. Biofilms from the working electrodes of both control and experimental soil chambers were collected weekly (every Thursday) throughout the six-week duration of the experiment. Each of the six parallel working electrodes in every soil chamber was

harvested once during the course of the experiment to obtain a time series of the microbial community. Biofilms were harvested by removing the ticket from the soil and scraping the biofilm into a 15-mL sterile centrifuge tube (#93000-026, VWR, USA) using a sterile blade. Samples were placed on wet ice immediately in the field, and then stored at -20^{o}C until the completion of the experiment. Following biofilm harvesting, the bare electrodes were returned to the soil to keep the WE surface area constant throughout the experiment. Genomic DNA was extracted using a PowerSoil® DNA Isolation Kit (MoBio, Carlsbad, CA). Extraction product was then amplified in duplicate 50-µL polymerase chain reactions (PCRs) according to Gilbert, Meyer [215] using 25 cycles. In short, duplicate 50-µL PCR reactions were conducted using: 28 µL molecular grade water, 20 µL mastermix (5Prime Hot MasterMix, Catalog # 2200110, 5Prime, Fischer Scientific, USA), 0.5 µL 515f forward primer [216], 0.5 µL 806r barcoded reverse primer [216], and 1 µL template DNA. Reactions were run under the following conditions: 94^{o}C for 3 minutes; then 94^{o}C for 45 seconds, 50^{o}C for 60 seconds, and 72^{o}C for 90 seconds (repeat 25 times); 72^{o}C for 10 minutes, and then hold at 4^{o}C. Duplicate PCR products were then pooled, confirmed with gel electrophoresis, and cleaned using the Mag-Bind® E-Z Pure Kit (Omega, Norcross, GA). Cleaned product was again confirmed with gel electrophoresis and pooled at equimolar ratios to a final concentration of 8 ng DNA µL^{-1}. The single, pooled amplicon mixture was sequenced at the Cornell University Biotechnology Resource Center using an Illumina MiSeq (2x250 bp, paired end). Sequences were assigned using barcodes using the Quantitative Insights Into Microbial Ecology (QIIME) platform (v 1.6) [217]. Then, the forward and reverse reads were joined using fastqjoin and the data returned to the QIIME platform for OTU picking, alpha diversity, beta diversity, and further analysis. Machine learning was

conducted using the pamR package in R [204], and constrained correspondence analysis was performed using the vegan package in R [218, 243].

5.3 Results & Discussion

Greenhouse Gas Emissions. In the unpoised electrode (control) chambers, methane emissions were much higher from the upstream site (1.96 ± 1.42 mg CH_4*m^{-2}*h^{-1}) than the downstream site (0.79 ± 0.65 mg CH_4*m^{-2}*h^{-1}) (**Table 5.1**). In the poised electrode chambers, methane emissions were similar from both the upstream (0.96 ± 0.86 mg CH_4*m^{-2}*h^{-1}) and downstream (0.93 ± 1.1 mg CH_4*m^{-2}*h^{-1}) sites. At the downstream site, emissions from the poised electrode chambers were similar to those from the unpoised electrode chambers but, at the upstream site, emissions from the poised electrode chambers were much lower than those from unpoised electrode chambers ($p=0.0009$). However, methane emissions for each chamber were highest at the beginning of the experiment and decreased throughout the six weeks. Therefore, to determine the effects of potentiostatic manipulation, average methane emissions (mg CH_4*m^{-2}*h^{-1}) from chambers with poised electrodes were normalized against the methane emissions from chambers with unpoised electrodes at each site for each measurement day. For the downstream site, which had lower soil temperatures, lower pH, more vegetation cover, and less direct sunlight, methane emissions were not significantly different in the chambers with poised electrodes ($p = 0.08$); however, at the upstream site, chambers with poised electrode experienced a suppression of methane emissions by 44% ($p=0.003$) (**Fig. 5.1a**). There were no differences in the average nitrous oxide emissions (μg N_2O-N*m^{-2}*h^{-1}), which were used as a measure of denitrification rates, between sites or treatments (**Table 5.1**). These rates were also normalized in the same manner as the methane emissions and expressed as nitrous oxide emission ratios, however, there was no effect on denitrification rates at either site ($p>0.41$, **Fig. 5.1b**).

Parameter	Downstream Unpoised	Downstream Poised	Upstream Unpoised	Upstream Poised
Nitrous Oxide Emissions ($\mu g\ N_2O\text{-}N*m^{-2}*h^{-1}$)	2179 ± 2873	2394 ± 3287	2138 ± 2136	1793 ± 1794
Methane Emissions ($mg\ CH_4*m^{-2}*h^{-1}$)	0.79 ± 0.65	0.93 ± 1.1	1.96 ± 1.42	0.96 ± 0.86
Chloride Concentration (ppm)	218 ± 142	103 ± 63.0	107 ± 41.2	88.5 ± 39.7
Sulfate Concentration (ppm)	45.5 ± 32.8	41.4 ± 35.8	38.2 ± 31.2	15.1 ± 14.6

Table 5.1. Average nitrous oxide emissions, methane emission, chloride concentrations, and sulfate concentrations from chambers with unpoised and poised electrodes at both the upstream and downstream sites. There were no differences in nitrous oxide emissions between sites or treatments. In the chambers with unpoised electrodes (controls), methane emissions from the upstream site were higher than the downstream site. Poising a potential on the electrodes had no effect on methane emissions at the downstream site, however, methane emissions at the upstream site were severely inhibited (50% reduction, $p=0.0009$). At the upstream site, sulfate concentrations were significantly lower at the upstream site in the chambers with poised electrodes ($p=0.0008$), while there were no differences between treatments at the downstream site. At the downstream site, chloride concentrations were lower in the chambers with poised electrodes ($p=0.0066$), while there was not a significant different between treatments at the upstream site.

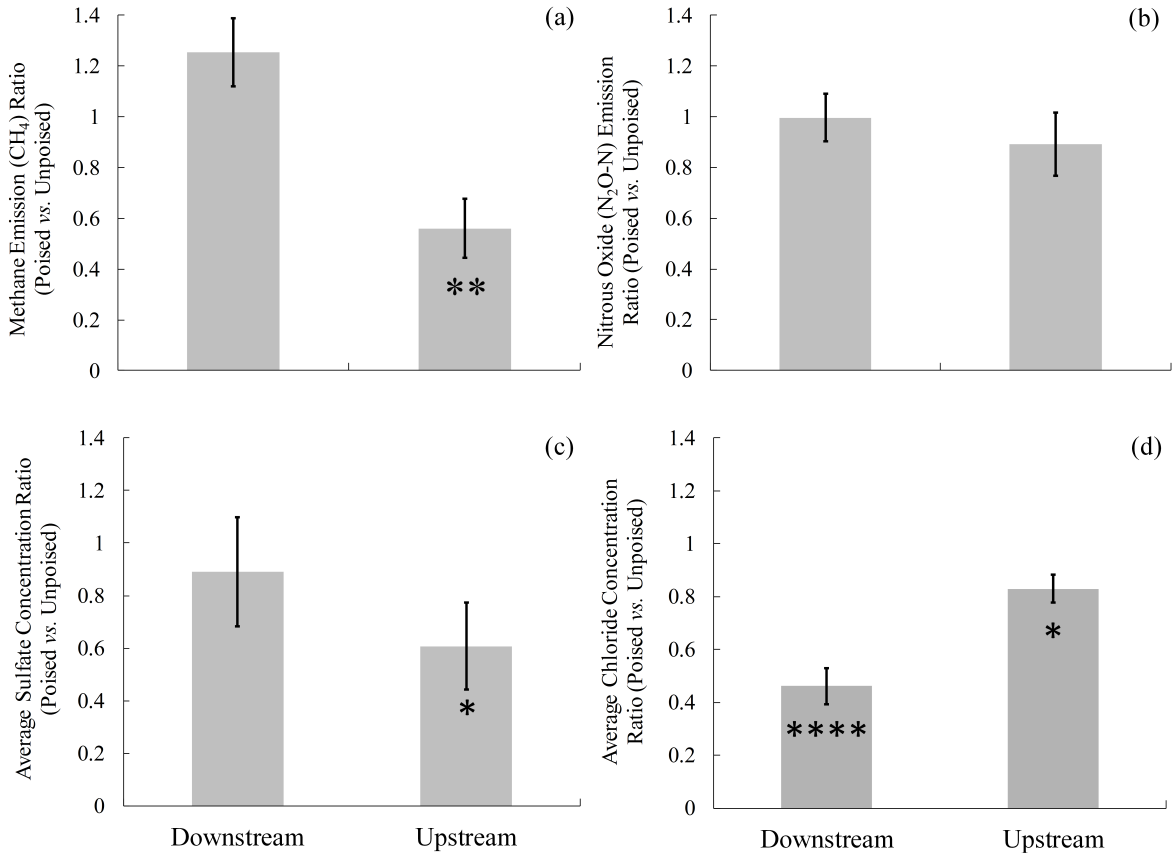

Figure 5.1. Average gas emission ratios (poised:unpoised) for methane (a) and nitrous oxide (b), as well as average sulfate (c) and chloride (d) concentration ratios for downstream and upstream sites during the duration of the experiment. At the upstream site, manipulation of the soil electrochemical environment using poised electrodes resulted in a 44% inhibition of methane emissions. Sulfate concentrations (c) were significantly lower in chamber containing poised electrodes at the upstream site but not the downstream site, while chloride concentrations (d) were significantly lower in chambers containing poised electrodes at both sites. Significant differences at are noted at the p=0.05(*), p=0.01(**) and p=0.0001(****) thresholds. Error bars indicate standard error.

Environmental Parameters. Soil temperature generally increased during the course of the experiment, and ranged between 6.8^{o}C and 19.1^{o}C. On a daily basis throughout the six weeks, the upstream site averaged soil temperatures 1.5^{o}C higher than that of the downstream site ($p<0.001$). pH across both sites was near neutral, with the upstream site averaging a pH of 7.3 ± 0.24 and the downstream site a pH of 7.2 ± 0.23. Dissolved oxygen was low across both sites, and both had average concentrations less than 1 mg L^{-1}. There were no differences in soil

electrical conductivity between sites or control and treatment collars; the average soil conductivity across both sites was 403 ± 165 μS/cm.

There was no difference between sites or treatments in total iron concentrations from soil pore water, which averaged 10.97 ± 9.0 μM. Nearly all of this (95%) iron was in the reduced form (Fe^{2+}), and there were no differences between sites or treatments in iron speciation. Both nitrate (NO_3^-) and nitrite (NO_2^-) were low (<1ppm) across sites and treatments, and were below detection limit (0.1 ppm) for most samples. Chloride concentrations were lower in pore water collected from chambers containing poised electrodes throughout the treatment (**Table 5.1**); these values were normalized in the same manner as gas emission rates. At the downstream site, chloride concentrations were, on average, 55% lower than in chambers with unpoised electrodes ($p<0.0001$); at the upstream sites, chambers with poised electrodes had chloride concentrations that were 17% lower than those with unpoised electrodes ($p=0.01$) (**Fig. 5.1d**). At the upstream site, sulfate concentrations were 39% lower in chambers with poised electrodes than those with unpoised electrodes ($p=0.04$), however there was not a significant difference in sulfate concentrations at the downstream site (**Fig. 5.1c**).

Microbial Community Composition. Compositions of the microbial communities were grouped by site location and treatment (i.e., unpoised or poised), and then grouped into the first two weeks and last two weeks of the experiment to determine the effects of poised electrodes on microbial communities over time (**Fig. 5.2**). For all groups, proteobacteria and bacteroidetes phyla comprised greater than 80% of the communities, and ten phyla accounted for >98% of all sequences in each group. At the upstream site, the unpoised electrodes had no significant effects on proteobacteria or bacteroidetes populations; however, the poised electrodes caused a 35% decrease in the abundance of bacteroidetes ($p=0.04$) (**Fig. 5.2a**). At the downstream site, both

unpoised and poised electrodes enriched for proteobacteria while causing a decrease in relative abundance of bacteroidetes over time (**Fig. 5.2b**). The unpoised electrodes caused a 20 % increase in proteobacteria and a 50% decrease in bacteroidetes ($p<0.01$ for both phyla), while the poised electrodes resulted in a 14% increase in proteobacteria and a 30% decrease in bacteroidetes ($p=0.06$ for both phyla). Verrucomicrobia, acidobacteria, actinobacteria, chloroflexi, firmicutes, cyanobacteria, planctomycetes, and gemmatimonadetes were the other phyla accounting for > 1% of the microbial communities, with relative abundances between 1-6%.

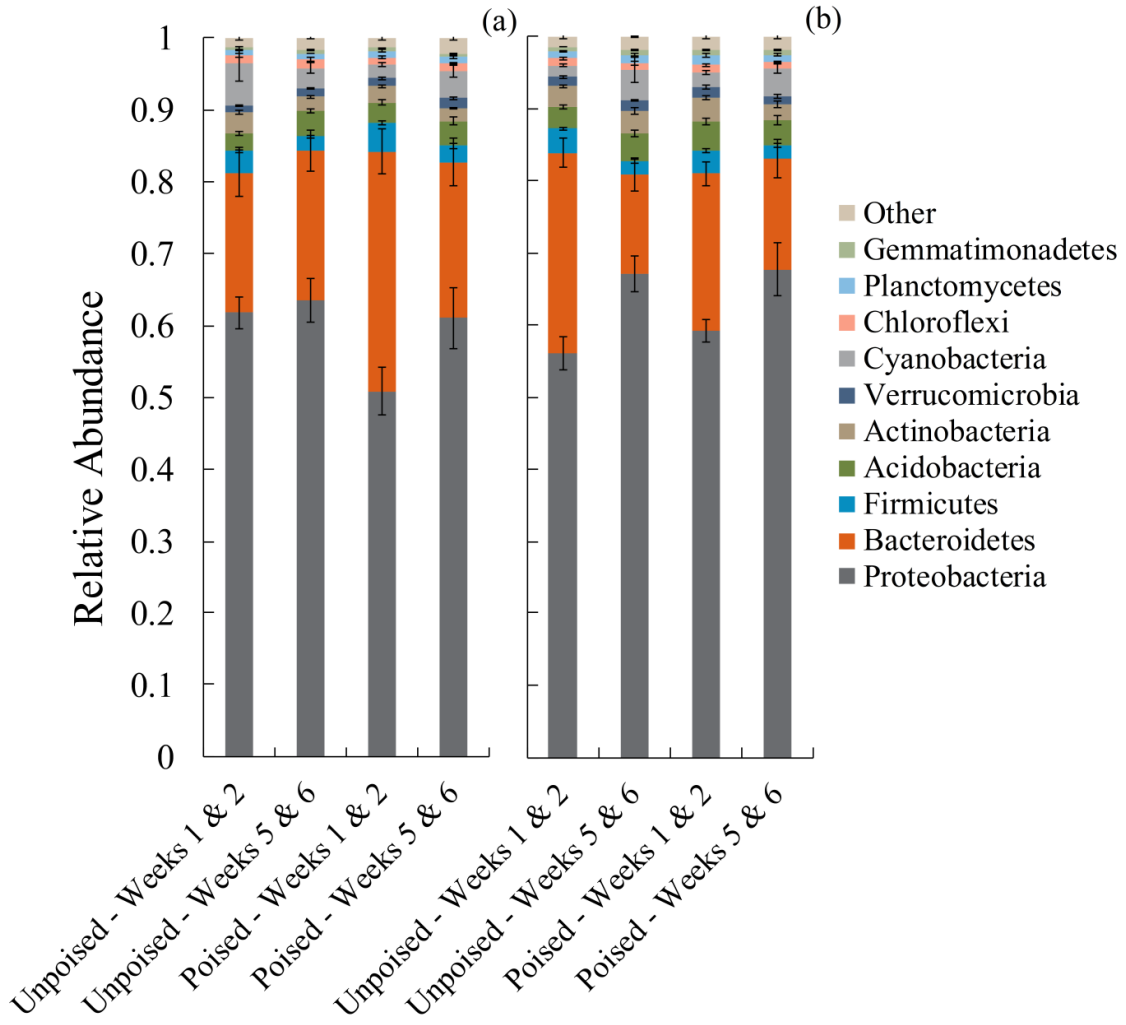

Figure 5.2. Average taxonomic summaries (phylum level) of the microbial communities from the upstream (a) and downstream (b) sites. Communities are grouped as the first two weeks and the last two weeks are shown to view the effects of long-term potentiostatic manipulation. At the upstream site (a) the unpoised electrodes had minimal effects on the microbial community, however, the poised electrodes enriched for proteobacteria at the expense of bacteroidetes. At the downstream site (b), both the unpoised and poised electrodes experienced increases in proteobacteria and decreases in bacteroidetes abundance over the duration of the experiment. Error bars indicate standard error.

Beta diversity, the difference in community structure between samples, was analyzed using UniFrac distances [203]. Principal coordinates analysis of both weighted (which takes into

account relative abundance of sequences within samples) and unweighted UniFrac distances did not reveal clustering of samples by site or treatment (**Fig. 5.3 a,b**). Unweighted UniFrac explained 8.5% of the total variation in samples in the first two principal coordinates (**Fig. 5.3a**), while the weighted method explained 55.8% of total variation (**Fig. 5.3b**). Samples were then separated by site (i.e., upstream *vs.* downstream) for the first two weeks and last two weeks of the experiment to view changes in community composition over time (**Fig. 5.4**). At the downstream site, both unweighted (**Fig 5.4a**) and weighted (**Fig. 5.4b**) UniFrac principal coordinates analysis revealed clustering of samples according to time (first two weeks or last two weeks) regardless of whether the electrodes were poised or unpoised. A similar trend was observed at the upstream site (**Fig. 5.4 c, d**). This suggests that changes in community occur over time regardless of whether the electrode is poised or unpoised, and supports the differences in community structure over time found in alpha diversity analysis (i.e., relative abundance) (**Fig. 5.2**).

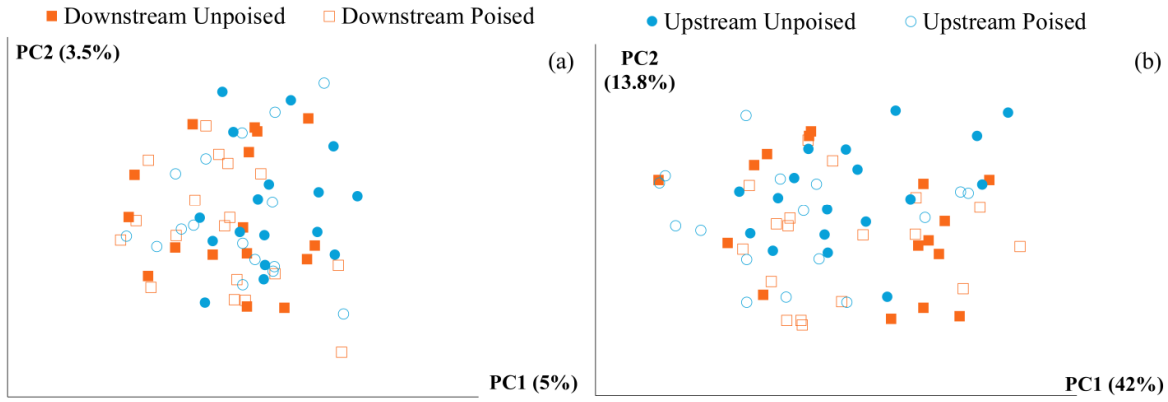

Figure 5.3. Principal coordinates analysis of the beta diversity of microbial communities shown using unweighted (a) and weighted (b) UniFrac distances. The weighted (b) method explains more variation (55.8%) in the first two principal coordinates than the unweighted (a) method (8.5%), however in both cases there are no clear clusters differentiating between sites (upstream or downstream) or treatment (unpoised or poised electrodes).

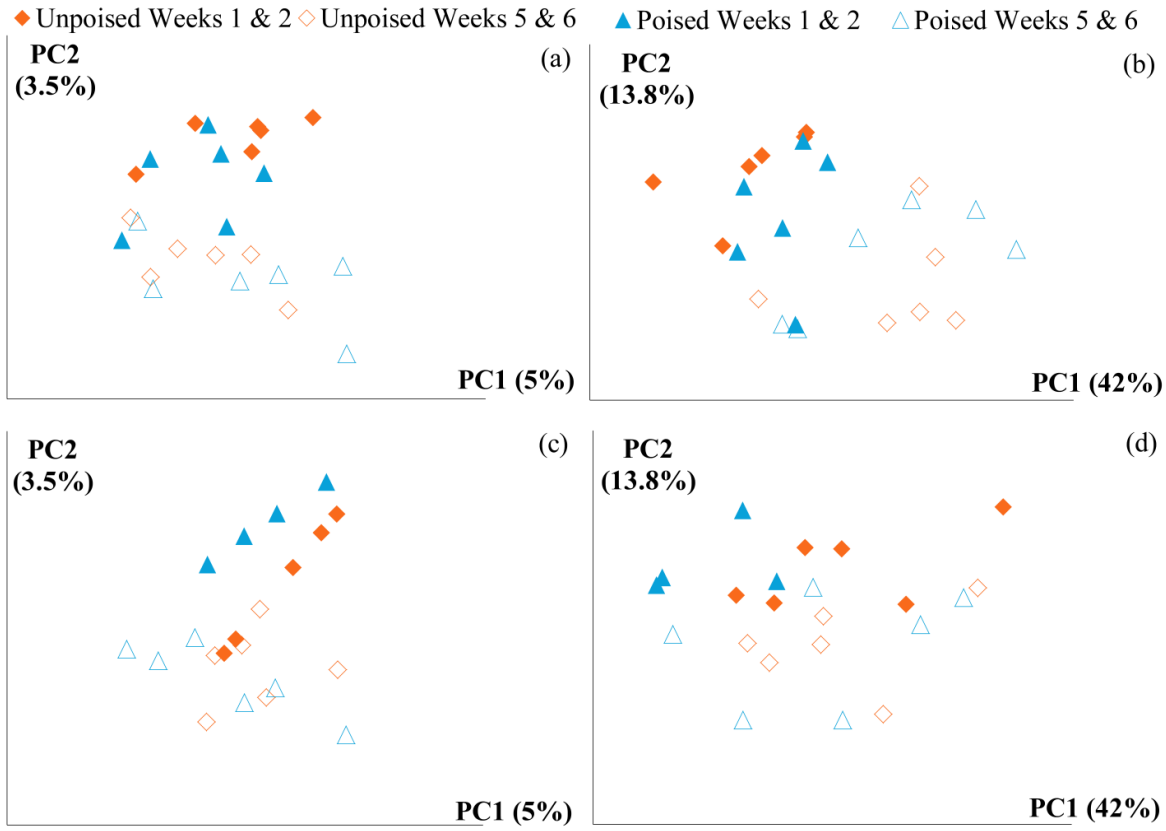

Figure 5.4. Principal coordinate analysis of beta diversity at the downstream and upstream sites using unweighted and weighed UniFrac distances: (a) downstream site, unweighted UniFrac; (b) downstream site, weighted UniFrac; (c) upstream site, unweighted UniFrac; and (d) upstream site, weighted UniFrac. Only samples from the first two weeks (shaded diamonds and triangles) and the last two weeks (open diamonds and triangles) are shown to observe changes in microbiome structure over the duration of the experiment. At the downstream site (a, b), there is a clear shift in community structure from the first two weeks to the last two weeks, and the temporal shift is larger than any differences between unpoised (diamonds) and poised (triangles) electrode communities. This trend is similar in samples from the upstream site (c, d).

To determine which environmental parameters were driving microbial community structure, we performed constrained correspondence analysis using rarified and filtered OTU tables with greenhouse gas fluxes and environmental metadata (**Fig. 5.5**). This analysis reveals correspondence between microbial samples and specific taxonomic groups, and shows which metadata is most influential towards microbial community structure. Across all sites and treatments, pH, nitrous oxide flux, soil conductivity, and chloride ion concentration were most

influential of microbial community structure within a sample (**Fig. 5.5a**). At the upstream site, where unpoised electrode chambers had higher methane emissions, methane emissions were the most influential parameter in describing community composition (**Fig. 5.5b**).

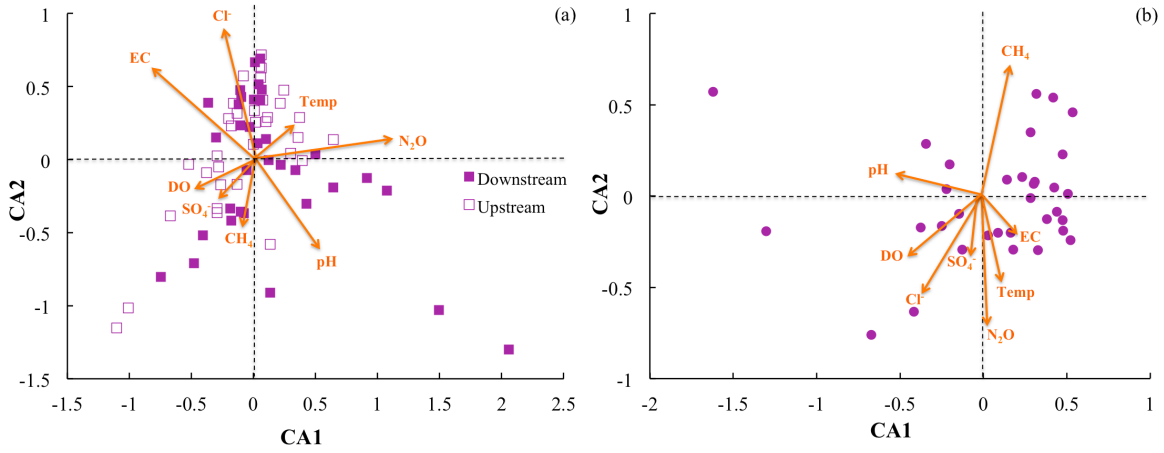

Figure 5.5. Constrained correspondence analysis (CCA) using rarified and filtered OTU tables, gas fluxes, and environmental metadata for (a) all samples and (b) only samples from the upstream site. Points indicate samples while arrows indicate vectors for both gas fluxes and environmental metadata, with longer arrows indicating higher influence for those parameters.

We used a machine learning approach to determine which OTUs were predictive of communities on poised and unpoised electrodes (**Fig. 5.6**). This approach finds OTUs predictive of a specific sample group (i.e., unpoised or poised electrodes) and creates an algorithm to predict the sample group of new samples. However, across both sites (**Fig. 5.6a**) and only within the upstream site (**Fig. 5.6b**), there was a high error rate (0.392 and 0.346 for both sites and only the upstream site, respectively). The error rate, which is the frequency with which the algorithm will incorrectly predict the sample group of a new sample, indicates that microbial communities on unpoised and poised electrodes are very similar and it is difficult to distinguish between sample groups.

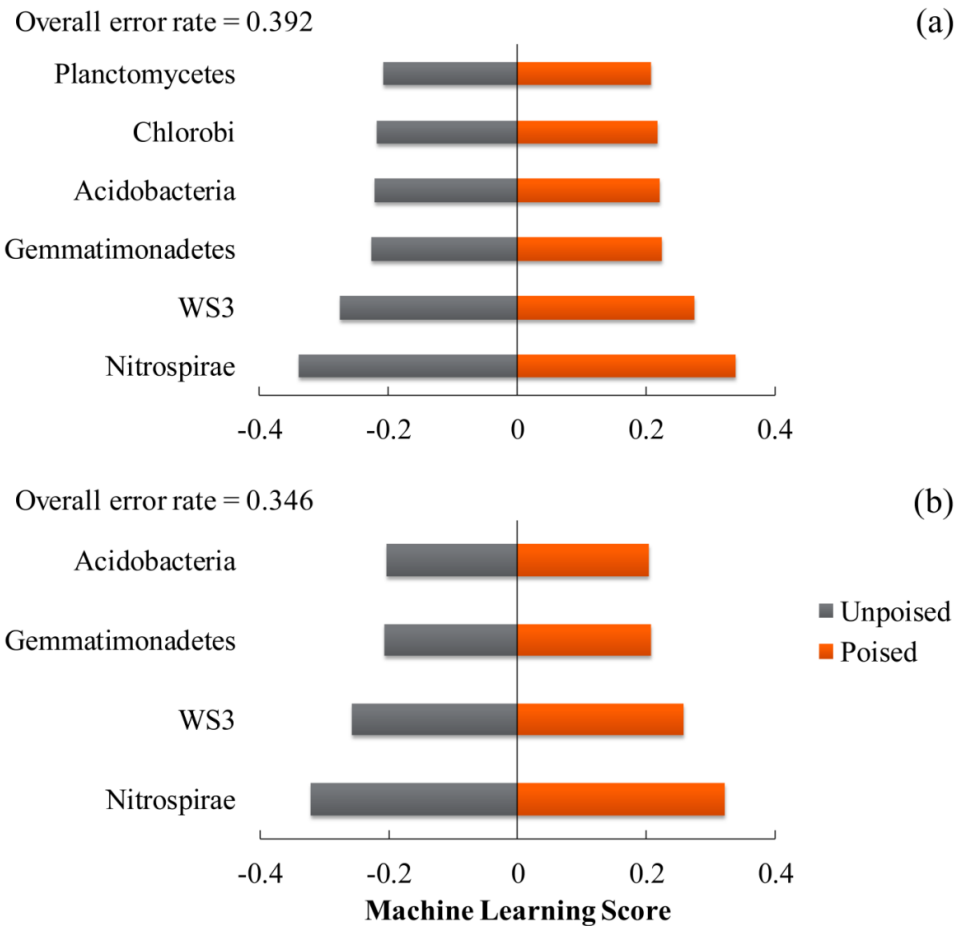

Figure 5.6. Machine learning analysis using phylum level taxonomy shows the phyla that are most indicative of unpoised or poised electrode communities across (a) both sites and (b) just the upstream site. However in both cases the error rate is high (0.392 for both sites and 0.346 for the upstream site), indicating that communities with electrodes are very similar at a phylum level with or without the application of an electrical potential.

Complex Biological, Chemical, & Physical Interactions Govern Ecosystem Function. Riparian zones have the capability to buffer aquatic ecosystems from the adjacent land and are important ecosystems for watershed management, especially in agricultural areas [222, 244]. Many studies have worked to directly link hydrologic parameters (e.g., water table depth, groundwater flow patterns) to both denitrification rates and greenhouse gas emissions [237, 245-247]. However, microbial communities are the drivers of subsurface biogeochemical transformations, and as such it is critical to link microbiome dynamics to ecosystem level parameters and functions [235,

236, 244]. There are often chemical or biological links (or both) between different ecosystem processes, such as temperature, groundwater flow, plant growth, and denitrification [155, 157, 219, 248, 249].

When we manipulated the soil redox environment using poised electrodes mimicking iron(III), there was a significant decrease in methane emissions from the upstream site (**Fig. 5.1a**) along with an increase in the relative abundance of proteobacteria (**Fig. 5.2a**). These results suggest that an increase in availability of an alternate electron acceptor with a higher energy yield for bacteria can cause a shift in microbial processes that has a measurable impact on the landscape level. Furthermore, manipulation resulted in a decrease in chloride and sulfate ions in soil porewater (**Fig. 5.1c,d**). The decrease in sulfate concentration is particularly interesting because sulfate reduction is also more energetically favorable than methanogenesis, and the proteobacteria phylum contains the largest group of sulfate-reducing bacteria [150, 250]. Furthermore, this shift in methane emissions and anion concentrations occurred at the upstream site, while the downstream site experienced the same enrichment of proteobacteria and decrease in chloride concentrations, but there were no effects on greenhouse gas emissions or sulfate concentrations.

5.4 Conclusions

We manipulated the soil redox environment by poising electrodes capable of being used as electron acceptors for iron(III)-reducing microbes and observed a clear response in ecosystem function (in this case, methane emissions). Poised electrodes provide an inexhaustible source of electron acceptor for iron reducers, and should allow them to out-compete methanogens for carbon sources and nutrients, since iron reduction is more energetically favorable than methanogenesis [150, 151]; this hypothesis is supported by the inhibition of methane emissions

at the upstream site. At this site, where emissions from chambers with unpoised electrodes (control) were twice as high as the downstream site, poising electrodes to mimic iron(III) resulted in a nearly 50% reduction in methane emissions and corresponded to an enrichment for proteobacteria and a decrease in bacteroidetes. However, at the downstream site, which had a lower magnitude of emissions (nearly 50%) from the chambers with unpoised electrodes (i.e., controls), poised electrodes had no effect on methane emissions. This is likely due to the lower methane emission rates at this site, which would preclude inhibition *via* bioelectrochemical manipulation since methanogenic activity is already low. The alteration of microbial community structure and suppression of methane emissions at the upstream site in conjunction with bioelectrochemical manipulation using electrodes demonstrates the fragile balance that governs biogeochemical cycles in these soils, and highlights the measurable impact that microbial competition has on ecosystem-scale processes. It is clear that microbial community structure and function is subject to influence from a wide array of biological, chemical, and physical factors. Accurate modeling of biogeochemical processes is important for predicting responses to climate change, determining regulatory limits for anthropogenic pollutants, and designing effective best management practices [158, 159, 219]. As such, a deeper comprehension of subsurface microbial ecosystems, their responses to environmental conditions across spatial and temporal gradients, and their impacts on larger-scale function, is critical for improving model accuracy, and further studies are certainly warranted.

Acknowledgements

The authors would like to acknowledge Andrea Fortman, Christine Georgakakos, & Shane DeGaetano for assistance in conducting field work and Julia Goodrich for assistance in

processing paired-end sequences. Partial funding provided by the Atkinson Center for a Sustainable Future and the Cornell University Program in Cross-Scale Biogeochemistry and Climate, which is supported by NSF-IGERT and the Atkinson Center for a Sustainable Future.

CHAPTER 6.

SUMMARY AND RECOMMENDATIONS FOR FUTURE WORK

This chapter is not published.

6.1 Summary

The biogeochemistry of subsurface ecosystems is complex and influenced by a wide array of biological, chemical, and physical factors. Although it is clear that the microbial communities in soils and sediments can impact greenhouse gas emissions, carbon and nutrient availability, plant productivity, and pollutant fate and transport, links between the microbial community and larger-scale ecosystem function are lacking. I have demonstrated the ability of potentiostatically poised electrodes to measure potential respiratory activity of dissimilatory metal-reducing bacteria in Arctic peat soils and linked microbial activity to daily changes in environmental factors (Chapter 3). Monitoring microbial respiration at three depths below the soil surface revealed an awakening of soils microbes in response to increasing temperature at deeper depths as the summer thaw progressed. These increases in microbial activity have the potential to impact the global carbon balance as Arctic soils that have been frozen year-round are subject to the warmer and longer summers associated with climate change. Currently most global methane models do not consider the impact of competing anaerobic microbial processes in wetland ecosystems, the single largest source of methane emissions to the atmosphere. However, it is clear that microbial community dynamics can have a large impact on methane emissions (Chapters 4 & 5). When potentiostatic manipulation was integrated with measures of greenhouse gas (CH_4 and CO_2) fluxes from soils, it was clear that small changes in subsurface conditions can alter microbial community structure and dynamics, and influence ecosystem function on the macro-scale. In the Arctic, potentiostatic

manipulation designed to enrich for iron- and humic acid-reduction microbial communities resulted in increased methane emissions from soils (Chapter 4). This response was unexpected, but is concerning as it demonstrates the high potential for production of an incredibly potent greenhouse gas in these carbon-rich environments. However, it was also evident that the response of microbial communities to manipulation was not uniform across spatial gradients within the ecosystem. In sediments of a riparian zone in upstate New York adjacent to an agricultural field, the same potentiostatic manipulation inhibited methane emissions by nearly 50%, although this response differed across a relatively small spatial gradient (Chapter 5). It is clear that within riparian zones, which provide critical services by acting as a buffer between aquatic and terrestrial ecosystems, there is high variability in processes across hydrologic and biogeochemical gradients. Many riparian areas are adjacent to agricultural fields and are important for watershed management, including the design of best management practices and establishment of regulatory limits on anthropogenic pollutants. The findings here demonstrate the high variability and complexity of subsurface microbial communities and their impacts on macro-scale ecosystem functions. In light of these findings, there are several recommendations for future work.

6.2 Recommendations for Future Work

Potentiostats for biosensing and bioremediation in natural and engineered systems

Microbes are capable of utilizing a wide array of substrates and electron acceptors for growth, and new capabilities are being discovered at an incredible rate. Many dissimilatory metal-reducing bacteria have been found to be able to degrade anthropogenic pollutants, such as aromatic hydrocarbons and uranium. This, combined with their ability to respire with potentiostatically controlled electrodes, opens the door for two exciting applications of

potentiostatically-controlled systems: biosensing and bioremediation. The monitoring of anthropogenic pollutants is often costly and labor intensive, and as a result it is easy to miss significant pollutants in natural environments. I have linked electrical current measurements of microbial respiration in the subsurface to environmental parameters (Chapter 3). By linking current measurements to pollutant degradation by DMRB, it would be possible to sense pollutants moving through natural (e.g., groundwater plumes, rivers) or engineered (e.g., water or wastewater treatment plants, agricultural areas) systems. For example, electroactive microbes can be genetically modified with inducible promotors to enable quantification of toxic compounds [251]. Furthermore, the use of robust, cost-effective sensors, such as potentiostats, would enable the deployment of a vast sensor network able to cover a wider area with greater resolution than is capable using traditional sampling techniques. Such systems would also minimize the lag time between sampling and measurement; currently there can be a significant lag between the sample time (i.e., when a pollutant is actually in the system) and the laboratory-based measurement (e.g., GC, HPLC), which creates the possibility of missing significant events. Direct correlation of electrical current production by bacteria with the presence of a pollutant provides near-instantaneous feedback. Another potential application of potenstatically poised electrodes in natural and engineered systems is the stimulation of microbial pollutant degradation. In either bioreactors or environmental systems (i.e, soils and sediments), potentiostatically poised electrodes could stimulate pollutant reduction by providing an inexhaustible electron acceptor for respiration and growing a robust biofilm community capable of enhanced pollutant remediation. Although both of these systems are far from practical implementation and require much work, they are certainly worth investigating.

Laboratory manipulations to augment field measurements

Climate change has the potential to alter subsurface conditions not only through temperature changes, but also through alterations in precipitation, groundwater hydrology, chemical transport and speciation, and plant productivity. All of these factors both impact and are impacted by subsurface microbial communities, and to understand the impacts that climate change can have on ecosystems as a whole, it is essential to conduct precisely designed manipulation experiments that examine ecosystem response on both a micro- and macro-scale. Field measurements are essential for providing realistic data regarding the response of ecosystems to manipulation. However in this case, it is obvious that natural subsurface systems are highly complex with many overlapping interactions and feedback processes. Despite precise experimental design, bioelectrochemical manipulation, micro- and macro-scale measurements, and extensive collection of environmental metadata, subsurface processes in both the mid- and high-latitudes exhibited a wide range of responses across small spatial and temporal gradients (Chapters 4 & 5). In the field, it is impossible to control fluctuations in temperature, precipitation, surface- and ground-water flow, and atmospheric chemical deposition, among others. For example, changing temperatures and severe storms during experimentation at the riparian zone in Freeville, New York vastly complicated data analysis and interpretation (Chapter 5). These changes make it correlating changes in specific processes to experimental manipulation difficult; therefore, laboratory-based manipulations may be required to augment field measurements. The laboratory allows control over many of the aforementioned environmental variables and thus simplifies statistical correlations by eliminating potential confounding factors. However, these experiments should be conducted to augment, and not in place of, field measurements. Laboratory experiments also allow for long-term manipulation experiments that are not possible due to changing seasons and other field logistics (e.g., electrical power, damage to equipment during

severe winter weather). Integrating laboratory and field experiments will be crucial to elucidating the complicated links between microbial community structure and macro-scale ecosystem function.

Isotopic tracking of carbon pathways through microbial communities

The data presented in this work demonstrates the complexity of subsurface ecosystems that had varying responses to stimuli across relatively small spatial gradients (Chapters 4 & 5). Within soil microcosms, there may be differences in carbon availability and speciation due to biological, chemical, and physical influences. Often, lignocellulosic plant material proceeds through sequential degradation by a mixed microbial consortium. Different groups of microbes consume varying types of organic material, such as biopolymers, monomers, low-molecular weight fatty acids, and alcohols, and their metabolic products are in turn utilized as a carbon source by other community constituents. Tracking the movement and accumulation of isotopically labeled lignocellulosic material within soil microbial communities is a powerful tool that can be applied in both laboratory and field settings [252]. Combined with measures of community structure and landscape-scale processes, these methods can help elucidate the fundamental links between community structure and function and improve our ability to model the responses of subsurface ecosystems to stimuli.

Integrating microbial- and landscape-scale measurements with global models

Wetlands account for approximately one third of total global methane emissions, and are the single largest natural methane source. In our experiments in the Arctic, I observed methane flux rates of 20.5-29.5 mg $CH_4 \times m^{-2} \times d^{-1}$; these are on the low end of other fluxes observed in Arctic environments, although emissions can have a high inter-annual variability due to weather conditions (e.g., temperature, precipitation) [158, 159]. However, global methane models are

highly subject to model assumptions, and small changes parameters can change predicted outputs by a factor of 2 [159]. Sensitivity analysis of the methane biogeochemical model of the Community Land Model 4.0 (CLM4CN) revealed that predicted methane emissions ranged from 150 – 346 Tg CH_4 yr^{-1}, and uncertainties in redox inhibition accounted for a major portion of this range (±45 Tg CH_4 yr^{-1}) [159]. There is undoubtedly a need for improved model parameters, and these improvements are best informed by increasing the amount of training sets for model development and testing, and improving our comprehension of the biological, physical, and chemical factors that govern subsurface wetland processes [158]. To do this, field and laboratory manipulation, such as those conducted here, should be simulated using models, and results should then be compared against measured gas emissions from both field and laboratory experiments. Models can then be improved by either altering existing parameters or adding new ones, if necessary. This type of close collaboration between scientists at the microbial, landscape, and global scales throughout the experimental process will improve scientific results and accuracy at all scales.

APPENDIX 1. SUPPLEMENTAL INFORMATION FOR: A COST-EFFECTIVE AND FIELD-READY POTENTIOSTAT THAT POISES SUBSURFACE ELECTRODES TO MONITOR BACTERIAL RESPIRATION

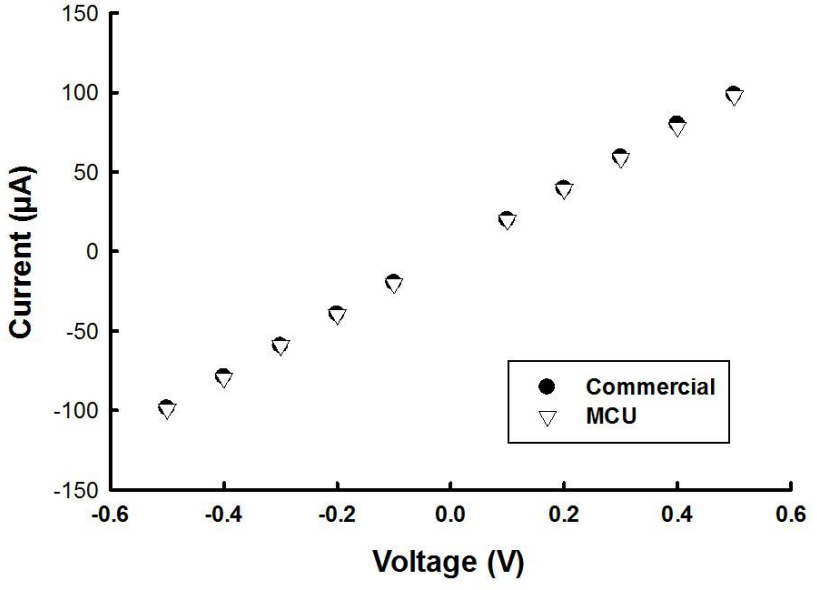

Fig. A1.S1: Comparison of our MCU-based with a commercial potentiostat using a resistor-capacitor (RC) system. The MCU-based potentiostat is accurate to the microamp level where the average error is 0.95 ± 0.58% (95% Confidence Limit).\

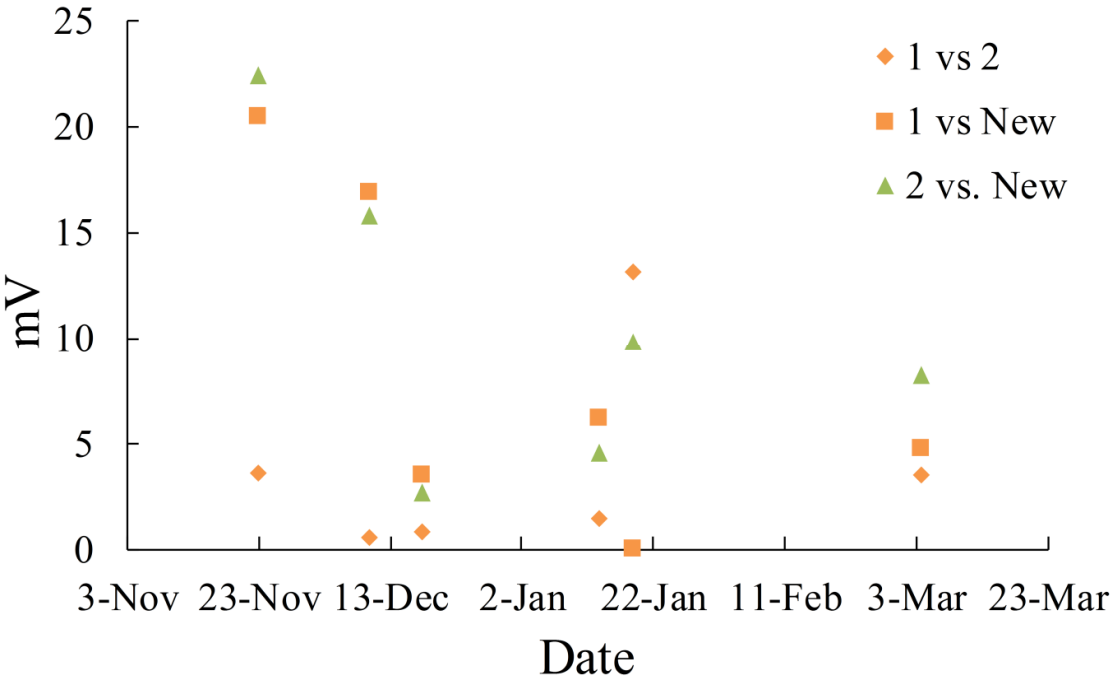

Fig. A1.S2. Tests of reference electrode accuracy over time in a cold room (3.3°C). Two reference electrodes (1 and 2) were placed in soil for a period of 3.5 months and periodically tested against both each other (orange diamonds) and a newly prepared reference electrode (orange squares and green triangles). These tests show that the reference electrodes stay relatively stable (within 20 mV) when deployed in cold soil environments over long periods of time.

A1.S1 Supplementary Design Information

A1.S1.1 Hardware Design

The ATmega 644 MCU was selected for its ability to function in extreme temperatures (-40°C to 85°C). In addition, this MCU has eight input/output (I/O) ports that are enabled with 10-bit internal analog-to-digital converters (ADCs), which are necessary for reading the applied potentials and currents. Circuit boards were designed using ExpressPCB (www.expresspcb.com).

A1.S1.2 Software Design

Interrupt service routines were used to run the peripherals (e.g., LCD, SD) based on a central timer. Upon startup of the potentiostat, the clock is set to a default time (Jan. 1, 2011, 0:00). Once the user sets the clock to the correct date and time, the timer is updated accordingly during the operating period. We programmed the current and potential to be recorded every min, although this parameter can be easily altered in the code.

The FatFS file system library (ChaN, Japan) was used for communicating between the MCU and SD card using the serial peripheral interface (SPI). The SD card runs in SPI mode 0, with the MCU acting as the master device. For SD card removal and data download, a reset button was included to allow the user to reinitialize SD card functions upon reinsertion into the unit. A new text file is created every time the unit is turned on or the reset button is pressed. Following a temporary power outage, the potentiostat will restart although the time will reset to default settings.

Upon turning the LCD switch on, the LCD drivers are reinitialized to ensure proper functionality. The LCD screen will initially show the date and time of the unit; four buttons below the LCD screen allow the user to navigate through screens and set parameters. Two buttons below the LCD screen allow the user to set the correct date and time. A third button allows the unit to cycle through three additional screens showing the voltage and current at each electrode depth. The fourth button can be pressed to force a manual update of the current and voltage.

A1.S2 Testing the MCU Potentiostat

We tested our MCU-based potentiostat using a commercial potentiostat (VSP, Biologic, Claix, France). This commercial unit measures currents on a range of 10 μA to 1 A with a resolution of 760 pA. The control voltage is a 20 V adjustable range with a 5 μV resolution.

A1.S3 Temperature Considerations

It should be noted that many of the components used to construct the MCU-based potentiostat exhibit changes in performance in response to temperature fluctuations. Therefore, it is of concern to ensure that the fluctuations in current recorded by the MCU-based potentiostat were indeed a result of microbial respiration and due to the response of electrical components to temperature fluctuations. For example, both thick film and carbon film resistors were used in the design, and these components have temperature coefficients of 0-200 ppm/K and 0-850 ppm/K, respectively. There are 39 resistors in each potentiostat, the highest temperature-based fluctuations in signal would be on the order of 33,150 ppm/K. The temperature fluctuations on any given day were only on the order of 2^{o}K; therefore, the fluctuations in electrical current recorded due to the temperature response of electrical components would be much less than the fluctuations recorded by the MCU-potentiostat. This confirms that the signal recorded was indeed from microbial respiration.

A1.S4 Parts List

Category	Component	Part #	Unit Price	Units	Total Price
Parts for One MCU Potentiostat					
MiniBoardPro 4-Layer Service	MCU Board (Minimum Order = 3)	PCB Express	98	0.33	32.34
MiniBoardPro 4-Layer Service	Electrode Board (Minimum Order = 3)	PCB Express	98	1	98.00
MiniBoardPro 4-Layer Service	Shifter Board (Minimum Order = 3)	PCB Express	98	0.33	32.34
MiniBoardPro 4-Layer Service	SD Board (Minimum Order = 3)	PCB Express	98	0.33	32.34
Capacitor	10 µF	Digikey 445-2863-ND	0.35	1	0.35
Capacitor	22 pF	Digikey 311-1154-1-ND	0.11	2	0.22
Capacitor	0.1 µF	Digikey 311-1179-1-ND	0.04	28	1.15
Capacitor	1 µF	Digikey 399-1254-1-ND	0.07	36	2.56
Capacitor	2.2 µF	Digikey 490-1799-1-ND	0.10	3	0.30
Capacitor	100 µF Aluminum	Digikey P5138-ND	0.08	4	0.31
Capacitor	330 µF	Digikey P12372-ND	0.19	1	0.19
Resistor	1 Ω	Digikey CF1/81JRCT-ND	0.06	1	0.06
Resistor	100 Ω	Digikey P100FCT-ND	0.11	1	0.11
Resistor	1 kΩ	Digikey P1.0KECT-ND	0.03	15	0.39
Resistor	100 kΩ	Digikey P100KECT-ND	0.09	1	0.09
Resistor	1 kΩ 1%	Digikey WHA1K0FECT-ND	0.87	1	0.87
Resistor	2 kΩ 1%	CMF2.0KHBCT-ND	0.16	1	0.16
Resistor	200 Ω 1%	WHA200FECT-ND	1.08	1	1.08
Resistor	400 Ω 1%	41F400E-ND	2.38	1	2.38
Resistor	2 kΩ	Digikey CF1/82KJRCT-ND	0.03	2	0.06
Resistor	300 Ω	Digikey P300FCT-ND	0.11	1	0.11
Resistor	5.1 kΩ	Digikey CF1/85.1KJRCT-ND	0.02	6	0.14
Resistor	10 kΩ	Digikey CF1/810KJRCT-ND	0.03	3	0.10
Resistor	56 kΩ	Digikey CF1/856KJRCT-ND	0.06	1	0.06
Resistor	240 kΩ	Digikey CF1/8240KJRCT-ND	0.06	1	0.06
Resistor Network	10 kΩ	Digikey 4116R-1-103LF-ND	0.40	3	1.19
Potentiometer	10 kΩ	Digikey 3057Y-103-ND	13.41	4	53.64
Inductor	330 µH	Digikey 445-3753-1-ND	1.35	4	5.40
Diode	1N4001	Digikey 1N4001DICT-ND	0.18	1	0.18

Diode	1N914	Digikey 1N914BCT-ND	0.04	3	0.12
Diode	1N5822	Digikey 1N5822-E3/54GICT-ND	0.35	1	0.35
Connector	10 Pin M	Digikey WM4208-ND	0.73	2	1.47
Connector	10 Pin F	Digikey WM2620-ND	0.65	2	1.31
Connector	14 Pin M	Digikey MHB14K-ND	1.56	1	1.56
Connector	4 Pin M	Digikey WM4302-ND	0.61	9	5.46
Connector	4 Pin F	Digikey WM2202-ND	0.35	9	3.18
Connector	3 Pin M	Digikey WM4301-ND	0.74	18	13.25
Connector	3 Pin F	Digikey WM2012-ND	0.16	3	0.48
Connector	Pin Connectors	Digikey WM1114-ND	0.09	53	4.51
Electronics - Misc	ATMEGA644 Microcontroller	Digikey ATEMGA644-20PU-ND	4.79	1	4.79
Electronics - Misc	16 MHz Crystal	Digikey 535-9912-1-ND	0.82	1	0.82
Electronics - Misc	3.3V Regulator	Digikey 296-8056-5-ND	1.46	1	1.46
Electronics - Misc	Toggle Switch	Digikey CKN10027-ND	4.63	1	4.63
Electronics - Misc	Push Button Switch	Digikey 401-1969-ND	0.90	1	0.90
Electronics - Misc	Power Jack 2.1MM	Digikey CP-002A-ND	0.30	1	0.30
Electronics - Misc	2.1mm Female Plug	Digikey CP3-1000-ND	0.73	1	0.73
Electronics - Misc	40 Pin DIP Socket	Digikey A24806-ND	2.92	1	2.92
Electronics - Misc	Jumper	Digikey S9001-ND	0.08	26	2.03
Electronics - Misc	Yellow LED	Digikey 160-1673-ND	0.24	1	0.24
Electronics - Misc	Spacers	Digikey 492-1108-ND	0.04	8	0.28
Electronics - Misc	5V Buck Regulator	Digikey 576-1516-5-ND	2.24	1	2.24
Electronics - Misc	1.25V Reference Chip	Digikey LTC6652AHMS8-1.25#PBF-ND	4.80	3	14.40
Electronics - Misc	Voltage Regulator +/-5V	Digikey DCP010505DBP-ND	10.60	3	31.80
Electronics - Misc	SD Card Connector	Digikey 3M5646CT-ND	1.06	1	1.06
Electronics - Misc	LT1007 Op Amp	Linear Technologies	3.75	3	11.25
Electronics - Misc	LT1097 Op Amp	Linear Technologies	2.25	15	33.75
Electronics - Misc	SD Card		29	1	29.00
Parts for Use in Extreme Environments					
Connector	3 Pin External F	708-1157-ND	15	1	15.00
Connector	3 Pin External M	708-1108-ND	11.21	1	11.21
Connector	6 Pin External F	708-1159-ND	16.98	1	16.98
Connector	6 Pin External M	708-1110-ND	12.59	1	12.59
Connector	External Cap	708-1180-ND	1.19	2	2.38

Connector	2 Pin External M	708-1107-ND	10.55	1	10.55
Connector	2 Pin External F	708-1156-ND	14.35	1	14.35
Case	Waterproof Case	Seahorse Cases SE-120	21.37	1	21.37
Parts That Can Be Used for More Than One Unit					
Electronics - Misc	Push Button Switch	Digikey 401-1969-ND	0.90	4	3.60
MiniBoardPro 4-Layer Service	LCD Board (Minimum Order =3)	PCB Express	98	0.33	32.34
Connector	14 Pin M	Digikey MHB14K-ND	1.56	4	6.24
Electronics - Misc	Solder paste	Digikey SMD291SNL-ND	14.25	1	14.25
Electronics - Misc	LCD Screen	Electronics 123	9.99	1	9.99
Electronics - Misc	Ribbon Cable (14) - 300 ft	Digikey AE14G-300-ND	47.95	1	47.95
Programming	AVRISP	Digikey AVRISP2-ND	35	1	35.00
Connector	14 Pin F	3M9091-ND	4.93	1	4.93
		Subtotal - One MCU Potentiostat			**440.41**
		Subtotal - Parts for Use in Extreme Environments			**104.43**
		Subtotal - Parts That Can Be Used for More Than One Unit			**154.30**

APPENDIX 2 SUPPLEMENTAL INFORMATION FOR: POTENTIOSTATICALLY-POISED ELECTRODES MIMIC IRON OXIDES AND INTERACT WITH SOIL MICROBIAL COMMUNITIES TO ALTER THE BIOGEOCHEMISTRY OF ARCTIC PEAT SOILS

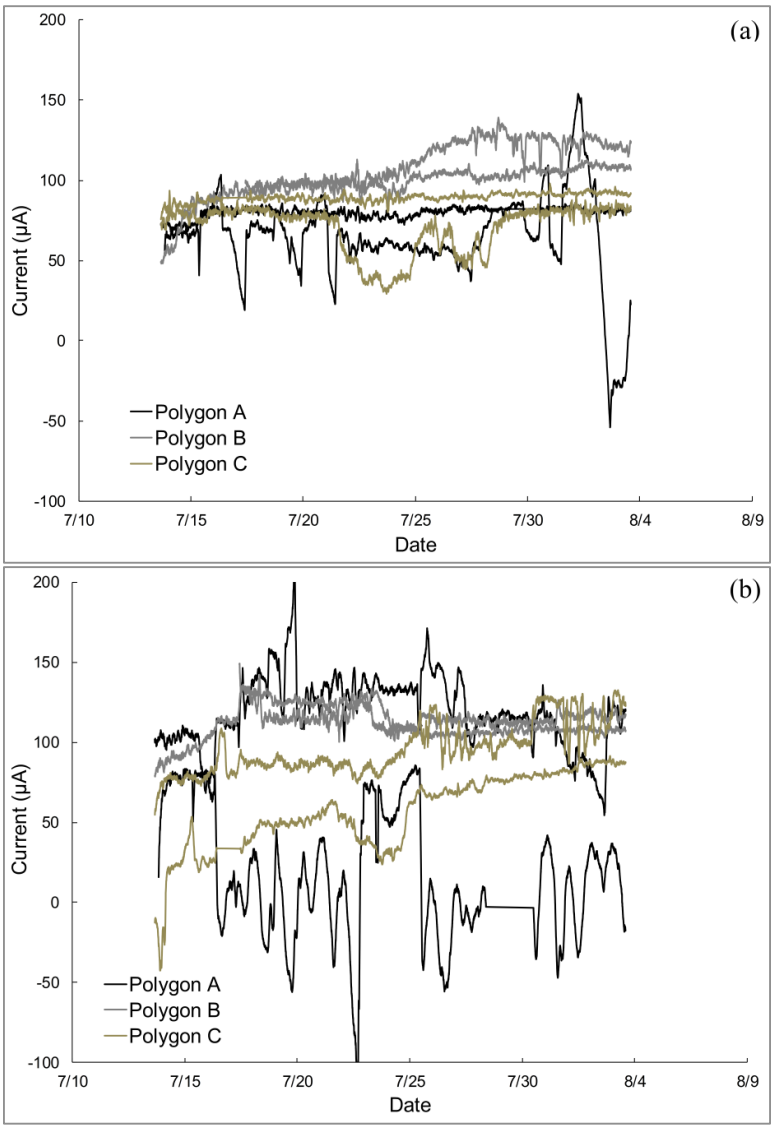

Figure A2.S1. Electrical current from poised electrodes at shallow (a) and deep (b) depths recorded by microcontroller-based potentiostats. At the shallow depth (a), all electrodes begin with similar currents and then change over the course of the five-week experiment, with the currents in polygon A increasing by ~40 μA in the middle of the experiment. Electrical current is more erratic in electrodes at deep depths (b).

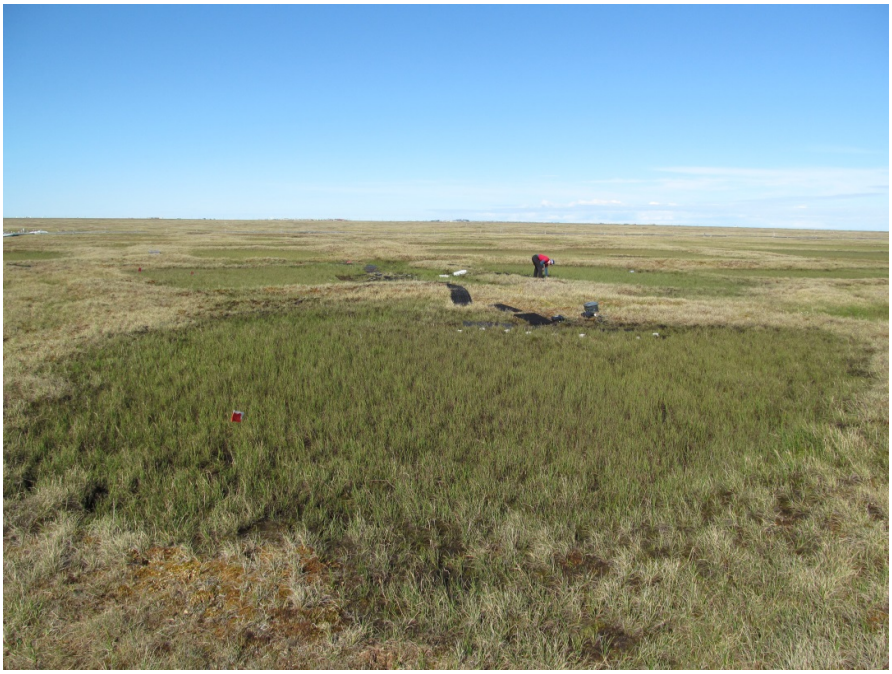

Figure A2.S2. The three replicate polygons studied in this experiment. The A polygon located in the back left, the B polygon in the back right, and the C polygon in the foreground. The entire site is located within a medium-aged drained thaw lake basin in the Barrow Environmental Obervatory.

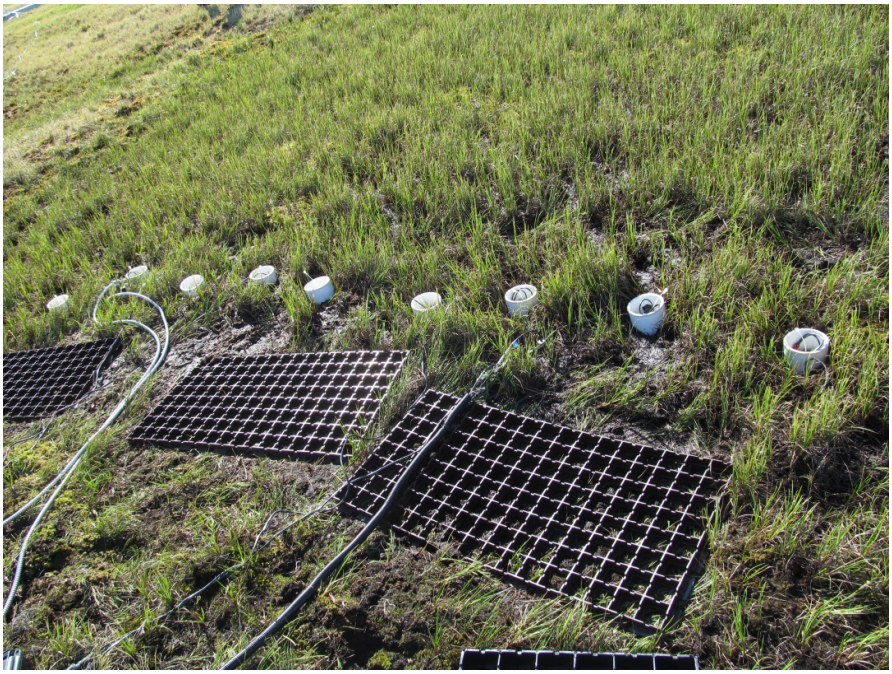

Figure A2.S3. Soil chambers deployed in the B polygon. Each polygon contained nine soil chambers. The mats pictured are to prevent disturbance of the study site while sampling.

Figure A2.S4. A soil chamber containing electrodes located in the depressed polygon of a medium-aged drained thaw lake basin outside Barrow, AK. The opaque device in the center of the chamber is a porous soil moisture sampler.

Figure A2.S5. Gas fluxes (CH_4, CO_2) being measured from a soil chamber outside Barrow, AK. One tube leads to the input of a greenhouse gas analyzer which is then returned to the chamber *via* the second tube. The chamber is vented using a needle in the center of the chamber top.

APPENDIX 3 SUPPLEMENTAL INFORMATION FOR: CHANGES IN MICROBIAL COMMUNITY STRUCTURE AND METHANE EMISSIONS FROM RIPARIAN ZONE SEDIMENTS IN RESPONSE TO BIOELECTROCHEMICAL MANIPULATION

Figure A3.S1. Soil chambers located in the riparian zone of Fall Creek in Freeville, NY. Chambers were installed at two site approximately 50 m apart: a downstream site (left) and an upstream site (right).

Figure A3.S2. Microcontroller-based potentiostats (black box) were used to poise electrode potentials to stimulate growth of iron reducing microbes. The potentiostats were powered using a car battery (located within the Styrofoam cooler).

Figure A3.S3. Methane and nitrous oxide emission were measured from soil chambers by placing a cap on the soil chamber (right) and measuring the change in gas concentrations over 30 min. While the caps were on the chambers, the chambers were vented using a needle to prevent pressure differentials between the soil and headspace.

Figure A3. S4. Even though the two sites were only ~50 m apart, the downstream site (top) had more vegetation cover which resulted in lower soil temperatures than the upstream site (bottom), which was more exposed.

APPENDIX 4: PROTOCOLS

A4.1 Iron^{2+}, Iron^{3+}, and Total Iron (Ferrozine Assay)

Materials:

0.5 N HCl
Hydroxylamine hydrochloride
HEPES (Sigma H-0891), FW 238.3
Ferrozine (Sigma P-9762 3-(2-Pyridyl)-5,6-bis(4-phenylsulfonic acid)-1,2,4-triazine)
Iron(II) salt for standards
200µL black 96-well plates
1 mL 96 well plate

Reagent Preparation:

1. Ferrozine Solution
    a. Obtain 400 ml Milli-Q water
    b. Add 5.98 grams HEPES
    c. Add 0.5 gram ferrozine
    d. Adjust pH to 7.0
    e. QS to 1 liter with Milli-Q water
    f. Store at 4°C
2. 1.4 M Hydroxylamine (prepare fresh daily)
    a. Dilute 9.7 grams of hydroxylamine hydrochloride in 100 mL of 0.5 N HCl.
3. HCl (0.5 N)
    a. Dilute 83 mL of concentrated (36%) HCl with 1917 mL of deionized water.

Standards:

1. Concentrated Standards (Store at 4^{o}C). Prepare in hood; $FeCl_2*4H_2O$ will oxidize rapidly under aerobic conditions at neutral pHs.
    a. 0 mM – 5 mL 0.5 N HCl
    b. 1 mM – Dissolve 0.99 mg $FeCl_2*4H_2O$ in 5 mL of 0.5 N HCl
    c. 5 mM – Dissolve 4.97 mg $FeCl_2*4H_2O$ in 5 mL of 0.5 N HCl
    d. 10 mM – Dissolve 9.94 mg $FeCl_2*4H_2O$ in 5 mL of 0.5 N HCl
    e. 20 mM – Dissolve 19.88 mg $FeCl_2*4H_2O$ in 5 mL of 0.5 N HCl
    f. 40 mM – Dissolve 39.76 mg $FeCl_2*4H_2O$ in 5 mL of 0.5 N HCl
2. Diluted Standards (prepare fresh)
    a. Dilute 0.1 mL of concentrated standards in 4.9 mL of 0.5 N HCl to get standards of 0, 20, 100, 200, 400, & 800 µM.
3. Making a Standard Curve
    a. In a black 96-well plate, combine 4 µL of diluted standards (in triplicate) with 196 µL of ferrozine reagent. Pipette up and down to mix.
    b. Read absorbance at 562 nm.
    c. Calculate standard curve.

Measuring Iron^{2+} in Samples:

Note: Fe^{2+} will rapidly oxidize at neutral pHs and aerobic conditions. To circumvent this, you may want to acidify your sample by mixing it 1:1 with 0.5 N HCl - this will dilute your sample by a factor of 2)

1. In a black 96-well plate, combine 4 µL of your sample with 196 µL of ferrozine reagent. Pipette up and down to mix.
2. Read fluorescence at 562 nm.
3. Calculate samples concentrations using standard curve.

Measuring Total Iron in Samples:

1. In a 1 mL 96-well plate, mix 0.1 mL acidified samples with 0.9 mL of 1.4 M hydroxylamine solution.
2. Apply centrifuge tape and shake on a plate shaker at room temperature for 15-30 minutes to reduce all iron to Fe^{2+}.
3. Combine 4 µL of the acid digest with 196 µL of ferrozine reagent. Pipette up and down to mix.
4. Read fluorescence at 562 nm.
5. Calculate total iron concentrations using standard curve. Remember, samples were diluted by a factor of 10 with hydroxylamine solution.

Calculating $Iron^{3+}$ in Samples

Calculate $iron^{3+}$ concentrations in samples by subtracting the $iron^{2+}$ concentrations from the total iron concentrations.

A4.2 Sequencing of Environmental Samples Using Illumina MiSeq: Preparation and Data Processing

Materials:

PowerSoil® DNA Isolation Kit
505f Forward primer
806r Barcoded reverse primer
5PRIME HotMaster Mix
Molecular grade H_2O
96 well PCR plates
Mag-Bind PCR Cleanup Solution
96 well Mag-Bind PCR Cleanup Plate
70% molecular grade ethanol
Magnetic separation stand
Elution Buffer (Solution C6 from PowerSoil® DNA Isolation Kit)
PicoGreen Reagent
Tris EDTA solution
Polypropylene reservoirs
Various single- and multi-channel pipettes
0.1-10 µL filter pipette tips
200 µL filter pipette tips
Eppendorf pipette tips

Procedure:

1. Extract genomic DNA from samples using the PowerSoil DNA Isolation Kit. Procedure: http://www.mobio.com/images/custom/file/protocol/12888.pdf
2. Run duplicate 50 µL polymerase chain reactions (PCRs) for each sample by combining (for each reaction): 0.5 µL of 10 µM 505f forward primer, 0.5 µL of 10 µM 806r barcoded reverse primer, 20 µL of 5PRIME HotMaster Mix, 28 µL of molecular grade H_2O, and 1 µL of DNA template (extraction product). The PCR sequence is titled 16SEMP25 on the thermocycler.
3. For each sample, combine the PCR product from duplicate reactions.
4. Run gels to confirm PCR product.
5. Purify PCR product with Mag-Bind PCR Cleanup Kit.
    a. Shake Mag-Bind Solution to resuspend any settled particles. Add 1.8X PCR product (1.8*80uL) of Mag-Bind to each well. [In DNA biosafety cabinet, rest of protocol outside hood in clean bench area]
    b. Transfer 80 uL of pooled PCR product to 96-well Mag-Bind PCR Cleanup Plate
    c. Mix each well by pipetting up and down 5-10 times (or vortexing for 30 seconds), then incubate at room temperature for 1 minute.
    d. Place the plate onto a magnetic separation stand to magnetize the Mag-Bind particles. Solution will be clear when beads have completely migrated toward the magnets [at least 5 minutes]. Leave plate on stand.
    e. Remove and discard the clear supernatant (don't disturb magnetic beads, should remove ~200 uL).

f. Add 200 uL of 70% ethanol to each well and incubate at room temperature for 1 minute.
g. Remove and discard the clear supernatant (don't disturb magnetic beads, remove ~200 uL).
h. Repeat steps f and g.
i. Allow the plate to dry on the magnetic for at least 10-15 minutes. Remove any liquid residue from the wells by pipetting [Make sure it is dry before proceeding; don't move plate at this step, the beads can be easily disturbed].
j. Remove from the separation stand (carefully!) and add 30-40 uL of Elution Buffer (10 mM Tris pH 8.5, TE Buffer, 0.1 mM EDTA, DI H2O, or Solution C6 from PowerSoil® DNA Isolation Kit) to each well to elute DNA from the magnetic particles. [Make sure the volume is above the magnetic beads].
k. Mix each well by pipetting up and down 20 times (or vortexing for 30 seconds), then incubate at room temperature for 2-3 minutes.
l. Place the plate onto the magnetic seperation stand to magnetize the Mag-Bind particles. Wait at least 5 minutes.
m. Transfer the cleared supernatant containing purified DNA to a new 96-well PCR plate. [Use 10 uL pipette, if you draw beads, put solution back and let settle, then retry; you should get ~30-35 uL out]
n. Seal the PCR plate with aluminum foil and store at -20^{o}C.

6. Run gels to confirm 250-450 bp bands.
7. Quantify DNA using PicoGreen.
    a. Take out PicoGreen to thaw.
    b. Make linear DNA standards from lamda-DNA stock.
    c. You will need 99 uL of TE and 100 uL green mix per sample. To calculate the amount of green mix you need (# of samples +1) x 100 = volume (uL) of green mix. To make green mix, make a 1:200 dilution of PicoGreen in TE. (For example, to make 1mL of green mix you would dilute 5uL PicoGreen in 995 uL sterile TE). Mix, and keep in the dark until ready to use.
    d. Using a black 96-well plate, first add 99uL of TE to each well that a sample or standard will go in.
    e. Add 1uL of sample or standard per well. Remember to have one 'blank' containing only TE and green mixture (no DNA).
    f. Add 100uL of green mixture to each well. Pipette up and down to mix well.
    g. Read fluorescence at Excitation 485/20; Emission 528/20; Sensitivity 50.
    h. Calculate DNA concentrations in samples using standard curve.
8. Pool 100 ng DNA from each sample into a single tude.
9. Sequence at the Cornell University Biotechnology Resource Center using the Illumina MiSeq (2x250bp; paired end).
10. You will receive three files from the sequencing center: forward reads, reverse reads, and the 12 base barcode read. Assign barcodes and join the forward and reverse reads by:
    a. Split libraries on each read separately. Sample syntax:
        i. Sample syntax for the forward reads: *MacQIIME microbe:Freeville $ split_libraries_fastq.py -i R1.fastq -o Forward/ -b I1.fastq --rev_comp_mapping_barcodes -m mappingfile.txt -q 25*

ii. You should see a result like this:
Quality filter results
Total number of input sequences: 11685911
Barcode not in mapping file: 189195
Read too short after quality truncation: 107473
Count of N characters exceeds limit: 3326
Illumina quality digit = 0: 0
Barcode errors exceed max: 8776708
Total number seqs written 2609209

iii. Sample syntax for the reverse reads: *MacQIIME microbe:Freeville $ split_libraries_fastq.py -i R2.fastq -o Reverse/ -b I1.fastq --rev_comp_mapping_barcodes -m mappingfile.txt -q 25*

iv. You should see a result like this:
Quality filter results
Total number of input sequences: 11685911
Barcode not in mapping file: 189195
Read too short after quality truncation: 329527
Count of N characters exceeds limit: 5796
Illumina quality digit = 0: 0
Barcode errors exceed max: 8776708
Total number seqs written 2384685

b. Grab only the sequences in each original run file that are in both split library files.
   i. Sample syntax: *MacQIIME microbe:Freeville $ python python_scripts/sortmatepairs.py R1.fastq R2.fastq Forward/seqs.fna Reverse/seqs.fna sortmatepairs*
   ii. You should see a result like this:
   2609209
   2384685
   2339767

c. Use fastqjoin to join the forward and reverse reads.
   i. Sample syntax: *MacQIIME microbe:Freeville $ ea-utils.1.1.2-537/fastq-join sortmatepairs_Read1seqs.fastq sortmatepairs_Read2seqs.fast -o fastqjoin*
   ii. You should see a result like this:
   Total reads: 2339767
   Total joined: 2334862
   Average join len: 244.62
   Stdev join len: 23.12

d. Make the joined files look like QIIME split library files.
   i. Sample syntax: *MacQIIME microbe:Freeville $ python python_scripts/imitate_splitlib_mod.py fastqjoinjoin Forward/seqs.fna split_lib_merged*

e. Pick OTUs and continue downstream data analysis as you would normally in QIIME (http://www.qiime.org).

A4.3 Operator Instructions for Microcontroller-Based Potentiostat

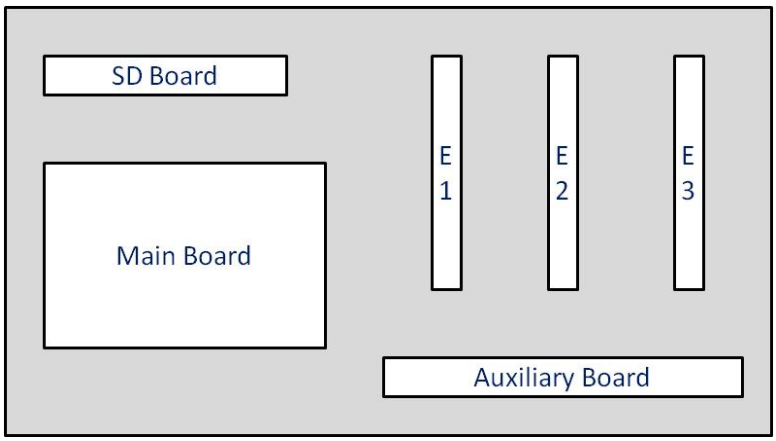

Figure A4.S1: Schematic diagram of the inside of the microcontroller potentiostat showing the six (6) circuit boards, labeled Main, SD, Auxiliary, E1, E2, & E3. In addition, there is a liquid crystal display (LCD) board that can be used by the user to check the operating parameters.

A. Standard Operation

Connecting the unit

1. There are three (3) cables at the rear of the black box. Connect the unlabeled six pin connector to the electrodes.
2. Connect the unlabeled three pin connector to the reference electrodes.
3. Connect the remaining connector, labeled with blue tape, to the power source. This will be either a two or three pin connector. This will power the unit on and begin operation.

Setting the clock and shift

1. Upon commencing operation of the potentiostat, the user must set the clock and an operating parameter called shift.
2. Plug the LCD into the gray connector on the bottom left corner of the main board. Then, on the SD board, flip the small white and black switch from left to right. The LCD screen should display a date, time, and shift value.
3. There are four buttons on the board (Figure 2). In order from left to right, these buttons are:

SET button	Goes into set mode so user can change data
INC button	Increments value
STAT button	Rotates between the clock screen and the electrode data
UPDT button	Quickly updates electrode data

4. To adjust the clock, hold the SET button down while on the clock screen. A cursor will begin to flash on the first parameter, the month.
5. To increment the value that the cursor is currently at, press and hold the INC button. Holding it down will allow the value to continue to increment.
6. When the correct value is set for month, press and hold the SET button to scroll to the next parameter. Continue this pattern until all parameters have been set.
7. To complete the operation, hold down the SET button until the cursor disappears. This will return the potentiostat to its normal operating mode and print a message on the SD card noting that the time was changed.

8. The shift is displayed on the second line of the LCD, below the date and time. For normal operation, this value should be set between 530-600. If it is not already in the correct range, adjust the value so that it is in the correct range.
9. To adjust the shift to the correct value, use the potentiometer located on the auxiliary board. To decrease the magnitude, turn the dial clockwise. To increase, turn the dial counter-clockwise. Changes in the shift value will be reflected on the LCD screen every 1 minute.
10. To remove the LCD screen, flip the switch on the SD card board to the left and pull the LCD screen and cable out of the main board. The switch will stop data from being sent to the LCD.

Setting the applied potential

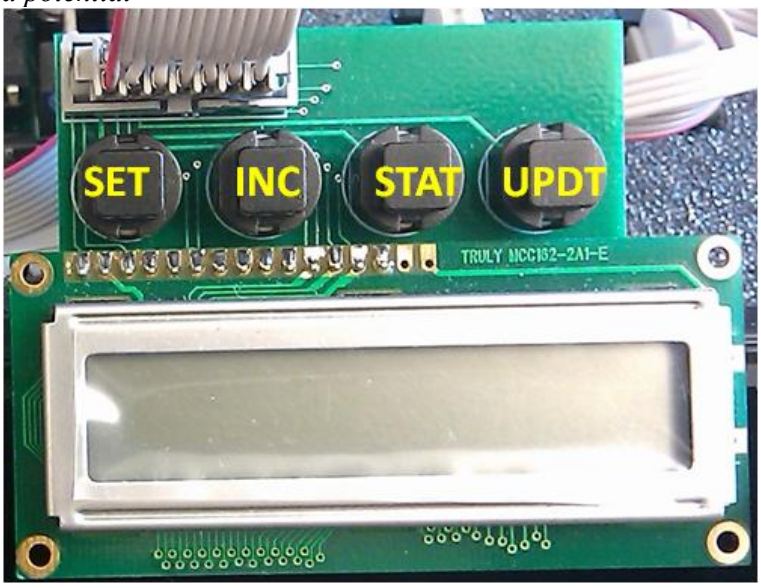

Figure A4.S2: LCD screen, showing the four different buttons

1. The potential of each electrode can be monitored using the LCD screen. Begin operation of the LCD screen as previously described.
2. From the date/time screen, press and hold the STAT button to scroll to the next screen, which will display the applied voltage and current of electrode 1. Press and hold the STAT button again to scroll to electrode 2, and again to scroll to electrode 3. Holding the STAT button while on electrode 3 will bring the LCD screen back to the date/time screen.
   Note: Only the magnitude of the applied voltage is displayed on the LCD screen. To check or change the polarity, refer to step 6.
3. Each screen will display the last taken measurement of the voltage being applied across the electrode and the current being read in. Pressing the UPDT button will cause the CPU to take a new measurement at that electrode and display the results on the LCD screen. No data will be written to the SD card.
4. To adjust the magnitude of the applied potential, use the screwdriver to turn the potentiometer (labeled P on Figure 3) on the board corresponding to the channel you are monitoring (E1, E2, or E3) To decrease the magnitude, turn the dial clockwise. To

increase, turn the dial counter-clockwise. Use the LCD screen ensure the correct potential is set.

5. To change the polarity of the applied potential, use the jumpers located on the electrode boards, shown in the figure below.
6. Jumpers 4, 5, & 6 control the polarity of the applied voltage to the working electrode. To apply a positive voltage, connect the center pin to the right pin of J4, J5, and J6. To apply a negative voltage, connect the center pin to the left pin of J4, J5, & J6.
7. The polarity of the potential displayed on the LCD screen must be manually set by the user. From the correct electrode screen, press and hold the SET key. The bottom line of the LCD will display something similar to this: "0 RES 1000." If the first number is a zero, the LCD will display a negative potential. If it is a one a positive potential will be displayed. Change the number using the INC button.
8. Confirm that the correct polarity is set *via* jumpers, and the correct magnitude with the LCD screen.
9. To remove the LCD screen, flip the switch on the SD card board to the left and pull the LCD screen and cable out of the main board. The switch will stop data from being sent to the LCD.

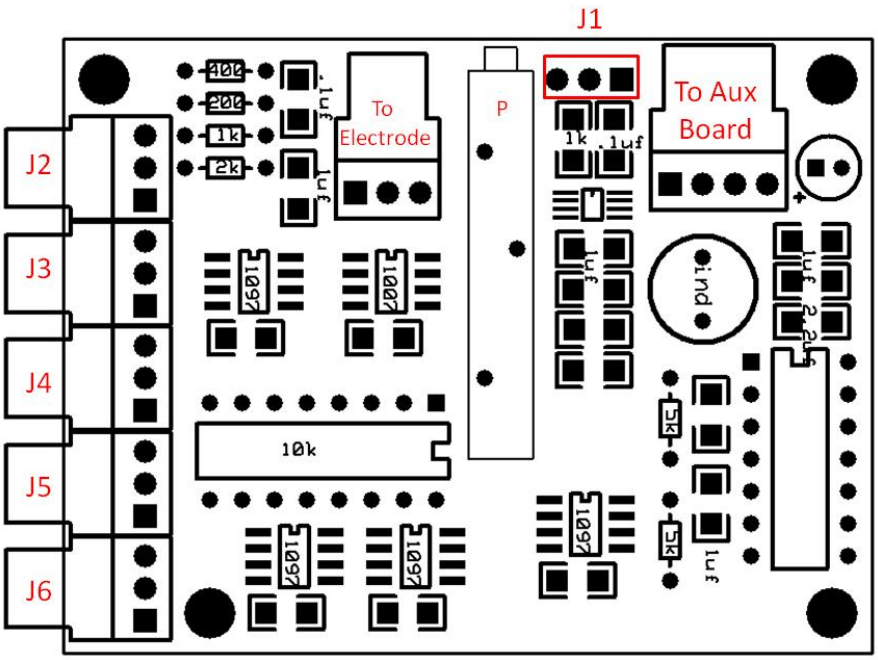

Figure A4.S3: Electrode circuit board showing location of jumpers used to set current range and applied voltage polarity.

Downloading data

1. To download data, remove the SD card by pressing the SD card into the SD card slot until it clicks and pops out. Insert the SD card into your computer and copy the data file. Data files are name "pot###," and the highest numbered file will be the most recent.
2. To resume data collection, insert the SD card into the SD card slot until it clicks. Start a new data file by pushing the black button on the SD board. If the LCD screen is plugged

in and on, and the screen is currently in the clock view, the second line of the LCD screen will read "SD card reset."

B. *Advanced Operation*

Changing the current range

1. There are four possible current ranges: 200 µA, 400 µA, 1mA, and 2mA. The unit will be set to the 1 mA range in the default mode.
2. To change the current range for a electrode, use jumpers J2 and J3 (shown on Figure A4.S3) and below:

Current Range	Jumper Setting
200 µA	J2, Center-Left pins connected
400 µA	J2, Center-Right pins connected
1 mA	J3, Center-Left pins connected
2 mA	J3, Center-Right pins connected

3. If the current range is changed, the value "RES" must be changed on the electrode LCD screen to ensure accurate data. From the correct electrode screen, press and hold the SET key. The bottom line of the LCD will display something similar to this: "0 RES 1000." Move the cursor to the '1000' and use the INC key to scroll to the correct current range. Note: Here all values are in µA, so a RES value of 1000 is the 1 mA current range.

Programming the microcontroller

1. If the need to program the chip arises, attach the programming device to your PC (*via* USB) and connect the other end to the 6 pins found near the bottom of the main board. The red wire should connect to the left side of the board. Make sure that the jumper connector below the 6 pins is inserted, otherwise the chip will not program.
2. Open up AVRstudio. Go to the project folder and open up *potentiostat.aps*. The project should open up. Follow the instructions found on this website to make sure that the data is stored correctly. http://winavr.scienceprog.com/avr-gcc-tutorial/using-sprintf--function-for-float-numbers-in-avr-gcc.html (instructions begin near the bottom, starting with "You may ask what to do with AVRStudio settings, where makefile is generated automatically. Well things are simple too in this situation." Then go to Project>>Configuration Options and make sure that the device is "Atmega644" and the frequency is set to "16000000" Hz.
3. The potentiostat is currently set to record data every minute. To change this setting, go to source files on the left bar. And open *main.c*. Right at the top there is a macro called *record_trigger()*. This tells the device when to record data. To set how often you want the potentiostat to record, change the (minute==xx) to be however often you want data recorded.
4. Hit F7 to program the device. If there are errors make sure you go and fix them. Go to Tools>>Program AVR>>Connect. Select the platform "AVRISP mkII" and Port "USB." Hit connect. A new window should appear. Go to the Program tab and in the Flash menu, hit the … to browse the file location. Go into the project folder "/default/potentiostat.hex". Then hit the program button. This should program the device.

Internal Connections

1. The unit should have all connections in the correct position at the beginning of use, but if the need arises to unplug or re-connect the boards, the correct configuration is outlined below:
   Auxiliary Board Connections:
   A1 – Connects to main board *via* 3-prong connector
   A2 – Connects to E1 board *via* 4-prong connector
   A3 – Connects to main board port labeled ‘E1’
   A4 – Connects to E2 board *via* 4-prong connector
   A5 – Connects to main board port labeled ‘E2’
   A6 – Connects to E3 board *via* 4-prong connector
   A7 – Connects to main board port labeled ‘E3’
2. The SD board connects to the main board *via* the 10-prong connectors on either board.
3. There are three 3-pronged connectors that enter the box *via* the hole in the back to connect to electrodes. They are labeled with red, blue, and black marker, and should be connected as follows:
   Red – Shallow electrode, connect to E1 board
   Blue – Medium electrode, connect to E2 board
   Black – Deep electrode, connect to E3 board

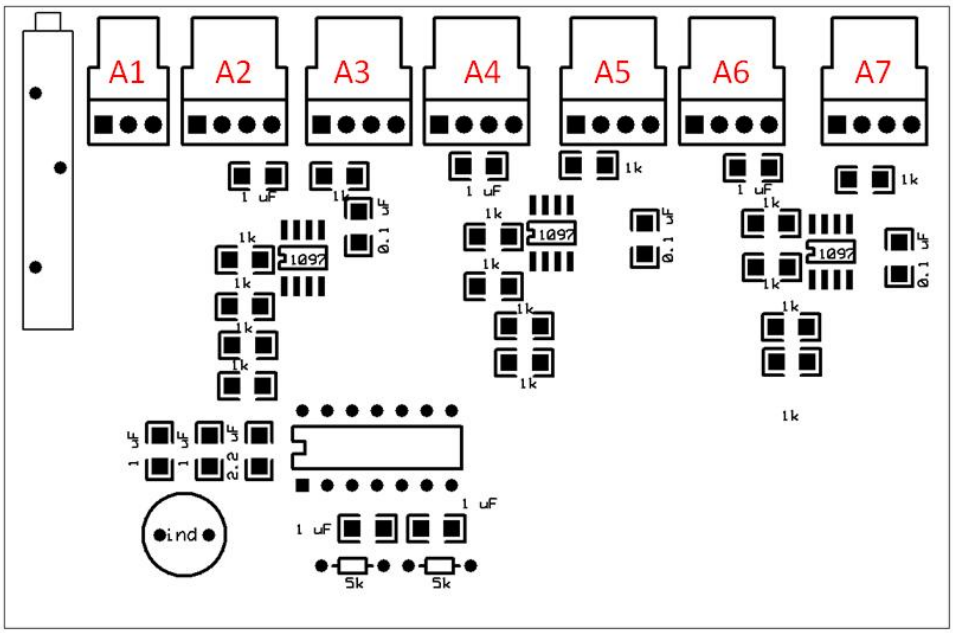

Figure A4.S4: Auxiliary board showing connections to other circuit boards (labeled A1 – A7).

A4.4 Measuring Gas Fluxes from Soil Chambers

Materials:
-Soil chamber
-Soil chamber cap
-Needles
-10 mL syringe with two-way valve
-10 mL glass vials
-Butyl rubber stopper
-Crimp caps for vials
-Vial crimper
-Vial de-crimper
-Stopwatch
-Vacuum pump (optional, but preferred)
-Gas standards for the gases of interest
-Gas chromatograph
-Beeswax-coated calcium carbide tablets (optional, for measuring denitrification rates *via* nitrous oxide emissions)

Procedure:

1. Cap vials using the butyl stoppers, crimp caps, and vial crimper. Cap four times the number of chambers you will be measuring.
2. Evacuate the vials using either a vacuum pump (preferred) or manually using a syringe.
3. If you are using nitrous oxide to measure denitrification flux, place 4-8 beeswax-coated calcium carbide tablets in the soil approximately 45 minutes prior to sampling. (Note: The number of tablets and time before sampling may change depending on environmental conditions, especially soil moisture.)
4. Place the cap on your soil chamber, place one needle into the vent septum, and start the stopwatch. Immediately remove 10 mL of gas using the syringe and a second needle, and then place the gas sample in an evacuated container.
5. Repeat at 10, 20, and 30 minutes after the time that the cap was placed on the soil chamber.
6. Remove the cap from the soil chamber.
7. In the lab, use the gas chromatograph to measure gas flux. For methane and nitrous oxide using the GC in the Soil & Water Lab, the method is "NOMEAC_3". This method also measures acetylene to confirm inhibition of nitrous oxide reduction.
8. Calculate the concentrations of gases using standard curves.
9. To calculate flux rates, plot take the slope of the linear regression lines for Gas Concentration *vs*. Time.
10. To convert this flux rate from ppm/min to $mg/m^2/h^1$, you will need the headspace volume of the chamber with the cap on, surface area of the chamber, and the molecular weight of the gas of interest. Calculate a conversion factor which is equal:

$$Conversion\ Factor = Headspace\ Volume * Molecular\ Weight\ of\ Gas$$

To calculate specific elemental flux (e.g., mg CH_4-C instead of mg CH_4, use the molecular fraction of the element of interest for the molecular weight. The flux rate ($mg/m^2/h^1$) is then calculated as:

$$Flux\ Rate\ \left(\frac{mg}{m^2h}\right) = \frac{\left(Slope\ of\ Linear\ Regression\ in \frac{ppm}{min}\right) * Conversion\ Factor}{(Surface\ Area\ of\ the\ Chamber) * 60}$$

REFERENCES

1. Davis, J.B. and H.F. Yarbrough, *Preliminary experiments on a microbial fuel cell.* Science, 1962. **137**(3530): p. 615-&.
2. Potter, M.C., *Electrical effects accompanying the decomposition of organic compounds.* Proceedings of the Royal Society of London Series B, 1911. **84**(571): p. 260-276.
3. Cohen, B., *The bacterial culture as an electrical half-cell.* Bacteriology, 1931. **1931**(21): p. 18-19.
4. Lovley, D.R., *Powering microbes with electricity: direct electron transfer from electrodes to microbes.* Environmental Microbiology Reports, 2011. **3**(1): p. 27-35.
5. Stams, A.J.M., F.A.M. de Bok, C.M. Plugge, M.H.A. van Eekert, J. Dolfing, and G. Schraa, *Exocellular electron transfer in anaerobic microbial communities.* Environmental Microbiology, 2006. **8**(3): p. 371-382.
6. Rabaey, K., N. Boon, M. Hofte, and W. Verstraete, *Microbial phenazine production enhances electron transfer in biofuel cells.* Environmental Science & Technology, 2005. **39**(9): p. 3401-8.
7. Reguera, G., K.D. McCarthy, T. Mehta, J.S. Nicoll, M.T. Tuominen, and D.R. Lovley, *Extracellular electron transfer via microbial nanowires.* Nature, 2005. **435**(7045): p. 1098-101.
8. Bond, D.R. and D.R. Lovley, *Electricity production by Geobacter sulfurreducens attached to electrodes.* Applied and Environment Microbiology, 2003. **69**(3): p. 1548-55.
9. Venkataraman, A., M. Rosenbaum, J.B.A. Arends, R. Halitschke, and L.T. Angenent, *Quorum sensing regulates electric current generation of Pseudomonas aeruginosa PA14 in bioelectrochemical systems.* Electrochemistry Communications, 2010. **12**(3): p. 459-462.
10. Dekker, A., A. Ter Heijne, M. Saakes, H.V.M. Hamelers, and C.J.N. Buisman, *Analysis and improvement of a scaled-up and stacked microbial fuel cell.* Environmental Science & Technology, 2009. **43**(23): p. 9038-9042.
11. Logan, B.E., *Scaling up microbial fuel cells and other bioelectrochemical systems.* Applied Microbiology and Biotechnology, 2010. **85**(6): p. 1665-71.
12. Rozendal, R.A., H.V.M. Hamelers, K. Rabaey, J. Keller, and C.J.N. Buisman, *Towards practical implementation of bioelectrochemical wastewater treatment.* Trends in Biotechnology, 2008. **26**(8): p. 450-459.
13. Lovley, D.R., *Microbial fuel cells: novel microbial physiologies and engineering approaches.* Current Opinion in Biotechnology, 2006. **17**(3): p. 327-332.
14. Borole, A.P., C.Y. Hamilton, T.A. Vishnivetskaya, D. Leak, C. Andras, J. Morrell-Falvey, M. Keller, and B. Davison, *Integrating engineering design improvements with exoelectrogen enrichment process to increase power output from microbial fuel cells.* Journal of Power Sources, 2009. **191**(2): p. 520-527.
15. Lovley, D.R., S.J. Giovannoni, D.C. White, J.E. Champine, E.J.P. Phillips, Y.A. Gorby, and S. Goodwin, *Geobacter-Metallireducens Gen-Nov Sp-Nov, a microorganism capable of coupling the complete oxidation of organic-compounds to the reduction of iron and other metals.* Archives of Microbiology, 1993. **159**(4): p. 336-344.
16. Lovley, D.R., *Dissimilatory Fe(III) and Mn(IV) reduction.* Microbiological Reviews, 1991. **55**(2): p. 259-287.
17. Burdige, D.J. and K.H. Nealson, *Microbial manganese reduction by enrichment cultures from coastal marine-sediments.* Applied and Environmental Microbiology, 1985. **50**(2): p. 491-497.
18. Nealson, K.H., B.M. Tebo, and R.A. Rosson, *Occurrence and mechanisms of microbial oxidation of manganese.* Advances in Applied Microbiology, 1988. **33**: p. 279-318.
19. Chapnick, S.D., W.S. Moore, and K.H. Nealson, *Microbially mediated manganese oxidation in a fresh-water lake.* Limnology and Oceanography, 1982. **27**(6): p. 1004-1014.

20. Rabaey, K. and W. Verstraete, *Microbial fuel cells: novel biotechnology for energy generation.* Trends in Biotechnology, 2005. **23**(6): p. 291-8.
21. Rabaey, K., N. Boon, S.D. Siciliano, M. Verhaege, and W. Verstraete, *Biofuel cells select for microbial consortia that self-mediate electron transfer.* Applied and Environmental Microbiology, 2004. **70**(9): p. 5373-82.
22. Gorby, Y.A., S. Yanina, J.S. McLean, K.M. Rosso, D. Moyles, A. Dohnalkova, T.J. Beveridge, I.S. Chang, B.H. Kim, K.S. Kim, D.E. Culley, S.B. Reed, M.F. Romine, D.A. Saffarini, E.A. Hill, L. Shi, D.A. Elias, D.W. Kennedy, G. Pinchuk, K. Watanabe, S. Ishii, B. Logan, K.H. Nealson, and J.K. Fredrickson, *Electrically conductive bacterial nanowires produced by Shewanella oneidensis strain MR-1 and other microorganisms.* Proceedings of the National Academy of Sciences of the United States of America, 2006. **103**(30): p. 11358-63.
23. Picioreanu, C., I.M. Head, K.P. Katuri, M.C.M. van Loosdrecht, and K. Scott, *A computational model for biofilm-based microbial fuel cells.* Water Research, 2007. **41**: p. 2921-2940.
24. Lovley, D.R., *The microbe electric: conversion of organic matter to electricity.* Current Opinion in Biotechnology, 2008. **19**(6): p. 564-71.
25. Marcus, A.K., C.I. Torres, and B.E. Rittmann, *Conduction-based modeling of the biofilm anode of a microbial fuel cell.* Biotechnology and Bioengineering, 2007. **98**(6): p. 1171-1182.
26. Harris, H.W., M.Y. El-Naggar, O. Bretschger, M.J. Ward, M.F. Romine, A.Y. Obraztsova, and K.H. Nealson, *Electrokinesis is a microbial behavior that requires extracellular electron transport.* Proceedings of the National Academy of Sciences of the United States of America, 2010. **107**(1): p. 326-331.
27. Okamoto, A., R. Nakamura, and K. Hashimoto. *In-vivo electrochemistry of flavin-mediated extracellular electron transfer in Shewanella biofilm*. in *3rd International Microbial Fuel Cell Conference*. 2011. Leeuwarden, The Netherlands.
28. Okamoto, A., R. Nakamura, K. Ishii, and K. Hashimoto, *In vivo electrochemistry of c-type cytochrome-mediated electron-transfer with chemical marking.* Chembiochem : A European Journal of Chemical Biology, 2009. **10**(14): p. 2329-2332.
29. Fornero, J.J., M. Rosenbaum, and L.T. Angenent, *Electric power generation from municipal, food, and animal wastewaters using microbial fuel cells.* Electroanalysis, 2010. **22**(7-8): p. 832-843.
30. Zhang, B., H. Zhao, S. Zhou, C. Shi, C. Wang, and J. Ni, *A novel UASB-MFC-BAF integrated system for high strength molasses wastewater treatment and bioelectricity generation.* Bioresource Technology, 2009. **100**(23): p. 5687-93.
31. Lu, N., Zhou, S. Zhang, J., Ni, J., *Electricity generation from starch processing wastewater using microbial fuel cell technology.* Biochemical Engineering Journal, 2009. **43**(3): p. 246-251.
32. Greenman, J., Galvez, A. Giusti, L. Jerepoulous, I., *Electricity from landfill leachate using microbial fuel cells; comparison with a biological aerated filter.* Enzyme and Microbial Technology, 2009. **44**: p. 112-119.
33. Sun, J., Y.Y. Hu, Z. Bi, and Y.Q. Cao, *Simultaneous decolorization of azo dye and bioelectricity generation using a microfiltration membrane air-cathode single-chamber microbial fuel cell.* Bioresource Technology, 2009. **100**(13): p. 3185-92.
34. Min, B. and B.E. Logan, *Continuous electricity generation from domestic wastewater and organic substrates in a flat plate microbial fuel cell.* Environmental Science & Technology, 2004. **38**(21): p. 5809-5814.
35. Adzic, R.R., ed. *Electrocatalysis*. Frontiers in electrochemistry, ed. J. Lipkowski and P.N. Ross. Vol. 5. 1998, VCH Publishers: New York. 197-241.
36. Tarasevich, M.R., Sadkowski, and E. Yeager, eds. *Comprehensive treatise of electrochemistry*. ed. B.E. Conway, et al. Vol. 7. 1983, Plenum Press: New York. 301-398.

37. Wang, J.X., N.M. Markovic, and R.R. Adzic, *Kinetic analysis of oxygen reduction on Pt(111) in acid solutions: Intrinsic kinetic parameters and anion adsorption effects.* Journal of Physical Chemistry B, 2004. **108**(13): p. 4127-4133.
38. Oh, S., B. Min, and B.E. Logan, *Cathode performance as a factor in electricity generation in microbial fuel cells.* Environmental Science & Technology, 2004. **38**(18): p. 4900-4904.
39. Rabaey, K. and R.A. Rozendal, *Microbial electrosynthesis - revisiting the electrical route for microbial production.* Nature Reviews Microbiology, 2010. **8**(10): p. 706-716.
40. Rabaey, K., G. Lissens, S.D. Siciliano, and W. Verstraete, *A microbial fuel cell capable of converting glucose to electricity at high rate and efficiency.* Biotechnology Letters, 2003. **25**(18): p. 1531-5.
41. Logan, B.E., B. Hamelers, R. Rozendal, U. Schroder, J. Keller, S. Freguia, P. Aelterman, W. Verstraete, and K. Rabaey, *Microbial fuel cells: methodology and technology.* Environmental Science & Technology, 2006. **40**(17): p. 5181-92.
42. He, Z. and L.T. Angenent, *Application of bacterial biocathodes in microbial fuel cells.* Electroanalysis, 2006. **18**(19-20): p. 2009-2015.
43. Fornero, J.J., M. Rosenbaum, M.A. Cotta, and L.T. Angenent, *Carbon dioxide addition to microbial fuel cell cathodes maintains sustainable catholyte pH and improves anolyte pH, alkalinity, and conductivity.* Environmental Science & Technology, 2010. **44**(7): p. 2728-2734.
44. Torres, C.I., A.K. Marcus, and B.E. Rittmann, *Proton transport inside the biofilm limits electrical current generation by anode-respiring bacteria.* Biotechnology and Bioengineering, 2008. **100**(5): p. 872-881.
45. Franks, A.E., N. Malvankar, and K.P. Nevin, *Bacterial biofilms: the powerhouse of a microbial fuel cell.* Biofuels, 2010. **1**(4): p. 589-604.
46. Nevin, K.P., B.C. Kim, R.H. Glaven, J.P. Johnson, T.L. Woodard, B.A. Methe, R.J. DiDonato, S.F. Covalla, A.E. Franks, A. Liu, and D.R. Lovley, *Anode biofilm transcriptomics reveals outer surface components essential for high density current production in Geobacter sulfurreducens fuel cells.* PLoS One, 2009. **4**(5).
47. Yuan, Y., B. Zhao, S.G. Zhou, S.K. Zhong, and L. Zhuang, *Electrocatalytic activity of anodic biofilm responses to pH changes in microbial fuel cells.* Bioresource Technology, 2011. **102**(13): p. 6887-6891.
48. Zhuang, L., S.G. Zhou, Y.T. Li, and Y. Yuan, *Enhanced performance of air-cathode two-chamber microbial fuel cells with high-pH anode and low-pH cathode.* Bioresource Technology, 2010. **101**(10): p. 3514-3519.
49. Fornero, J.J., M. Rosenbaum, M.A. Cotta, and L.T. Angenent, *Microbial fuel cell performance with a pressurized cathode chamber.* Environmental Science & Technology, 2008. **42**(22): p. 8578-8584.
50. Fornero, J.J., *Improving the cathode conditions by pressurizing and carbon dioxide addition to enhance the practicality of MFC treatment of wastewater*, in *Department of Energy, Environmental, and Chemical Engineering*2009, Washington University in St. Louis: St. Louis. p. 238.
51. Harnisch, F. and U. Schroder, *From MFC to MXC: chemical and biological cathodes and their potential for microbial bioelectrochemical systems.* Chemical Society Reviews, 2010. **39**(11): p. 4433-4448.
52. Pinto, R.P., B. Srinivasan, S.R. Guiot, and B. Tartakousky, *The effect of real-time external resistance optimization on microbial fuel cell performance.* Water Research, 2011. **45**(4): p. 1571-1578.

53. Woodward, L., M. Perrier, B. Srinivasan, R.P. Pinto, and B. Tartakovsky, *Comparison of Real-Time Methods for Maximizing Power Output in Microbial Fuel Cells.* Aiche Journal, 2010. **56**(10): p. 2742-2750.
54. Woodward, L., M. Perrier, B. Srinivasan, and B. Tartakovsky, *Maximizing Power Production in a Stack of Microbial Fuel Cells Using Multiunit Optimization Method.* Biotechnology Progress, 2009. **25**(3): p. 676-682.
55. Gopinath, A.V. and D. Russell, *An inexpensive field-portable programmable potentiostat.* Chemical Educator, 2006. **11**(1): p. 23-28.
56. Fricke, K., F. Harnisch, and U. Schroder, *On the use of cyclic voltammetry for the study of anodic electron transfer in microbial fuel cells.* Energy & Environmental Science, 2008. **1**(1): p. 144-147.
57. Vieira, M.J., I.A. Pinho, S. Giao, and M.I. Montenegro, *The use of cyclic voltammetry to detect biofilms formed by Pseudomonas fluorescens on platinum electrodes.* Biofouling, 2003. **19**(4): p. 215-222.
58. Barsoukov, E. and J.R. Macdonald, *Impedance Spectroscopy Theory, Experiment, and Applications*. 2nd ed. 2005, Hoboken, NJ: Wiley-Interscience.
59. He, Z., N. Wagner, S.D. Minteer, and L.T. Angenent, *An upflow microbial fuel cell with an interior cathode: assessment of the internal resistance by impedance spectroscopy.* Environmental Science & Technology, 2006. **40**(17): p. 5212-5217.
60. He, Z. and F. Mansfeld, *Exploring the use of electrochemical impedance spectroscopy (EIS) in microbial fuel cell studies.* Energy & Environmental Science, 2009. **2**(2): p. 215-219.
61. Smith, L.S., *Impedance spectroscopy theory, experiment, and applications.* Choice: Current Reviews for Academic Libraries, 2005. **43**(1): p. 130-130.
62. Manohar, A.K., O. Bretschger, K.H. Nealson, and F. Mansfeld, *The use of electrochemical impedance spectroscopy (EIS) in the evaluation of the electrochemical properties of a microbial fuel cell.* Bioelectrochemistry, 2008. **72**(2): p. 149-154.
63. Min, B.K., S.A. Cheng, and B.E. Logan, *Electricity generation using membrane and salt bridge microbial fuel cells.* Water Research, 2005. **39**(9): p. 1675-1686.
64. Oh, S.E. and B.E. Logan, *Proton exchange membrane and electrode surface areas as factors that affect power generation in microbial fuel cells.* Applied Microbiology and Biotechnology, 2006. **70**(2): p. 162-9.
65. Lettinga, G., A.F.M. Vanvelsen, S.W. Hobma, W. Dezeeuw, and A. Klapwijk, *Use of the upflow sludge blanket (USB) reactor concept for biological wastewater-treatment, especially for anaerobic treatment.* Biotechnology and Bioengineering, 1980. **22**(4): p. 699-734.
66. Rabaey, K., P. Clauwaert, P. Aelterman, and W. Verstraete, *Tubular microbial fuel cells for efficient electricity generation.* Environmental Science & Technology, 2005. **39**(20): p. 8077-8082.
67. He, Z., S.D. Minteer, and L.T. Angenent, *Electricity generation from artificial wastewater using an upflow microbial fuel cell.* Environmental Science & Technology, 2005. **39**(14): p. 5262-7.
68. Kim, B., I.S. Chang, J.K. Jang, and G.C. Gil, *Membraneless and mediatorless microbial fuel cell*, 2003.
69. Reimers, C.E., L.M. Tender, S. Fertig, and W. Wang, *Harvesting energy from the marine sediment--water interface.* Environmental Science & Technology, 2001. **35**(1): p. 192-5.
70. Tender, L.M., C.E. Reimers, H.A. Stecher, 3rd, D.E. Holmes, D.R. Bond, D.A. Lowy, K. Pilobello, S.J. Fertig, and D.R. Lovley, *Harnessing microbially generated power on the seafloor.* Nature Biotechnology, 2002. **20**(8): p. 821-5.
71. Nielsen, M.E., C.E. Reimers, and H.A. Stecher, 3rd, *Enhanced power from chambered benthic microbial fuel cells.* Environmental Science & Technology, 2007. **41**(22): p. 7895-900.

72. Nielsen, M.E., *Utilization of natural and supplemental biofuels for harvesting energy from marine sediments*, in *College of Oceanic and Atmospheric Sciences*2008, Oregon State Univeristy: Corvallis, OR. p. 137.
73. Rabaey, K., L.T. Angenent, U. Schroder, and J. Keller, eds. *Bioelectrochemical systems: from extracellular electron transfer to biotechnological application*. 2010, IWA Publishing: London, UK.
74. He, Z., H.B. Shao, and L.T. Angenent, *Increased power production from a sediment microbial fuel cell with a rotating cathode.* Biosensors and Bioelectronics, 2007. **22**(12): p. 3252-3255.
75. Tender, L.M., S.A. Gray, E. Groveman, D.A. Lowy, P. Kauffman, J. Melhado, R.C. Tyce, D. Flynn, R. Petrecca, and J. Dobarro, *The first demonstration of a microbial fuel cell as a viable power supply: powering a meteorological buoy.* Journal of Power Sources, 2008. **179**(2): p. 571-575.
76. Donovan, C., A. Dewan, D. Heo, and H. Beyenal, *Batteryless, wireless sensor powered by a sediment microbial fuel cell.* Environmental Science & Technology, 2008. **42**(22): p. 8591-8596.
77. Dumas, C., A. Mollica, D. Feron, R. Basseguy, L. Etcheverry, and A. Bergel, *Marine microbial fuel cell: use of stainless steel electrodes as anode and cathode materials.* Electrochimica Acta, 2007. **53**(2): p. 468-473.
78. Ter Heijne, A., H.V.M. Hamelers, V. De Wilde, R.A. Rozendal, and C.J.N. Buisman, *A bipolar membrane combined with ferric iron reduction as an efficient cathode system in microbial fuel cells.* Environmental Science & Technology, 2006. **40**(17): p. 5200-5205.
79. Rabaey, K., S.T. Read, P. Clauwaert, S. Freguia, P.L. Bond, L.L. Blackall, and J. Keller, *Cathodic oxygen reduction catalyzed by bacteria in microbial fuel cells.* Isme Journal, 2008. **2**(5): p. 519-527.
80. Zuo, Y., S. Cheng, and B.E. Logan, *Ion exchange membrane cathodes for scalable microbial fuel cells.* Environmental Science & Technology, 2008. **42**(18): p. 6967-6972.
81. Cheng, S.A. and B.E. Logan, *Ammonia treatment of carbon cloth anodes to enhance power generation of microbial fuel cells.* Electrochemistry Communications, 2007. **9**(3): p. 492-496.
82. Niessen, J., U. Schroder, M. Rosenbaum, and F. Scholz, *Fluorinated polyanilines as superior materials for electrocatalytic anodes in bacterial fuel cells.* Electrochemistry Communications, 2004. **6**(6): p. 571-575.
83. Liu, H., R. Ramnarayanan, and B.E. Logan, *Production of electricity during wastewater treatment using a single chamber microbial fuel cell.* Environmental Science & Technology, 2004. **38**(7): p. 2281-5.
84. Zhao, F., F. Harnisch, U. Schroder, F. Scholz, P. Bogdanoff, and I. Herrmann, *Application of pyrolysed iron(II) phthalocyanine and CoTMPP based oxygen reduction catalysts as cathode materials in microbial fuel cells.* Electrochemistry Communications, 2005. **7**(12): p. 1405-1410.
85. Rosenbaum, M., F. Aulenta, M. Villano, and L.T. Angenent, *Cathodes as electron donors for microbial metabolism: Which extracellular electron transfer mechanisms are involved?* Bioresource Technology, 2011. **102**(1): p. 324-333.
86. Schroder, U., J. Niessen, and F. Scholz, *A generation of microbial fuel cells with current outputs boosted by more than one order of magnitude.* Angewandte Chemie, 2003. **42**(25): p. 2880-3.
87. Gil, G.C., I.S. Chang, B.H. Kim, M. Kim, J.K. Jang, H.S. Park, and H.J. Kim, *Operational parameters affecting the performannce of a mediator-less microbial fuel cell.* Biosensors and Bioelectronics, 2003. **18**(4): p. 327-34.
88. Rozendal, R.A., H.V. Hamelers, and C.J. Buisman, *Effects of membrane cation transport on pH and microbial fuel cell performance.* Environmental Science & Technology, 2006. **40**(17): p. 5206-11.

89. Harnisch, F., U. Schroder, and F. Scholz, *The suitability of monopolar and bipolar ion exchange membranes as separators for biological fuel cells.* Environmental Science & Technology, 2008. **42**(5): p. 1740-1746.
90. Rozendal, R.A., T.H.J.A. Sleutels, C.J.N. Buisman, and H.V.M. Hamelers, *Effect of the type of ion exchange membrane on performance, ion transport, and pH in biocatalyzed electrolysis of wastewater.* Water Science & Technology, 2008. **57**(11): p. 1757-1762.
91. Harnisch, F., R. Warmbier, R. Schneider, and U. Schroder, *Modeling the ion transfer and polarization of ion exchange membranes in bioelectrochemical systems.* Bioelectrochemistry, 2009. **75**(2): p. 136-141.
92. Sleutels, T.H.J.A., H.V.M. Hamelers, and C.J.N. Buisman, *Effect of mass and charge transport speed and direction in porous anodes on microbial electrolysis cell performance.* Bioresource Technology, 2011. **102**(1): p. 399-403.
93. Liu, H. and B.E. Logan, *Electricity generation using an air-cathode single chamber microbial fuel cell in the presence and absence of a proton exchange membrane.* Environmental Science & Technology, 2004. **38**(14): p. 4040-4046.
94. Fan, Y.Z., H.Q. Hu, and H. Liu, *Enhanced coulombic efficiency and power density of air-cathode microbial fuel cells with an improved cell configuration.* Journal of Power Sources, 2007. **171**(2): p. 348-354.
95. Rosenbaum, M., M.A. Cotta, and L.T. Angenent, *Aerated Shewanella oneidensis in continuously fed bioelectrochemical systems for power and hydrogen production.* Biotechnology and Bioengineering, 2010. **105**(5): p. 880-888.
96. Foley, J.M., R.A. Rozendal, C.K. Hertle, P.A. Lant, and K. Rabaey, *Life Cycle Assessment of High-Rate Anaerobic Treatment, Microbial Fuel Cells, and Microbial Electrolysis Cells.* Environmental Science & Technology, 2010. **44**(9): p. 3629-3637.
97. Franks, A.E. and K.P. Nevin, *Microbial fuel cells, a current review.* Energies, 2010. **3**(5): p. 899-919.
98. Nevin, K.P., T.L. Woodard, A.E. Franks, Z.M. Summers, and D.R. Lovley, *Microbial electrosynthesis: feeding microbes electricity to convert carbon dioxide and water to multicarbon extracellular organic compounds.* Mbio, 2010. **1**(2).
99. Liu, H., S. Grot, and B.E. Logan, *Electrochemically assisted microbial production of hydrogen from acetate.* Environmental Science & Technology, 2005. **39**(11): p. 4317-4320.
100. Rozendal, R.A., H.V.M. Hamelers, G.J.W. Euverink, S.J. Metz, and C.J.N. Buisman, *Principle and perspectives of hydrogen production through biocatalyzed electrolysis.* International Journal of Hydrogen Energy, 2006. **31**(12): p. 1632-1640.
101. Clauwaert, P., R. Toledo, D. Van der Ha, R. Crab, W. Verstraete, H. Hu, K.M. Udert, and K. Rabaey, *Combining biocatalyzed electrolysis with anaerobic digestion.* Water Science & Technology, 2008. **57**(4): p. 575-579.
102. Villano, M., F. Aulenta, M. Beccaru, and M. Majone, *Microbial generation of H_2 or CH_4 coupled to wastewater treatment in bioelectrochemical systems.* Chemical Engineering Transactions, 2010. **20**: p. 163-168.
103. Cheng, S.A., D.F. Xing, D.F. Call, and B.E. Logan, *Direct biological conversion of electrical current into methane by electromethanogenesis.* Environmental Science & Technology, 2009. **43**(10): p. 3953-3958.
104. Rozendal, R.A., E. Leone, J. Keller, and K. Rabaey, *Efficient hydrogen peroxide generation from organic matter in a bioelectrochemical system.* Electrochemistry Communications, 2009. **11**(9): p. 1752-1755.

105. Strycharz, S.M., S.M. Gannon, A.R. Boles, A.E. Franks, K.P. Nevin, and D.R. Lovley, *Reductive dechlorination of 2-chlorophenol by Anaeromyxobacter dehalogenans with an electrode serving as the electron donor.* Environmental Microbiology Reports, 2010. **2**(2): p. 289-294.
106. Strycharz, S.M., T.L. Woodard, J.P. Johnson, K.P. Nevin, R.A. Sanford, F.E. Loffler, and D.R. Lovley, *Graphite electrode as a sole electron donor for reductive dechlorination of tetrachlorethene by Geobacter lovleyi.* Applied and Environmental Microbiology, 2008. **74**(19): p. 5943-5947.
107. Aulenta, F., A. Canosa, M. Majone, S. Panero, P. Reale, and S. Rossetti, *Trichloroethene dechlorination and H-2 evolution are alternative biological pathways of electric charge utilization by a dechlorinating culture in a bioelectrochemical system.* Environmental Science & Technology, 2008. **42**(16): p. 6185-6190.
108. Wang, H.Y. and J.H. Qu, *Combined bioelectrochemical and sulfur autotrophic denitrification for drinking water treatment.* Water Research, 2003. **37**(15): p. 3767-3775.
109. Clauwaert, P., K. Rabaey, P. Aelterman, L. De Schamphelaire, T.H. Ham, P. Boeckx, N. Boon, and W. Verstraete, *Biological denitrification in microbial fuel cells.* Environmental Science & Technology, 2007. **41**(9): p. 3354-3360.
110. Gregory, K.B. and D.R. Lovley, *Remediation and recovery of uranium from contaminated subsurface environments with electrodes.* Environmental Science & Technology, 2005. **39**(22): p. 8943-8947.
111. Schink, B., *Energetics of syntrophic cooperation in methanogenic degradation.* Microbiology and Molecular Biology Reviews, 1997. **61**(2): p. 262-&.
112. Thauer, R.K., K. Jungermann, and K. Decker, *Energy conservation in chemotrophic anaerobic bacteria.* Bacteriological Reviews, 1977. **41**(1): p. 100-180.
113. Du, X., B. Boonchayaanant, W.-M. Wu, S. Fendorf, J. Bargar, and C.S. Criddle, *Reduction of uranium(VI) by soluble iron(II) conforms with thermodynamic predictions.* Environmental Science & Technology, 2011. **45**(11): p. 4718-4725.
114. Dolfing, J. and D.B. Janssen, *Estimates of Gibbs free energies of formation of chlorinated aliphatic compounds.* Biodegradation, 1994. **5**(1): p. 21-28.
115. Dolfing, J. and B.K. Harrison, *Gibbs free energy of formation of halogenated aromatic compounds and their potential role as electron acceptors in anaerobic environments.* Environmental Science & Technology, 1992. **26**(11): p. 2213-2218.
116. Steinbusch, K.J.J., H.V.M. Hamelers, J.D. Schaap, C. Kampman, and C.J.N. Buisman, *Bioelectrochemical ethanol production through mediated acetate reduction by mixed cultures.* Environmental Science & Technology, 2010. **44**(1): p. 513-517.
117. Cusick, R.D., B. Bryan, D.S. Parker, M.D. Merrill, M. Mehanna, P.D. Kiely, G.L. Liu, and B.E. Logan, *Performance of a pilot-scale continuous flow microbial electrolysis cell fed winery wastewater.* Applied Microbiology and Biotechnology, 2011. **89**(6): p. 2053-2063.
118. Turner, J.A., *Sustainable hydrogen production.* Science, 2004. **305**(5686): p. 972-974.
119. Ditzig, J., H. Liu, and B.E. Logan, *Production of hydrogen from domestic wastewater using a bioelectrochemically assisted microbial reactor (BEAMR).* International Journal of Hydrogen Energy, 2007. **32**(13): p. 2296-2304.
120. Hamelers, H.V.M., A. Ter Heijne, T.H.J.A. Sleutels, A.W. Jeremiasse, D.P.B.T.B. Strik, and C.J.N. Buisman, *New applications and performance of bioelectrochemical systems.* Applied Microbiology and Biotechnology, 2010. **85**(6): p. 1673-1685.
121. Hori, Y., A. Murata, and R. Takahashi, *Formation of hydrocarbons in the electrochemical reduction of carbon-dioxide at a copper electrode in aqueous-solution.* Journal of the Chemical Society, Faraday Transactions 1: Physical Chemistry in Condensed Phases, 1989. **85**: p. 2309-2326.

122. Agler, M.T., M.L. Garcia, E.S. Lee, M. Schlicher, and L.T. Angenent, *Thermophilic anaerobic digestion to increase the net energy balance of corn grain ethanol.* Environmental Science & Technology, 2008. **42**(17): p. 6723-6729.
123. Ragauskas, A.J., C.K. Williams, B.H. Davison, G. Britovsek, J. Cairney, C.A. Eckert, W.J. Frederick, J.P. Hallett, D.J. Leak, C.L. Liotta, J.R. Mielenz, R. Murphy, R. Templer, and T. Tschaplinski, *The path forward for biofuels and biomaterials.* Science, 2006. **311**(5760): p. 484-489.
124. Marsili, E., D.B. Baron, I.D. Shikhare, D. Coursolle, J.A. Gralnick, and D.R. Bond, *Shewanella secretes flavins that mediate extracellular electron transfer.* Proceedings of the National Academy of Sciences of the United States of America, 2008. **105**(10): p. 3968-3973.
125. von Canstein, H., J. Ogawa, S. Shimizu, and J.R. Lloyd, *Secretion of flavins by Shewanella species and their role in extracellular electron transfer.* Applied and Environmental Microbiology, 2008. **74**(3): p. 615-623.
126. Campos-Martin, J.M., G. Blanco-Brieva, and J.L. Fierro, *Hydrogen peroxide synthesis: an outlook beyond the anthraquinone process.* Angewandte Chemie International Edition, 2006. **45**(42): p. 6962-84.
127. Lozano, J. *Enhanced anaerobic digestion using Fenton's reagent*. in *83rd Annual Water Environment Federation Technical Exhibition and Conference (WEFTEC)*. 2010. New Orleans, LA.
128. Pletcher, D., *Indirect oxidations using electrogenerated hydrogen peroxide.* Acta Chemica Scandinavica, 1999. **53**(10): p. 745-750.
129. Oloman, C. and A.P. Watkinson, *Hydrogen-Peroxide Production in Trickle-Bed Electrochemical Reactors.* Journal of Applied Electrochemistry, 1979. **9**(1): p. 117-123.
130. Brillas, E., F. Alcaide, and P.L. Cabot, *A small-scale flow alkaline fuel cell for on-site production of hydrogen peroxide.* Electrochimica Acta, 2002. **48**(4): p. 331-340.
131. Brillas, E., A. Maestro, M. Moratalla, and J. Casado, *Electrochemical extraction of oxygen from air via hydroperoxide ion.* Journal of Applied Electrochemistry, 1997. **27**(1): p. 83-92.
132. Alvarez-Gallegos, A. and D. Pletcher, *The removal of low level organics via hydrogen peroxide formed in a reticulated vitreous carbon cathode cell, Part 1. The electrosynthesis of hydrogen peroxide in aqueous acidic solutions.* Electrochimica Acta, 1998. **44**(5): p. 853-861.
133. Qiang, Z.M., J.H. Chang, and C.P. Huang, *Electrochemical generation of hydrogen peroxide from dissolved oxygen in acidic solutions.* Water Research, 2002. **36**(1): p. 85-94.
134. Rabaey, K., S. Butzer, S. Brown, J. Keller, and R.A. Rozendal, *High Current Generation Coupled to Caustic Production Using a Lamellar Bioelectrochemical System.* Environmental Science & Technology, 2010. **44**(11): p. 4315-4321.
135. Kyazze, G., A. Popov, R. Dinsdale, S. Esteves, F. Hawkes, G. Premier, and A. Guwy, *Influence of catholyte pH and temperature on hydrogen production from acetate using a two chamber concentric tubular microbial electrolysis cell.* International Journal of Hydrogen Energy, 2010. **35**(15): p. 7716-7722.
136. Hu, H.Q., Y.Z. Fan, and H. Liu, *Hydrogen production using single-chamber membrane-free microbial electrolysis cells.* Water Research, 2008. **42**(15): p. 4172-4178.
137. Freguia, S., K. Rabaey, Z. Yuan, and J. Keller, *Non-catalyzed cathodic oxygen reduction at graphite granules in microbial fuel cells.* Electrochimica Acta, 2007. **53**(2): p. 598-603.
138. Olivares-Ramirez, J.M., M.L. Campos-Cornelio, J.U. Godinez, E. Borja-Arco, and R.H. Castellanos, *Studies on the hydrogen evolution reaction on different stainless steels.* International Journal of Hydrogen Energy, 2007. **32**(15): p. 3170-3173.
139. Call, D.F., M.D. Merrill, and B.E. Logan, *High surface area stainless steel brushes as cathodes in microbial electrolysis cells.* Environmental Science & Technology, 2009. **43**(6): p. 2179-2183.
140. Yang, K.S., G. Mul, and J.A. Moulijn, *Electrochemical generation of hydrogen peroxide using surface area-enhanced Ti-mesh electrodes.* Electrochimica Acta, 2007. **52**(22): p. 6304-6309.

141. Cheng, S.A. and B.E. Logan, *High hydrogen production rate of microbial electrolysis cell (MEC) with reduced electrode spacing.* Bioresource Technology, 2011. **102**(3): p. 3571-3574.
142. Tartakovsky, B., M.F. Manuel, H. Wang, and S.R. Guiot, *High rate membrane-less microbial electrolysis cell for continuous hydrogen production.* International Journal of Hydrogen Energy, 2009. **34**(2): p. 672-677.
143. Aelterman, P., K. Rabaey, H. The Pham, N. Boon, and W. Verstraete, *Continuous electricity generation at high voltages and currents using stacked microbial fuel cells.* Communications in agricultural and applied biological sciences, 2006. **71**(1): p. 63-6.
144. Oh, S.E. and B.E. Logan, *Voltage reversal during microbial fuel cell stack operation.* Journal of Power Sources, 2007. **167**(1): p. 11-17.
145. Venkataraman, A., M. Rosenbaum, S.D. Perkins, J.M. Werner, and L.T. Angenent, *Metabolite-based mutualism between Pseudomonas aeruginosa PA14 and Enterobacter aerogenes enhances current generation in bioelectrochemical systems.* Energy & Environmental Science, 2011.
146. Torres, C.I., R. Krajmalnik-Brown, P. Parameswaran, A.K. Marcus, G. Wanger, Y.A. Gorby, and B.E. Rittmann, *Selecting Anode-Respiring Bacteria Based on Anode Potential: Phylogenetic, Electrochemical, and Microscopic Characterization.* Environmental Science & Technology, 2009. **43**(24): p. 9519-9524.
147. Li, Z.J., M.A. Rosenbaum, A. Venkataraman, T.K. Tam, E. Katz, and L.T. Angenent, *Bacteria-based AND logic gate: a decision-making and self-powered biosensor.* Chemical Communications, 2011. **47**(11): p. 3060-3062.
148. Burdige, D.J. and K.H. Nealson, *Chemical and Microbiological Studies of Sulfide-Mediated Manganese Reduction.* Geomicrobiology Journal, 1986. **4**(4): p. 361-387.
149. Lovley, D.R., J.D. Coates, E.L. BluntHarris, E.J.P. Phillips, and J.C. Woodward, *Humic substances as electron acceptors for microbial respiration.* Nature, 1996. **382**(6590): p. 445-448.
150. Regnier, P., A.W. Dale, S. Arndt, D.E. LaRowe, J. Mogollon, and P. Van Cappellen, *Quantitative analysis of anaerobic oxidation of methane (AOM) in marine sediments: A modeling perspective.* Earth-Science Reviews, 2011. **106**(1-2): p. 105-130.
151. Bethke, C.M., R.A. Sanford, M.F. Kirk, Q.S. Jin, and T.M. Flynn, *The thermodynamic ladder in geomicrobiology.* American Journal of Science, 2011. **311**(3): p. 183-210.
152. Wagner, D., S. Kobabe, E.M. Pfeiffer, and H.W. Hubberten, *Microbial controls on methane fluxes from a polygonal tundra of the Lena Delta, Siberia.* Permafrost and Periglacial Processes, 2003. **14**(2): p. 173-185.
153. Nemergut, D.R., E.K. Costello, A.F. Meyer, M.Y. Pescador, M.N. Weintraub, and S.K. Schmidt, *Structure and function of alpine and arctic soil microbial communities.* Research in Microbiology, 2005. **156**(7): p. 775-784.
154. Natali, S.M., E.A.G. Schuur, and R.L. Rubin, *Increased plant productivity in Alaskan tundra as a result of experimental warming of soil and permafrost.* Journal of Ecology, 2012. **100**(2): p. 488-498.
155. Dubinsky, E.A., W.L. Silver, and M.K. Firestone, *Tropical forest soil microbial communities couple iron and carbon biogeochemistry.* Ecology, 2010. **91**(9): p. 2604-2612.
156. Chacon, N., W.L. Silver, E.A. Dubinsky, and D.F. Cusack, *Iron reduction and soil phosphorus solubilization in humid tropical forests soils: The roles of labile carbon pools and an electron shuttle compound.* Biogeochemistry, 2006. **78**(1): p. 67-84.
157. Liptzin, D. and W.L. Silver, *Effects of carbon additions on iron reduction and phosphorus availability in a humid tropical forest soil.* Soil Biology & Biochemistry, 2009. **41**(8): p. 1696-1702.
158. Riley, W.J., Z.M. Subin, D.M. Lawrence, S.C. Swenson, M.S. Torn, L. Meng, N.M. Mahowald, and P. Hess, *Barriers to predicting changes in global terrestrial methane fluxes: analyses using*

CLM4Me, a methane biogeochemistry model integrated in CESM. Biogeosciences, 2011. **8**(7): p. 1925-1953.

159. Meng, L., P.G.M. Hess, N.M. Mahowald, J.B. Yavitt, W.J. Riley, Z.M. Subin, D.M. Lawrence, S.C. Swenson, J. Jauhiainen, and D.R. Fuka, *Sensitivity of wetland methane emissions to model assumptions: application and model testing against site observations.* Biogeosciences Discuss., 2011. **8**(3): p. 6095-6160.
160. Tarnocai, C., J.G. Canadell, E.A.G. Schuur, P. Kuhry, G. Mazhitova, and S. Zimov, *Soil organic carbon pools in the northern circumpolar permafrost region.* Global Biogeochemical Cycles, 2009. **23**.
161. Lee, H., E.A.G. Schuur, K.S. Inglett, M. Lavoie, and J.P. Chanton, *The rate of permafrost carbon release under aerobic and anaerobic conditions and its potential effects on climate.* Global Change Biology, 2012. **18**(2): p. 515-527.
162. Pastor, J., J. Solin, S.D. Bridgham, K. Updegraff, C. Harth, P. Weishampel, and B. Dewey, *Global warming and the export of dissolved organic carbon from boreal peatlands.* Oikos, 2003. **100**(2): p. 380-386.
163. Bell, T., K. Callender, L. Whyte, and C. Greer, *Microbial competition in polar soils: a review of an understudied but potentially important control on productivity.* Biology, 2013. **2**(2): p. 533-554.
164. Schmidt, M.W.I., M.S. Torn, S. Abiven, T. Dittmar, G. Guggenberger, I.A. Janssens, M. Kleber, I. Kogel-Knabner, J. Lehmann, D.A.C. Manning, P. Nannipieri, D.P. Rasse, S. Weiner, and S.E. Trumbore, *Persistence of soil organic matter as an ecosystem property.* Nature, 2011. **478**(7367): p. 49-56.
165. Mackelprang, R., M.P. Waldrop, K.M. DeAngelis, M.M. David, K.L. Chavarria, S.J. Blazewicz, E.M. Rubin, and J.K. Jansson, *Metagenomic analysis of a permafrost microbial community reveals a rapid response to thaw.* Nature, 2011. **480**(7377): p. 368-U120.
166. Graham, D.E., M.D. Wallenstein, T.A. Vishnivetskaya, M.P. Waldrop, T.J. Phelps, S.M. Pfiffner, T.C. Onstott, L.G. Whyte, E.M. Rivkina, D.A. Gilichinsky, D.A. Elias, R. Mackelprang, N.C. VerBerkmoes, R.L. Hettich, D. Wagner, S.D. Wullschleger, and J.K. Jansson, *Microbes in thawing permafrost: the unknown variable in the climate change equation.* ISME Journal, 2011.
167. Tront, J.M., J.D. Fortner, M. Plotze, J.B. Hughes, and A.M. Puzrin, *Microbial fuel cell biosensor for in situ assessment of microbial activity.* Biosensors & Bioelectronics, 2008. **24**(4): p. 586-590.
168. Chang, I.S., J.K. Jang, G.C. Gil, M. Kim, H.J. Kim, B.W. Cho, and B.H. Kim, *Continuous determination of biochemical oxygen demand using microbial fuel cell type biosensor.* Biosensors and Bioelectronics, 2004. **19**(6): p. 607-613.
169. Kang, K.H., J.K. Jang, T.H. Pham, H. Moon, I.S. Chang, and B.H. Kim, *A microbial fuel cell with improved cathode reaction as a low biochemical oxygen demand sensor.* Biotechnology Letters, 2003. **25**(16): p. 1357-1361.
170. Kumlanghan, A., J. Liu, P. Thavarungkul, P. Kanatharana, and B. Mattiasson, *Microbial fuel cell-based biosensor for fast analysis of biodegradable organic matter.* Biosensors and Bioelectronics, 2007. **22**(12): p. 2939-2944.
171. Hinkel, K.M., W.R. Eisner, J.G. Bockheim, F.E. Nelson, K.M. Peterson, and X.Y. Dai, *Spatial extent, age, and carbon stocks in drained thaw lake basins on the Barrow Peninsula, Alaska.* Arctic, Antarctic, and Alpine Research, 2003. **35**(3): p. 291-300.
172. Lipson, D.A., M. Jha, T.K. Raab, and W.C. Oechel, *Reduction of iron (III) and humic substances plays a major role in anaerobic respiration in an Arctic peat soil.* Journal of Geophysical Research, 2010. **115**: p. G00I06.
173. Allen, B., D. Willner, W.C. Oechel, and D. Lipson, *Top-down control of microbial activity and biomass in an Arctic soil ecosystem.* Environmental Microbiology, 2010. **12**(3): p. 642-648.

174. Oechel, W.C., G.L. Vourlitis, S.J. Hastings, and S.A. Bochkarev, *Change in Arctic CO_2 flux over 2 decades - effects of climate-change at Barrow, Alaska.* Ecological Applications, 1995. **5**(3): p. 846-855.
175. Bockheim, J.G., K.M. Hinkel, and F.E. Nelson, *Predicting carbon storage in tundra soils of arctic Alaska.* Soil Science Society of America Journal, 2003. **67**(3): p. 948-950.
176. Hoj, L., R.A. Olsen, and V.L. Torsvik, *Effects of temperature on the diversity and community structure of known methanogenic groups and other archaea in high Arctic peat.* Isme Journal, 2008. **2**(1): p. 37-48.
177. Metje, M. and P. Frenzel, *Methanogenesis and methanogenic pathways in a peat from subarctic permafrost.* Environmental Microbiology, 2007. **9**(4): p. 954-964.
178. Moore, T.R. and M. Dalva, *Methane and carbon dioxide exchange potentials of peat soils in aerobic and anaerobic laboratory incubations.* Soil Biology & Biochemistry, 1997. **29**(8): p. 1157-1164.
179. Lovley, D.R. and S. Goodwin, *Hydrogen concentrations as an indicator of the predominant terminal electron-accepting reactions in aquatic sediments.* Geochimica Et Cosmochimica Acta, 1988. **52**(12): p. 2993-3003.
180. Lovley, D.R. and E.J.P. Phillips, *Competitive mechanisms for inhibition of sulfate reduction and methane production in the zone of ferric iron reduction in sediments.* Applied and Environmental Microbiology, 1987. **53**(11): p. 2636-2641.
181. Achtnich, C., F. Bak, and R. Conrad, *Competition for electron-donors among nitrate reducers, ferric iron reducers, sulfate reducers, and methanogens in anoxic paddy soil.* Biology and Fertility of Soils, 1995. **19**(1): p. 65-72.
182. Cervantes, F.J., F.A.M. de Bok, D.D. Tuan, A.J.M. Stams, G. Lettinga, and J.A. Field, *Reduction of humic substances by halorespiring, sulphate-reducing and methanogenic microorganisms.* Environmental Microbiology, 2002. **4**(1): p. 51-57.
183. Schuur, E.A.G., J. Bockheim, J.G. Canadell, E. Euskirchen, C.B. Field, S.V. Goryachkin, S. Hagemann, P. Kuhry, P.M. Lafleur, H. Lee, G. Mazhitova, F.E. Nelson, A. Rinke, V.E. Romanovsky, N. Shiklomanov, C. Tarnocai, S. Venevsky, J.G. Vogel, and S.A. Zimov, *Vulnerability of permafrost carbon to climate change: Implications for the global carbon cycle.* Bioscience, 2008. **58**(8): p. 701-714.
184. Schuur, E.A.G., B.W. Abbott, W.B. Bowden, V. Brovkin, P. Camill, J.G. Canadell, J.P. Chanton, F.S. Chapin, III, T.R. Christensen, P. Ciais, B.T. Crosby, C.I. Czimczik, G. Grosse, J. Harden, D.J. Hayes, G. Hugelius, J.D. Jastrow, J.B. Jones, T. Kleinen, C.D. Koven, G. Krinner, P. Kuhry, D.M. Lawrence, A.D. McGuire, S.M. Natali, J.A. O'Donnell, C.L. Ping, W.J. Riley, A. Rinke, V.E. Romanovsky, A.B.K. Sannel, C. Schädel, K. Schaefer, J. Sky, Z.M. Subin, C. Tarnocai, M.R. Turetsky, M.P. Waldrop, K.M. Walter Anthony, K.P. Wickland, C.J. Wilson, and S.A. Zimov, *Expert assessment of vulnerability of permafrost carbon to climate change.* Climatic Change, 2013. **119**(2): p. 359-374.
185. IPCC, *Climate change 2007 : the physical science basis : contribution of Working Group I to the Fourth Assessment Report of the Intergovernmental Panel on Climate Change*, S. Solomon, et al., Editors. 2007, Cambridge University Press: Cambridge ; New York. p. 996.
186. Schuur, E.A.G., B. Abbott, and P.C. Network, *High risk of permafrost thaw.* Nature, 2011. **480**(7375): p. 32-33.
187. Nealson, K.H. and D. Saffarini, *Iron and Manganese in Anaerobic Respiration - Environmental Significance, Physiology, and Regulation.* Annual Review of Microbiology, 1994. **48**: p. 311-343.
188. Venkateswaran, K., M.E. Dollhopf, R. Aller, E. Stackebrandt, and K.H. Nealson, *Shewanella amazonensis sp. nov., a novel metal-reducing facultative anaerobe from Amazonian shelf muds.* International Journal of Systematic Bacteriology, 1998. **48**: p. 965-972.

189. Huang, D.Y., S.G. Zhou, Q. Chen, B. Zhao, Y. Yuan, and L. Zhuang, *Enhanced anaerobic degradation of organic pollutants in a soil microbial fuel cell.* Chemical Engineering Journal, 2011. **172**(2-3): p. 647-653.
190. Morris, J.M., S. Jin, B. Crimi, and A. Pruden, *Microbial fuel cell in enhancing anaerobic biodegradation of diesel.* Chemical Engineering Journal, 2009. **146**(2): p. 161-167.
191. Heitmann, T., T. Goldhammer, J. Beer, and C. Blodau, *Electron transfer of dissolved organic matter and its potential significance for anaerobic respiration in a northern bog.* Global Change Biology, 2007. **13**(8): p. 1771-1785.
192. Keller, J.K. and K.K. Takagi, *Solid-phase organic matter reduction regulates anaerobic decomposition in bog soil.* Ecosphere, 2013. **4**(5): p. art54.
193. Lipson, D.A., T.K. Raab, D. Goria, and J. Zlamal, *The contribution of Fe(III) and humic acid reduction to ecosystem respiration in drained thaw lake basins of the Arctic Coastal Plain.* Global Biogeochemical Cycles, 2013: p. 1-12.
194. Lipson, D.A., M. Jha, T.K. Raab, and W.C. Oechel, *Reduction of iron (III) and humic substances plays a major role in anaerobic respiration in an Arctic peat soil.* Journal of Geophysical Research. G. Biogeosciences, 2010. **115**.
195. Friedman, E.S., M.A. Rosenbaum, A.W. Lee, D.A. Lipson, B.R. Land, and L.T. Angenent, *A cost-effective and field-ready potentiostat that poises subsurface electrodes to monitor bacterial respiration.* Biosensors and Bioelectronics, 2012. **32**(1): p. 309-313.
196. Lonergan, D.J., H.L. Jenter, J.D. Coates, E.J.P. Phillips, T.M. Schmidt, and D.R. Lovley, *Phylogenetic analysis of dissimilatory Fe(III)-reducing bacteria.* Journal of Bacteriology, 1996. **178**(8): p. 2402-2408.
197. Gault, A.G., A. Ibrahim, S. Langley, R. Renaud, Y. Takahashi, C. Boothman, J.R. Lloyd, I.D. Clark, F.G. Ferris, and D. Fortin, *Microbial and geochemical features suggest iron redox cycling within bacteriogenic iron oxide-rich sediments.* Chemical Geology, 2011. **281**(1-2): p. 41-51.
198. Kostka, J.E. and K.H. Nealson, *Dissolution and reduction of magnetite by bacteria.* Environmental Science & Technology, 1995. **29**(10): p. 2535-2540.
199. Inceoglu, O., W. Abu Al-Soud, J.F. Salles, A.V. Semenov, and J.D. van Elsas, *Comparative analysis of bacterial communities in a potato field as determined by pyrosequencing.* Plos One, 2011. **6**(8).
200. Hou, S.B., K.S. Makarova, J.H.W. Saw, P. Senin, B.V. Ly, Z.M. Zhou, Y. Ren, J.M. Wang, M.Y. Galperin, M.V. Omelchenko, Y.I. Wolf, N. Yutin, E.V. Koonin, M.B. Stott, B.W. Mountain, M.A. Crowe, A.V. Smirnova, P.F. Dunfield, L. Feng, L. Wang, and M. Alam, *Complete genome sequence of the extremely acidophilic methanotroph isolate V4, Methylacidiphilum infernorum, a representative of the bacterial phylum Verrucomicrobia.* Biology Direct, 2008. **3**.
201. Freitas, S., S. Hatosy, J.A. Fuhrman, S.M. Huse, D.B.M. Welch, M.L. Sogin, and A.C. Martiny, *Global distribution and diversity of marine Verrucomicrobia.* Isme Journal, 2012. **6**(8): p. 1499-1505.
202. Pol, A., K. Heijmans, H.R. Harhangi, D. Tedesco, M.S.M. Jetten, and H.J.M.O. den Camp, *Methanotrophy below pH1 by a new Verrucomicrobia species.* Nature, 2007. **450**(7171): p. 874-U17.
203. Lozupone, C. and R. Knight, *UniFrac: a new phylogenetic method for comparing microbial communities.* Applied and Environmental Microbiology, 2005. **71**(12): p. 8228-8235.
204. Tibshirani, R., T. Hastie, B. Narasimhan, and G. Chu, *Diagnosis of multiple cancer types by shrunken centroids of gene expression.* Proceedings of the National Academy of Sciences, USA, 2002. **99**(10): p. 6567-6572.

205. Erable, B., L. Etcheverry, and A. Bergel, *From microbial fuel cell (MFC) to microbial electrochemical snorkel (MES): maximizing chemical oxygen demand (COD) removal from wastewater.* Biofouling, 2011. **27**(3): p. 319-326.
206. Hoover, C.M., *Field Measurements for Forest Carbon Monitoring: A Landscape Scale Approach*. 2008, New York: Springer Science + Business Media B.V.
207. Friedman, E.S., *Bioelectrochemical systems as tools to study subsurface biogeochemical processes*, in *Department of Biological & Environmental Engineering*2013, Cornell University.
208. Callaghan, T.V., L.O. Bjorn, Y. Chernov, T. Chapin, T.R. Christensen, B. Huntley, R.A. Ims, M. Johansson, D. Jolly, S. Jonasson, N. Matveyeva, N. Panikov, W. Oechel, and G. Shaver, *Effects on the function of arctic ecosystems in the short- and long-term perspectives.* Ambio, 2004. **33**(7): p. 448-458.
209. Agler, M.T., B.A. Wrenn, S.H. Zinder, and L.T. Angenent, *Waste to bioproduct conversion with undefined mixed cultures: the carboxylate platform.* Trends in Biotechnology, 2011. **29**(2): p. 70-78.
210. Thomas, F., J.H. Hehemann, E. Rebuffet, M. Czjzek, and G. Michel, *Environmental and gut bacteroidetes: the food connection.* Frontiers in Microbiology, 2011. **2**: p. 93.
211. Olefeldt, D. and N.T. Roulet, *Effects of permafrost and hydrology on the composition and transport of dissolved organic carbon in a subarctic peatland complex.* Journal of Geophysical Research-Biogeosciences, 2012. **117**.
212. Lee, H., E.A.G. Schuur, and J.G. Vogel, *Soil CO_2 production in upland tundra where permafrost is thawing.* Journal of Geophysical Research, 2010. **115**(G1).
213. Hinkel, K.M., F. Paetzold, F.E. Nelson, and J.G. Bockheim, *Patterns of soil temperature and moisture in the active layer and upper permafrost at Barrow, Alaska: 1993-1999.* Global and Planetary Change, 2001. **29**(3-4): p. 293-309.
214. Zona, D., W.C. Oechel, J. Kochendorfer, K.T.P. U, A.N. Salyuk, P.C. Olivas, S.F. Oberbauer, and D.A. Lipson, *Methane fluxes during the initiation of a large-scale water table manipulation experiment in the Alaskan Arctic tundra.* Global Biogeochemical Cycles, 2009. **23**.
215. Gilbert, J.A., F. Meyer, J. Jansson, J. Gordon, N. Pace, J. Tiedje, R. Ley, N. Fierer, D. Field, N. Kyrpides, F.O. Glockner, H.P. Klenk, K.E. Wommack, E. Glass, K. Docherty, R. Gallery, R. Stevens, and R. Knight, *The Earth Microbiome Project: Meeting report of the "1st EMP meeting on sample selection and acquisition" at Argonne National Laboratory October 6(th) 2010.* Standards in Genomic Sciences, 2010. **3**(3): p. 249-253.
216. Caporaso, J.G., C.L. Lauber, W.A. Walters, D. Berg-Lyons, J. Huntley, N. Fierer, S.M. Owens, J. Betley, L. Fraser, M. Bauer, N. Gormley, J.A. Gilbert, G. Smith, and R. Knight, *Ultra-high-throughput microbial community analysis on the Illumina HiSeq and MiSeq platforms.* Isme Journal, 2012. **6**(8): p. 1621-1624.
217. Caporaso, J.G., J. Kuczynski, J. Stombaugh, K. Bittinger, F.D. Bushman, E.K. Costello, N. Fierer, A.G. Pena, J.K. Goodrich, J.I. Gordon, G.A. Huttley, S.T. Kelley, D. Knights, J.E. Koenig, R.E. Ley, C.A. Lozupone, D. McDonald, B.D. Muegge, M. Pirrung, J. Reeder, J.R. Sevinsky, P.J. Tumbaugh, W.A. Walters, J. Widmann, T. Yatsunenko, J. Zaneveld, and R. Knight, *QIIME allows analysis of high-throughput community sequencing data.* Nature Methods, 2010. **7**(5): p. 335-336.
218. R Core Team, *R: A Language and Environment for Statistical Computing.* 2013. **Vienna, Austria. 2013.** http://www.R-project.org.
219. Vidon, P., C. Allan, D. Burns, T.P. Duval, N. Gurwick, S. Inamdar, R. Lowrance, J. Okay, D. Scott, and S. Sebestyen, *Hot spots and hot moments in riparian zones: potential for improved water quality management1.* Journal of the American Water Resources Association, 2010. **46**(2): p. 278-298.

220. Burgin, A.J., P.M. Groffman, and D.N. Lewis, *Factors regulating denitrification in a riparian wetland.* Soil Science Society of America Journal, 2010. **74**(5): p. 1826-1833.
221. Groffman, P.M., A.J. Gold, and R.C. Simmons, *Nitrate dynamics in riparian forests - microbial studies.* Journal of Environmental Quality, 1992. **21**(4): p. 666-671.
222. McClain, M.E., E.W. Boyer, C.L. Dent, S.E. Gergel, N.B. Grimm, P.M. Groffman, S.C. Hart, J.W. Harvey, C.A. Johnston, E. Mayorga, W.H. McDowell, and G. Pinay, *Biogeochemical hot spots and hot moments at the interface of terrestrial and aquatic ecosystems.* Ecosystems, 2003. **6**(4): p. 301-312.
223. Groffman, P.M., K. Butterbach-Bahl, R.W. Fulweiler, A.J. Gold, J.L. Morse, E.K. Stander, C. Tague, C. Tonitto, and P. Vidon, *Challenges to incorporating spatially and temporally explicit phenomena (hotspots and hot moments) in denitrification models.* Biogeochemistry, 2009. **93**(1-2): p. 49-77.
224. Ranalli, A.J. and D.L. Macalady, *The importance of the riparian zone and in-stream processes in nitrate attenuation in undisturbed and agricultural watersheds - A review of the scientific literature.* Journal of Hydrology, 2010. **389**(3-4): p. 406-415.
225. Rosenbaum, M.A., H.Y. Bar, Q.K. Beg, D. Segre, J. Booth, M.A. Cotta, and L.T. Angenent, *Shewanella oneidensis in a lactate-fed pure-culture and a glucose-fed co-culture with Lactococcus lactis with an electrode as electron acceptor.* Bioresource Technology, 2011. **102**(3): p. 2623-2628.
226. Morris, J.M. and S. Jin, *Enhanced biodegradation of hydrocarbon-contaminated sediments using microbial fuel cells.* Journal of Hazardous Materials, 2012. **213**: p. 474-477.
227. Chang, I.S., H. Moon, J.K. Jang, and B.H. Kim, *Improvement of a microbial fuel cell performance as a BOD sensor using respiratory inhibitors.* Biosensors and Bioelectronics, 2005. **20**(9): p. 1856-1859.
228. TerAvest, M.A., Z.J. Li, and L.T. Angenent, *Bacteria-based biocomputing with Cellular Computing Circuits to sense, decide, signal, and act.* Energy & Environmental Science, 2011. **4**(12): p. 4907-4916.
229. Friedman, E.S., K.M. Miller, D.A. Lipson, and L.T. Angenent, *Potentiostatically-poised electrodes mimic iron oxides and interact with soil microbial communities to alter the biogeochemistry of Arctic peat soils.* Submitted to *Minerals*, 2013.
230. Zhang, T., S.M. Gannon, K.P. Nevin, A.E. Franks, and D.R. Lovley, *Stimulating the anaerobic degradation of aromatic hydrocarbons in contaminated sediments by providing an electrode as the electron acceptor.* Environmental Microbiology, 2010. **12**(4): p. 1011-1020.
231. Williams, K.H., K.P. Nevin, A. Franks, A. Englert, P.E. Long, and D.R. Lovley, *Electrode-based approach for monitoring in situ microbial activity during subsurface bioremediation.* Environmental Science & Technology, 2010. **44**(1): p. 47-54.
232. Weber, K.A., L.A. Achenbach, and J.D. Coates, *Microorganisms pumping iron: anaerobic microbial iron oxidation and reduction.* Nature Reviews Microbiology, 2006. **4**(10): p. 752-764.
233. Palmer, M.A. and C.M. Febria, *The heartbeat of ecosystems.* Science, 2012. **336**(6087): p. 1393-1394.
234. Wood, T.E., M.A. Cavaleri, and S.C. Reed, *Tropical forest carbon balance in a warmer world: a critical review spanning microbial- to ecosystem-scale processes.* Biological Reviews, 2012. **87**(4): p. 912-927.
235. Morales, S.E. and W.E. Holben, *Linking bacterial identities and ecosystem processes: can 'omic' analyses be more than the sum of their parts?* Fems Microbiology Ecology, 2011. **75**(1): p. 2-16.
236. Raes, J. and P. Bork, *Molecular eco-systems biology: towards an understanding of community function.* Nature Reviews Microbiology, 2008. **6**(9): p. 693-699.

237. McPhilips, L.E., M.T. Walter, P.M. Groffman, and C.L. Goodale, *Hydrologic and biogeochemical drivers of denitrification in a stream riparian area.* In Preparation, 2013.
238. Hutchinson, G.L. and A.R. Mosier, *Improved soil cover method for field measurement of nitrous-oxide fluxes.* Soil Science Society of America Journal, 1981. **45**(2): p. 311-316.
239. Groffman, P.M., M.A. Altabet, J.K. Bohlke, K. Butterbach-Bahl, M.B. David, M.K. Firestone, A.E. Giblin, T.M. Kana, L.P. Nielsen, and M.A. Voytek, *Methods for measuring denitrification: Diverse approaches to a difficult problem.* Ecological Applications, 2006. **16**(6): p. 2091-2122.
240. Thompson, R.B., *Using calcium carbide with the acetylene inhibition technique to measure denitrification from a sprinkler irrigated vegetable crop.* Plant and Soil, 1996. **179**(1): p. 9-16.
241. Freney, J.R., C.J. Smith, and A.R. Mosier, *Effect of a new nitrification inhibitor (wax coated calcium carbide) on transformations and recovery of fertilizer nitrogen by irrigated wheat.* Fertilizer Research, 1992. **32**(1): p. 1-11.
242. Braunschweig, J., J. Bosch, K. Heister, C. Kuebeck, and R.U. Meckenstock, *Reevaluation of colorimetric iron determination methods commonly used in geomicrobiology.* Journal of Microbiological Methods, 2012. **89**(1): p. 41-48.
243. Oksanen, J., F.G. Blanchet, R. Kindt, P. Legendre, H.H. Stevens, and H. Wagner, *vegan: Community Ecology Package. R package version 2.0-8.* 2013.
244. Burt, T., G. Pinay, and S. Sabater, *What do we still need to know about the ecohydrology of riparian zones?* Ecohydrology, 2010. **3**(3): p. 373-377.
245. Audet, J., J.R. Johansen, P.M. Andersen, A. Baattrup-Pedersen, K.M. Brask-Jensen, L. Elsgaard, C. Kjaergaard, S.E. Larsen, and C.C. Hoffmann, *Methane emissions in Danish riparian wetlands: Ecosystem comparison and pursuit of vegetation indexes as predictive tools.* Ecological Indicators, 2013. **34**(0): p. 548-559.
246. Aronson, E.L., D.R. Vann, and B.R. Helliker, *Methane flux response to nitrogen amendment in an upland pine forest soil and riparian zone.* Journal of Geophysical Research-Biogeosciences, 2012. **117**.
247. Vidon, P. and A.R. Hill, *Denitrification and patterns of electron donors and acceptors in eight riparian zones with contrasting hydrogeology.* Biogeochemistry, 2004. **71**(2): p. 259-283.
248. Teh, Y.A., E.A. Dubinsky, W.L. Silver, and C.M. Carlson, *Suppression of methanogenesis by dissimilatory Fe(III)-reducing bacteria in tropical rain forest soils: implications for ecosystem methane flux.* Global Change Biology, 2008. **14**(2): p. 413-422.
249. Frei, S., K.H. Knorr, S. Peiffer, and J.H. Fleckenstein, *Surface micro-topography causes hot spots of biogeochemical activity in wetland systems: A virtual modeling experiment.* J. Geophys. Res., 2012. **117**: p. G00N12.
250. Muyzer, G. and A.J.M. Stams, *The ecology and biotechnology of sulphate-reducing bacteria.* Nature Reviews Microbiology, 2008. **6**(6): p. 441-454.
251. Webster, D.P., M.A. TerAvest, S.T. Chen, S.T. Chen, C.Q. Paduano, C.M. Radens, S. Sureka, J.A. Gralnick, and L.T. Angenent, *An arsenic-specific biosensor with genetically engineered Shewanella oneidensis in a bioelectrochemical system.* Submitted to *Biosensors & Bioelectronics*, 2013.
252. Campbell, A.N., Personal Communication, 2013.